IL
NUOVO CIMENTO
ORGANO DELLA SOCIETÀ ITALIANA DI FISICA
SOTTO GLI AUSPICI DEL CONSIGLIO NAZIONALE DELLE RICERCHE

VOL. XII, N. 4 *Serie nona* 1° Ottobre 1954

Sur le changement de variables dans les distributions et leurs tranformées de Fourier.

R. SCARFIELLO
Buenos Aires

(ricevuto il 14 Giugno 1954)

Résumé. — On étudie le changement de variables dans les distributions en les considérant comme courants, soit de degré zéro, soit de degré n, dans un espace euclidien. On définit après la transformée de Fourier d'un courant et on applique les résultats antérieurs au cas de changement de variables dans la transformée de Fourier d'une distribution.

1. – Soit X un espace vectoriel à n dimensions orienté c'est-à-dire l'espace euclidien R^n, dont chaque point x est défini si l'on choisit une base par ses coordonnées: $x_1, x_2, ..., x_n$.

Soit $\overset{p}{\mathcal{D}}$ l'espace des formes différentielles extérieures à support compact de degré p, espace des formes d'expression canonique:

$$\overset{p}{\varphi} = \sum_I f_I \, \mathrm{d}x_I$$

dont les coefficients f_I sont des fonctions indéfiniment dérivables à support compact.

I est un ensemble de p entiers de $[1, n]$; $I = (i_1, ..., i_p)$ avec $i_1 < ... < i_p$. $\cdot \mathrm{d}x_I = \mathrm{d}x_{i_1} \wedge ... \wedge \mathrm{d}x_{i_p}$.

$\overset{n-p}{\mathcal{D}}$ son dual, espace des courants de degré $(n - p)$, c'est-à-dire, l'espace des

$\overset{p}{\mathcal{S}}_x$ sera l'espace des formes de degré p indéfiniment dérivables à decroissance rapide dans X, c'est-à-dire l'espace des formes d'expression canonique:

$$\overset{p}{\varphi} = \sum_{I|} f_I \, dx_I$$

telles que les coéfficients f_I sont des fonctions indéfiniment dérivables sur R^n au sens usuel et decroissant à l'infini plus rapidement que toute puissance de $1/|x|$ ainsi que chacune de leurs dérivées; $\overset{n-p}{\mathcal{S}}'_x$ son dual, espace des courants tempérés de degré $(n-p)$, c'est-à-dire, l'espace des formes linéaires continues sur $\overset{p}{\mathcal{S}}_x$.

Considérons une application linéaire $\overset{0}{\mathcal{S}}'_x \to \overset{0}{\mathcal{S}}'_x$ de l'espace des courants tempérés de degré zéro dans lui même.

Nous allons démontrer qu'elle se prolonge par continuité en une application linéaire $\overset{p}{\mathcal{S}}'_x \to \overset{p}{\mathcal{S}}'_x$ de l'espace des courants de degré p dans lui même.

En effet: soit $\overset{p}{\wedge} X$ l'espace vectoriel puissance extérieure d'ordre p de X. Puisque donner une forme de degré p c'est donner un p-champ vectoriel covariant, c'est-à-dire, c'est donner une fonction définie sur X à valeurs dans $\overset{p}{\wedge} Y$ on pourra poser, si on indique avec le signe $\otimes$, le produit tensoriel de deux espaces:

$$\overset{p}{\mathcal{S}}_x = \overset{0}{\mathcal{S}}_x \otimes \overset{p}{\wedge} Y \ (^3). \tag{14}$$

Considérons d'autre part l'espace $\overset{p}{\mathcal{S}}'_x$ et le produit tensoriel $\overset{0}{\mathcal{S}}'_x \otimes \overset{p}{\wedge} Y$.

Un élément du premier s'exprime par $\sum_J T_J \, dx_J$, tandis qu'un élément du deuxième s'exprime per $\sum_J T_J e'_J$, où les e'_J forment une base de $\overset{p}{\wedge} Y$. On voit que ces deux expressions sont les mêmes.

D'ailleurs si les T_J tendent vers zéro, $\sum_J T_J \, dx_J$ et $\sum_J T_J e'_J$ tendent aussi vers zéro.

On peut donc poser:

$$\overset{p}{\mathcal{S}}'_x = \overset{0}{\mathcal{S}}'_x \otimes \overset{p}{\wedge} Y \, , \tag{15}$$

formule qui définit un isomorphisme biunivoque et bicontinu entre $\overset{p}{\mathcal{S}}'_x$ et $\overset{0}{\mathcal{S}}'_x \otimes \overset{p}{\wedge} Y$.

Or, comme la formule (14) est intrinsèque et comme les espaces $\overset{0}{\mathcal{S}}_x$ et $\overset{p}{\mathcal{S}}_x$ sont denses dans $\overset{0}{\mathcal{S}}'_x$ et $\overset{p}{\mathcal{S}}'_x$ respectivement, alors la formule (15) est intrinsèque,

(3) Nous prenons X et Y réels, mais les fonctions et les formes sont à valeurs complexes; donc $\wedge X$ et $\wedge Y$ désignent les complexifiés des espaces désignés habituellement par $\wedge X$ et $\wedge Y$, c'est-à-dire: $\wedge X + i \wedge X$ et $\wedge Y + i \wedge Y$.

c'est-à-dire ne dépend pas du système d'axes choisi. (Un changement de base le montrerait si on faisait les calculs).

Si on revient à l'hypothèse, qu'on avait une application de $\overset{0}{\mathcal{S}}'_x$ dans $\overset{0}{\mathcal{S}}'_x$, la formule (15) montre que la même application applique $\overset{p}{\mathcal{S}}_x$ dans $\overset{p}{\mathcal{S}}_x$. ($\overset{p}{\wedge} Y$ étant appliqué sur lui même).

Considérons maintenant la transformée de Fourier $\mathcal{F}$ d'une forme différentielle de degré n appartenant à $\overset{n}{\mathcal{S}}_x$:

$$(16) \qquad \mathcal{F}\overset{n}{\varphi} = \mathcal{F}(\varphi(x)\,\mathrm{d}x_1 \wedge \ldots \wedge \mathrm{d}x_n) = \int_{R^n} \exp\,[-2\pi i\langle x, y\rangle]\varphi(x)\,\mathrm{d}x = \psi(y)\,,$$

et sa coniugée $\overline{\mathcal{F}}$:

$$(17) \qquad \overline{\mathcal{F}}\overset{n}{\varphi} = \overline{\mathcal{F}}(\varphi(x)\mathrm{d}x_1 \wedge \ldots \wedge \mathrm{d}x_n) = \int_{R^n} \exp.[2\pi i\langle x, y\rangle]\varphi(x)\,\mathrm{d}x = \tau(y)\,,$$

où $\psi(y)$ et $\tau(y)$ sont des fonctions ou si on veut, formes différentielles de degré zéro, appartenants à $\overset{0}{\mathcal{S}}_y$.

On pourrait aussi écrire:

$$(18) \qquad \begin{cases} \mathcal{F}\overset{n}{T} = \mathcal{F}(T\,\mathrm{d}x_1 \wedge \ldots \wedge \mathrm{d}x_n) = \mathcal{F}T = V\,, \\ \overline{\mathcal{F}}\overset{n}{T} = \overline{\mathcal{F}}(T\,\mathrm{d}x_1 \wedge \ldots \wedge \mathrm{d}x_n) = \overline{\mathcal{F}}T = W\,, \end{cases}$$

où les derniers membres sont les transformées de Fourier de la distributions T.

Si on considère que les transformées de Fourier sont des applications continues dans $\mathcal{S}'$; que $\overset{n}{\mathcal{S}}_x$ et $\overset{0}{\mathcal{S}}_y$ sont des sous-espaces denses dans $\overset{n}{\mathcal{S}}'_x$ et $\overset{0}{\mathcal{S}}'_y$ respectivement, et que (16) et (17) ne dépendent pas du système d'axes choisi, on voit que les formules (18) sont indépendents du système d'axes.

On peut conclure alors, que la transformation de Fourier $\mathcal{F}$ et sa conjugée $\overline{\mathcal{F}}$ définissent deux applications qui font passer des courants de degré n sur un espace, aux courants de degré zéro sur le dual.

Nous indiquerons symboliquement avec $\overset{n\to 0}{\mathcal{F}}$ et $\overset{n\to 0}{\overline{\mathcal{F}}}$ ces applications.

Supposons donc qu'on a, en général une application:

$$(19) \qquad \overset{n}{\mathcal{S}}'_x \to \overset{0}{\mathcal{S}}'_y$$

des courants tempérés de degré n sur X dans les courants de degré zéro sur Y.

Nous démontrerons sous cette hypothèse qu'on a:

$$(19\text{-}bis) \qquad \overset{n-p}{\mathcal{S}}'_x \to \overset{p}{\mathcal{S}}'_y\,,$$

c'est-à-dire, l'application donnée se prolonge en une application qui fait passer des courants tempérés de degré $(n-p)$ sur X aux courants tempérés de degré p sur Y.

En effet: soit $\overset{n-p}{T}$ un courant de degré $(n-p)$, et soit $\overset{p}{\omega}$ la forme identique de degré p sur X et à valeurs dans $\overset{p}{\wedge} X$, autrement dit la forme de degré p sur X telle qu'à tout p-vecteur sur X, elle lui fait correspondre le même p-vecteur comme élément de $\overset{p}{\wedge} X$.

Si on fait le produit extérieur de $\overset{n-p}{T}$ et $\overset{p}{\omega}$, on obtiendra un courant de degré n à valeur dans $\overset{p}{\wedge} X$, c'est-à-dire

$$\overset{n-p}{T} \wedge \overset{p}{\omega} = \overset{n}{S}, \tag{20}$$

ou $\overset{n}{S}$ est un courant de degré n à valeur dans $\overset{p}{\wedge} X$, ce que revient à dire que $\overset{n}{S}$ est un élément du produit tensoriel:

$$\overset{n}{\mathcal{S}}'_x \otimes \overset{p}{\wedge} X. \tag{21}$$

Mais par hypothèse on avait l'application $\overset{n}{\mathcal{S}}'_x \to \overset{0}{\mathcal{S}}'_y$, et en appliquant $\overset{p}{\wedge} X$ sur lui même, on aura:

$$\overset{n}{\mathcal{S}}'_x \otimes \overset{p}{\wedge} X \to \overset{0}{\mathcal{S}}'_y \otimes \overset{p}{\wedge} X = \overset{p}{\mathcal{S}}'_y, \tag{22}$$

car le produit tensoriel $\overset{0}{\mathcal{S}}'_y \otimes \overset{p}{\wedge} X$ donne bien l'espace des courants de degré p définis sur Y (voir (14)).

En somme: grâce à la multiplication extérieure par $\overset{p}{\omega}$ l'application $\overset{n}{\mathcal{S}}'_x \to \overset{0}{\mathcal{S}}'_y$ se prolonge en une application qui fait passer des courants de degré $(n-p)$ sur X, aux courants de degré p sur Y.

Lorsque l'application de la démonstration précedente est la transformée de Fourier ou sa conjuguée, on doit alors prolonger $\overset{n\to 0}{\mathcal{F}}$ et $\overset{n\to 0}{\overline{\mathcal{F}}}$ au moyen de la multiplication extérieure par ω.

On obtient dans ce cas: $\mathcal{F}_\omega$, ${}_\omega\mathcal{F}$, $\overline{\mathcal{F}}_\omega$, ${}_\omega\overline{\mathcal{F}}$, selon que l'on fait le produit extérieur par ω, à droite ou à gauche.

Si on tient compte qu'on a fait:

$$\overset{n-p\to p}{\mathcal{F}_\omega} \cdot \overset{n-p}{T} = \overset{n\to 0}{\mathcal{F}} \cdot (\overset{n-p}{T} \wedge \overset{p}{\omega}), \qquad \text{et:} \quad \overset{n-p\to p}{{}_\omega\mathcal{F}} \cdot \overset{n-p}{T} = \overset{n\to 0}{\mathcal{F}} \cdot (\overset{p}{\omega} \wedge \overset{n-p}{T}),$$

on pourra écrire symboliquement:

(23) $\overset{n\to 0}{\mathcal{F}}$ se prolonge en $\overset{n-p\to p}{\mathcal{F}_\omega}$ ou en $\overset{n-p\to p}{{}_\omega\mathcal{F}}$,

(24) $\overset{n\to 0}{\overline{\mathcal{F}}}$ » » $\overset{n-p\to p}{\overline{\mathcal{F}}_\omega}$ » $\overset{n-p\to p}{{}_\omega\overline{\mathcal{F}}}$.

Vérifions ces résultats en faisant les calculs avec un systeme d'axes. On a:

$$\overset{n-p}{T} = \sum_J T_J \, dx_J , \tag{25}$$

expression d'un courant de degré $(n-p)$ au moyen des $\binom{n}{p}$ distributions $T_J \in \mathcal{S}'_x$ [4]

$$\overset{p}{\omega} = \sum_K \boldsymbol{e}_K dx_K , \tag{26}$$

où les $\boldsymbol{e}_K$ forment une base de $\overset{p}{\wedge} X$.

On a alors:

$$\overset{n-p}{T} \wedge \overset{p}{\omega} = \sum \delta_I^{J,K} T_J \boldsymbol{e}_K \, dx_1 \wedge \ldots \wedge dx_n , \tag{27}$$

qui est une somme de courants de degré zéro T_J, multipliés par les vecteurs $\boldsymbol{e}_K$.

$\delta_I^{J,K}$ désigne le symbole de Kronecker, avec $I = (1, \ldots, n)$; $J = (j_1, \ldots, j_{n-p})$; $K = (k_1, \ldots, k_p)$. Si on fait la transformation de Fourier $\mathcal{F}$ de (27), on obtient:

$$\sum \delta_I^{J,K} V_J \boldsymbol{e}_K = \overset{p}{V} , \tag{28}$$

où on a fait:

$$\mathcal{F} T_J dx_1 \wedge \ldots \wedge dx_n = V_J , \tag{29}$$

avec $V_J \in \mathcal{S}'_y$.

L'expression (28) peut être considérée comme courant de degré zéro sur Y à valeur dans $\overset{p}{\wedge} X$, c'est-à-dire comme élément du produit tensoriel $\overset{0}{\mathcal{S}}'_y \otimes \overset{p}{\wedge} X$, ou si on veut comme courant de degré p sur Y.

On peut alors écrire d'accord avec (25):

$$\overset{p}{V} = \sum \delta_I^{J,K} V_J \, dy_K . \tag{30}$$

Soit d'ailleurs

$$\overset{n-p}{\omega'} = \sum_L \boldsymbol{e}'_L dy_L , \tag{30}$$

la forme identique de degré $(n-p)$ sur Y à valeur dans $\overset{p}{\wedge} Y$.

Les $\boldsymbol{e}'_L$ forment une base de $\overset{p}{\wedge} Y$.

---

[4] Voir [2], p. 30.

On a:

$$(32) \qquad {}^{n-p}\omega^{I} \wedge {}^{p}V = \sum \delta_{I}^{L,K} \cdot \delta_{I}^{J,K} e'_{L} V_{J} \, dy_1 \wedge \ldots \wedge dy_n .$$

On peut se passer du produit des symboles $\delta_I^{L,K}$, $\delta_I^{J,K}$ car ils sont les mêmes quand on fait $L = J$, alors:

$$(32\text{-}bis) \qquad {}^{n-p}\omega^{I} \wedge {}^{p}V = \sum_{J} e'_{J} V_{J} \, dy_1 \wedge \ldots \wedge dy_n .$$

Si on applique la transformée de Fourier conjuguée à (32-*bis*) on aura:

$$(33) \qquad \sum_{J} e'_{J} T_{J} = {}^{n-p}\bar{T},$$

car

$$\bar{\mathcal{F}} V_J \, dy_1 \wedge \ldots \wedge dy_n = T_J .$$

La formule (33) est alors l'expression d'un courant de degré zéro sur X à valeur dans ${}^{p}\wedge Y$ qui coïncide bien avec ${}^{n-p}\bar{T}$.

Alors, symboliquement:

$$(34) \qquad {}_{\omega}^{p\to n-p}\bar{\mathcal{F}} \circ {}^{n-p\to p}\bar{\mathcal{F}}_{\omega} = {}^{n-p}I ,$$

où I désigne l'identité.

3. – Soit maintenant H un isomorphisme de X sur lui même; un tel isomorphisme définit sur le dual Y l'isomorphisme contragrédient $\overset{\vee}{H}$ par la relation

$$(35) \qquad \langle H(x), \overset{\vee}{H}(y) \rangle = \langle x, y \rangle .$$

On aura une image directe de ${}^{n-p}\bar{S}'_x$ par H, et par conséquence une image directe de ${}^{p}\bar{S}'_y$ par $\overset{\vee}{H}$, et parce qu'il y a transport de structure on pourra écrire

$$(36) \qquad \begin{cases} {}^{n-p\to p}\bar{\mathcal{F}}_{\omega} \, H \, {}^{n-p}\bar{T} = \overset{\vee}{H} \, {}^{p}\bar{V} = \overset{\vee}{H} \, {}^{n-p\to p}\bar{\mathcal{F}}_{\omega} \, {}^{n-p}\bar{T} , \\ {}_{\omega}^{p\to n-p}\bar{\mathcal{F}} \, \overset{\vee}{H} \, {}^{p}\bar{V} = H \, {}^{n-p}\bar{T} = H \, {}_{\omega}^{p\to n-p}\bar{\mathcal{F}} \, {}^{p}\bar{V} , \end{cases}$$

et en fin, symboliquement:

$$(37) \qquad \begin{cases} {}^{n-p\to p}\bar{\mathcal{F}}_{\omega} \circ H = \overset{\vee}{H} \circ {}^{p\to n-p}\bar{\mathcal{F}}_{\omega} , \\ {}_{\omega}^{p\to n-p}\bar{\mathcal{F}} \circ \overset{\vee}{H} = H \circ {}_{\omega}^{n-p\to p}\bar{\mathcal{F}} . \end{cases}$$

A titre d'exemple nous obtiendrons la première des formules (37), dans le cas d'un courant de degré zéro, en faisant les calculs explicitement.

On peut poser:

$$\langle \mathcal{F} H \overset{0}{T}, \overset{0}{\varphi} \rangle = \langle H \overset{0}{T}, \mathcal{F} \overset{0}{\varphi} \rangle , \tag{38}$$

où les deux membres ont un sens bien défini car $\mathcal{F} H \overset{0}{T}$ est un courant de degré n, $H \overset{0}{T}$ un courant de degré zéro et $\mathcal{F} \overset{0}{\varphi}$ est une forme de degré n.

En tenant compte des formules (3) et (5), on aura:

$$\langle H \overset{0}{T}, \mathcal{F} \overset{0}{\varphi} \rangle = \langle \overset{0}{T}, H' \mathcal{F} \overset{0}{\varphi} \rangle . \tag{39}$$

Si on pose:

$$\mathcal{F} \overset{0}{\varphi} = \overset{n}{\psi}(x) = \int_{\overset{\cdot}{R}^n} \exp [-2\pi i \langle x, y \rangle] \varphi(y) \, dy , \tag{40}$$

on aura:

$$H' \mathcal{F} \overset{0}{\varphi} = H' \overset{n}{\psi} = \psi(H(x)) \cdot |H| = \tag{41}$$

$$= |H| \cdot \int_{\overset{\cdot}{R}^n} \exp [-2\pi i \langle H(x), y \rangle] \varphi(y) \, dy = |H| \int_{\overset{\cdot}{R}^n} \exp [-2\pi i \langle x, {}^t H(y) \rangle] \varphi(y) \, dy .$$

Si on fait: ${}^t H(y) = \xi$; $y = {}^t H^{-1}(\xi)$ on obtient de (41)

$$|H| \int_{\overset{\cdot}{R}^n} \exp [-2\pi i \langle \xi, x \rangle] \varphi({}^t H^{-1}(\xi)) \, |{}^t H^{-1}| \, d\xi = \tag{42}$$

$$= |H| \cdot |{}^t H^{-1}| \int_{\overset{\cdot}{R}^n} \exp [-2\pi i \langle \xi, x \rangle \varphi({}^t H^{-1}(\xi)) \, d\xi =$$

$$= \int_{\overset{\cdot}{R}^n} \exp[-2\pi i \langle \xi, x \rangle] \varphi({}^t H^{-1}(\xi)) d\xi = \mathcal{F} \varphi({}^t H^{-1}(\xi)) = \mathcal{F} \overset{0}{\varphi}(\overset{\vee}{H}(\xi)) = \mathcal{F} \overset{\vee}{H}' \overset{0}{\varphi} ,$$

ou on a indiqué par $\overset{\vee}{H}$ l'isomorphisme contragrédient ${}^t H^{-1}$ de H.

On a donc:

$$H' \mathcal{F} \overset{0}{\varphi} = \mathcal{F} \overset{\vee}{H}' \overset{0}{\varphi} . \tag{43}$$

En remplaçant dans (39) on aura:

$$\langle \overset{0}{T}, H' \mathcal{F} \overset{0}{\varphi} \rangle = \langle \overset{0}{T}, \mathcal{F} \overset{\vee}{H}' \overset{0}{\varphi} \rangle = \langle \mathcal{F} \overset{0}{T}, \overset{\vee}{H}' \overset{0}{\varphi} \rangle = \langle \overset{\vee}{H} \mathcal{F} \overset{0}{T}, \overset{0}{\varphi} \rangle , \tag{44}$$

et par comparaison avec le premier membre de (38) on obtient:

$$\mathcal{F}H\overset{0}{T} = \overset{\vee}{H}\mathcal{F}\overset{0}{T}. \tag{45}$$

Je tiens à remercier ici, M. L. SCHWARTZ, qui m'a suggéré de faire cette note et maintes fois m'a aidé avec ses conseilles, M. J. LIONS dont les discussions m'on été si utiles, et la Direccion Nacional de la Energía Atómica de Buenos Aires, qui m'a permis de rester comme boursier à Paris.

APPLICATION

Soit $X = R$, $n = 1$, $T = \lg|x|$, H l'homotétie de rapport $\lambda > 0$ (5).

a) Considérons d'abord T comme courant de degré zéro.
Il est facile de voir que:

$$H\overset{0}{T} = \lg\left|\frac{x}{\lambda}\right| = \lg|x| - \lg\lambda .$$

Alors:

$$\mathcal{F}H\overset{0}{T} = \mathcal{F}\lg|x| - \mathcal{F}\lg\lambda =$$

$$= -\frac{1}{2}Pf\frac{1}{|y|} - K\delta - \delta\lg\lambda = -\frac{1}{2}Pf\frac{1}{|y|} - (K + \lg\lambda)\delta ,$$

où on a fait:

$$\mathcal{F}\lg|x| = -\frac{1}{2}Pf\frac{1}{|y|} - K\delta , \tag{47}$$ (6)

avec $K = C + \lg 2\pi$ et $C =$ const. d'Euler.

Considérons maintenant: $\overset{\vee}{H}\mathcal{F}\overset{0}{T}$; on aura:

$$\overset{\vee}{H}\left(-\frac{1}{2}Pf\frac{1}{|y|} - K\delta\right) = \overset{\vee}{H}\overset{1}{S}. \tag{48}$$

où $\left(-\frac{1}{2}Pf(1/|y|) - K\delta\right) = \overset{1}{S}$ doit être considéré comme courant de degré un, et H est l'homothétie de rapport $1/\lambda$.
On aura

$$\langle H\overset{1}{S}, \overset{0}{\varphi}\rangle = \langle \overset{1}{S}, \overset{\vee}{H}\overset{0}{\varphi}\rangle = \left\langle \overset{1}{S}, \overset{0}{\varphi}\left(\frac{y}{\lambda}\right)\right\rangle = \left\langle \left(-\frac{1}{2}Pf\frac{1}{|y|} - K\delta\right), \varphi\left(\frac{y}{\lambda}\right)\right\rangle = \tag{49}$$

$$= \left\langle -\frac{1}{2}Pf\frac{1}{|y|}, \varphi\left(\frac{y}{\lambda}\right)\right\rangle - \left\langle K\delta, \varphi\left(\frac{y}{\lambda}\right)\right\rangle =$$

$$= -\frac{1}{2}Pf\int_{-\infty}^{\infty}\frac{1}{|y|}\varphi\left(\frac{y}{\lambda}\right)dy - K\varphi(0) .$$

(5) Voir [5], p. 1012.
(6) Voir [1], II, p. 114.

Considérons le premier terme du dernier membre de (49)

$$(50)\qquad -\frac{1}{2}\,Pf\int_{-\infty}^{\infty}\frac{1}{|y|}\,\varphi\left(\frac{y}{\lambda}\right)dy =$$

$$= -\frac{1}{2}\lim_{\varepsilon\to 0}\left[\int_{\varepsilon}^{\infty}\frac{1}{y}\,\varphi\left(\frac{y}{\lambda}\right)dy - \int_{-\infty}^{-\varepsilon}\frac{1}{y}\,\varphi\left(\frac{y}{\lambda}\right)dy + \varphi(0)\lg\varepsilon + \varphi(0)\lg\varepsilon\right] =$$

$$= -\frac{1}{2}\lim_{\varepsilon\to 0}\left[2\int_{\varepsilon}^{\infty}\frac{\varphi\left(\frac{y}{\lambda}\right)+\varphi\left(-\frac{y}{\lambda}\right)}{y}\,dy + 2\varphi(0)\lg\varepsilon\right].$$

Si on fait:

$$\frac{y}{\lambda} = \xi\,; \qquad \frac{\varepsilon}{\lambda} = \eta\,.$$

On aura (50) égal à:

$$(51)\qquad -\frac{1}{2}\lim_{\eta\to 0}\left[2\int_{\eta}^{\infty}\frac{\varphi(\xi)+\varphi(-\xi)}{\xi}\,d\xi + 2\varphi(0)\lg\lambda\eta\right] =$$

$$= -\frac{1}{2}\lim_{\eta\to 0}\left[2\int_{\eta}^{\infty}\frac{\varphi(\xi)+\varphi(-\xi)}{\xi}\,d\xi + 2\varphi(0)\lg\eta + 2\varphi(0)\lg\lambda\right] =$$

$$= -\frac{1}{2}\,Pf\int_{-\infty}^{\infty}\frac{1}{|\xi|}\,\varphi(\xi)\,d\xi - \varphi(0)\lg\lambda\,.$$

En ramenant ce résultat à (49), on obtient:

$$(52)\qquad \overset{\mathrm{V}}{H}\overset{1}{S} = -\frac{1}{2}\,Pf\,\frac{1}{|y|} - K\delta - \delta\lg\lambda = -\frac{1}{2}\,Pf\,\frac{1}{|y|} - (K+\lg\lambda)\delta\,,$$

ce qui coïncide avec (45).

b) Si l'on considère T comme courant de degré un on aura

$$\overset{1}{H}T = \frac{1}{\lambda}\lg\left|\frac{x}{\lambda}\right|,$$

et

$$(53)\qquad \mathcal{F}\overset{1}{H}T = \frac{1}{\lambda}\mathcal{F}(\lg|x| - \lg\lambda) =$$

$$= \frac{1}{\lambda}[\mathcal{F}\lg|x| - \mathcal{F}\lg\lambda] = \frac{1}{\lambda}\left[-\frac{1}{2}\,Pf\,\frac{1}{|y|} - (K+\lg\lambda)\delta\right].$$

Considérons maintenant:

$$\overset{\vee}{H}\mathcal{F}\overset{1}{T} = \overset{\vee}{H}\overset{0}{S}\,.$$

On obtient:

$$(54)\qquad \langle \overset{\vee}{H}\overset{0}{S},\ \overset{1}{\varphi}\rangle = \left\langle \overset{0}{S},\ \frac{1}{\lambda}\varphi\left(\frac{x}{\lambda}\right)\right\rangle = \left\langle \left(-\frac{1}{2}Pf\,\frac{1}{|y|} - K\delta\right),\ \frac{1}{\lambda}\varphi\left(\frac{x}{\lambda}\right)\right\rangle,$$

et finalement

$$(55)\qquad \overset{\vee}{H}\overset{0}{S} = \frac{1}{\lambda}\left[-\frac{1}{2}Pf\,\frac{1}{|y|} - (K + \lg\lambda)\delta\right],$$

résultat que coïncide avec (53).

Pour $\lambda < 0$ on obtient le même résultat en remplaçant λ par $|\lambda|$ comme on le voit très facilement en effectuant les mêmes calculs antérieurs.

BIBLIOGRAPHIE

[1] L. Schwartz: *Théorie des distributions*, I, II (Paris, 1950-51).
[2] G. de Rham et K. Kodaira: *Harmonic Integrals* (Princeton, 1950).
[3] M. Cugiani et S. Albertoni: *Nuovo Cimento*, **10**, 157 (1953).
[4] W. Güttinger: *Phys. Rev.*, **89**, 1004 (1953).
[5] N. Boubaki: *Eléments de Mathématique*, VI, livre II, ch. II.

RIASSUNTO (*)

Si studia il cambiamento di variabili nelle distribuzioni considerandole come correnti, sia di grado zero che di grado n in uno spazio euclideo. In seguito si definisce la trasformata di Fourier di una corrente e si applicano i precedenti risultati al caso del cambiamento di variabili nella trasformata di Fourier di una distribuzione.

(*) *Traduzione a cura della Redazione.*

IL NUOVO CIMENTO Vol. XII, N. 4 1° Ottobre 1954

Diffusion proton-proton aux énergies intermédiaires.

A. Martin et L. Verlet

Laboratoire de Physique de l'École Normale Supérieure - Paris

(ricevuto il 2 Luglio 1954)

Summary. — Proton-proton scattering at intermediate energies has been studied with the potential derived from the *PS-PS* Theory. The validity of Born approximation in *P* and *D* states, the influence of *P-F* coupling, and of non-perturbation corrections to the potential have been investigated. A comparison with experiment shows a good agreement at 18.3 MeV, but a definite disagreement at 32 MeV.

1. – Introduction.

L'interaction entre deux nucléons déduite de la théorie mésique pseudoscalaire (avec couplage pseudoscalaire) peut, aux faibles énergies, être approchée par un potentiel statique (1). Celui-ci a déjà été confronté avec l'expérience à ces énergies par Lévy, et, également, par Jastrow (2) avec une forme légèrement modifiée que nous emploierons ci-après (équation (1)). A ces énergies les résultats sont acceptables dans un domaine de variation assez large des paramètres.

Il nous a paru bon de voir si des expériences de diffusion aux énergies intermédiaires confirment cet accord et la latitude correspondante dans le choix des paramètres. D'autre part, ces énergies sont particulièrement inté-

(1) M. Lévy: *Phys. Rev.*, **86**, 806 (1952); **88**, 725 (1952) que nous appellerons L; voir aussi A. Klein: *Phys. Rev.*, **90**, 1101 (1953); **91**, 740 (1953); **92**, 1017 (1953).

(2) R. Jastrow: *Phys. Rev.*, **91**, 749 (1953). J. M. Blatt et M. H. Kalos (*Phys. Rev.*, **92**, 1563 (1953)) se sont servi du même potentiel pour déterminer les propriétés des nucléons aux basses énergies. Mais ils se sont imposés un choix de paramètres donnant exactement le moment quadrupolaire du Deutéron, critère beaucoup trop sévère vu l'importance des effets mésiques en ce qui concerne cette quantité (F. Villars: *Phys. Rev.*, **86**, 476 (1952) et S. Déser: *Phys. Rev.*, **92**, 1542 (1053)).

ressantes parce qu'elles sont de l'ordre de l'énergie cinétique des nucléons dans le deutéron (quelques dizaines de MeV) et représentent probablement une limite de l'approximation statique faite par LÉVY même si l'on utilise la dépendance de l'énergie du potentiel statique provenant des corrections de non perturbation.

Des expériences de diffusion neutron-proton ont été effectuées à 40 MeV et les résultats ont été analysés dans L; mais outre le fait que cette énergie est probablement au delà du domaine de validité du potentiel, l'usage de l'approximation de Born dans les états P n'est pas justifié comme nous le verrons plus loin (§ 3). Il paraissait donc intéressant d'analyser les expériences précises de diffusion proton-proton qui ont été faites à 18 MeV ([3]), et à 32 MeV ([4]). Nous avons publié un compte rendu préliminaire de cette étude ([5]) qui souffrait également de l'utilisation de l'approximation de Born dans les états P. On trouvera ici une analyse plus complète et plus correcte de ces expériences.

Nous avons utilisé le potentiel ([6]):

$$(1)\qquad \left\{\begin{aligned} V(r) &= \infty \quad \text{pour} \quad r < r_c = 0.38\,, \\ V(r) &= V_c(r) + S_{12} V_t(r)\,, \\ V_c(r) &= \frac{G^2}{4\pi}\left(\frac{1}{2M}\right)^2 \frac{(\tau_1\cdot\tau_2)(\sigma_1\cdot\sigma_2)}{3}\,\frac{e^{-r}}{r} - 3\lambda\left(\frac{G^2}{4\pi}\right)^2\left(\frac{1}{2M}\right)^2 \frac{2}{\pi}\,\frac{K_1(2r)}{r^2}\,, \\ V_t(r) &= \frac{G^2}{4\pi}\left(\frac{1}{2M}\right)^2 \frac{(\tau_1\cdot\tau_2)}{3}\left|1 + \frac{3}{r} + \frac{3}{r^2}\right|\frac{e^{-r}}{r}\,. \end{aligned}\right.$$

qui est, à quelques modifications près, le potentiel statique déduit par LÉVY de la théorie pseudoscalaire des forces nucléaires (L).

Ces modifications sont les suivantes:

Nous n'avons gardé que le terme principal du quatrième ordre; nous avons multiplié ce terme par un paramètre ajustable λ dont l'introduction est justifiée dans une certaine mesure par des considérations théoriques (corrections radiatives ([7]), diffusion méson-méson ([8])) et permet de tenir compte d'une partie des termes abandonnés.

Nous avons étudié au § 2 la diffusion proton-proton avec le potentiel (1). Les déphasages des états S, P et D ont été obtenus à la fois par le calcul

([3]) J. L. YNTEMA et M. G. WHITE: *Technical Report* N10 3478 *Princeton University* (1952).

([4]) B. CORK, L. JOHNSTON et C. RICHMAN: *Phys. Rev.*, **79**, 71 (1950); F. FILLMORE: *Phys. Rev.*, **83**, 1252 (1951).

([5]) A. MARTIN et L. VERLET: *Phys. Rev.*, **89**, 519 (1953).

([6]) Nous nous plaçons dans un système d'unités où $\hbar = c = \mu_\pi = 1$.

([7]) Voir référence ([1]) et aussi M. RUDERMAN: *Phys. Rev.*, **90**, 183 (1953).

([8]) G. BONNEVAY: *Compt. Rend.*, **16**, 1641 (1954).

direct et par l'approximation de Born dont l'insuffisance dans les états P a été démontrée. On peut trouver pour un large domaine de variation du paramètre un accord avec l'expérience en ce qui concerne la section efficace à 18,3 MeV. A 32 MeV un tel accord n'est pas possible. La prise en considération du couplage ${}^3P_2$-${}^3F_2$ modifie extrêmement peu les sections efficaces précédemment calculées.

Au § 3 nous avons tenu compte des corrections non adiabatiques au potentiel. Si elles amènent à modifier les valeurs de λ et de $G^2/4\pi$ pour lesquelles les sections efficaces à 90° sont en accord avec l'expérience, il n'en résulte pas un changement sensible des conclusions du § 2.

2. – Calculs des déphasages et distributions angulaires.

2·1. *Sections efficaces différentielles en se limitant aux états S, P et D.* – Les équations de Schrödinger pour les fonctions d'onde radiales (9) sont intégrées, soit dans l'approximation de Born, soit rigoureusement, et fournissent les déphasages K_0 pour l'état S, $K_1^{(0)}K_1^{(1)}K_1^{(2)}$ pour les états $P(J = 0, 1, 2)$, K_2 pour l'état D.

L'approximation de Born, pour un potentiel comprenant un cœur répulsif, est donnée par:

$$K_L^{(J)} = -M\int_{r_c}^{\infty}[F_L(kr) - \varrho_L(kr_c)G_L(kr)]^2 V_L^{(J)}(r)\,\mathrm{d}r - (-1)^L\varrho_L(kr_c)\,,$$

où F_L et G_L sont respectivement les fonctions coulombiennes régulière et irrégulière et $\varrho_L(kr_c) = F_L(kr_c)/G_{L(kr_c)}$.

Les déphasages exacts sont obtenus par une méthode d'intégration qui permet de passer d'un point au suivant en négligeant seulement des termes de l'ordre de la puissance sixième de l'intervalle. Nous nous sommes toujours placés dans des cas où la précision de cette méthode était excellente.

L'intégration est conduite à partir du cœur et les déphasages sont déterminés en comparant la fonction d'onde à une combinaison linéaire des fonctions coulombiennes (10) en un point où le potentiel nucléaire ne se fait plus sentir.

On pouvait espérer que l'approximation de Born s'appliquerait aux états de moment orbital non nul (référence (5) et (L)); alors que, pour les états D,

(9) F. Rohrlich et J. Eisenstein: *Phys. Rev.*, **75**, 705 (1949).

(10) I. Bloch, M. H. Hull, A. A. Broyles, W. G. Bouricius, B. E. Freeman et G. Breit: *Rev. Mod. Phys.*, **23**, n. 2 (1951).

on vérifie par intégration directe qu'il en est bien ainsi, on arrive, en ce qui concerne les états P à une conclusion toute autre:

les résultats obtenus par intégration directe sont toujours différents de ceux obtenus par l'approximation de Born; le désaccord peut être énorme: par exemple pour $\lambda = 1{,}1$, $G^2/4\pi = 10{,}4$, $E = 32$ MeV:

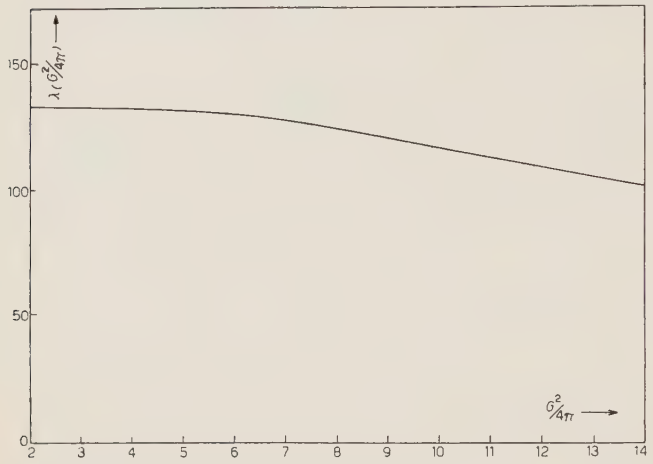

Fig. 1.

$$K_1^{(0)} \text{ direct} = 55^\circ\,,$$

$$K_1^{(0)} \text{ Born} = 12^\circ\,.$$

Même dans le cas où les déphasages sont petits, la différence est très appréciable; par exemple pour $\lambda = 20$, $G^2/4\pi = 2{,}6$, $E = 18{,}3$ MeV, l'intégration directe donne:

$$K_1^{(0)} = 6^\circ{,}4 \qquad K_1^{(1)} = 2^\circ{,}4 \qquad K_1^{(2)} = 4^\circ{,}4\,.$$

L'approximation de Born:

$$K_1^{(0)} = 3^\circ{,}2 \qquad K_1^{(1)} = 1^\circ{,}1 \qquad K_1^{(2)} = 2^\circ{,}2\,.$$

Les déphasages, calculés pour $\lambda = 20$; 5,8; 1,1; 0,5 sont reproduits dans le tableau I. Pour une valeur donnée de λ on a ajusté la constante de couplage de manière à avoir un accord avec l'expérience à 90° pour $E = 18{,}3$ MeV. On a obtenu ainsi une relation entre λ et $G^2/4\pi$ (fig. 1). Nous avons reproduit (fig. 2) les sections efficaces différentielles [11] correspondant à la valeur de λ qui donne un accord avec l'expérience, à 90°, pour 18,3 et 32 MeV. L'accord avec l'expérience [3,4] aux autres angles est correct pour 18,3 MeV, mauvais pour 32 MeV.

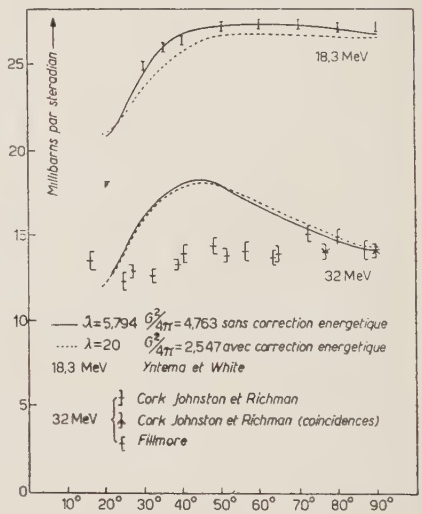

Fig. 2.

(11) G. Breit, C. Kittel et H. M. Thaxton: *Phys. Rev.*, **57**, 255 (1940).

TABLEAU I.

$G^2/4\pi$	λ	E	K_0	$K_1^{(0)}$	$K_1^{(1)}$	$K_1^{(2)}$	K_2
14.2	0.5	18 MeV	32°,8	35°,6	— 3°,0	2°,1	0°,46
		32 MeV	28°,1	71°,5	— 4°,7	6°,9	1°,0
10.2	1.1	18 MeV	47°,0	20°,3	— 1°,0	3°,2	0°,35
		32 MeV	40°,9	46°,8	— 1°,4	6°,8	0°,86
4.76	5.8	18 MeV	52°,7	9°,0	1°,5	4°,0	0°,24
		32 MeV	46°,6	20°,6	2°,9	6°,8	0°,56
2.59	20	18 MeV	53°,0	6°,4	2°,4	4°,4	0°,19
		32 MeV	47°,2	11°,9	4°,7	6°,8	0°,45

2·2. *Influence du couplage* ${}^3P_2$-${}^3F_2$. – Nous nous sommes aperçus que le couplage de l'état ${}^3P_2$ et de l'état ${}^3F_2$ par la force tenseur ne changeait pas sensiblement les résultats à 32 MeV. Ces déphasages correspondant aux états ${}^3P_2$ et ${}^3F_2$ sont remplacés du fait du couplage par les déphasages $K_\alpha^{(2)}$ et $K_\gamma^{(2)}$ des deux solutions propres (9). Une solution propre est une superposition des deux états ayant le même comportement radial aux grandes distances. Les fonctions d'onde radiales obéissent aux équations:

$$\left\{\frac{\mathrm{d}^2}{\mathrm{d}r^2}+\frac{ME}{2}-\frac{2}{r^2}-M\left(V_c-\frac{4}{10}\,V_t\right)\right\}u_1=-\frac{12}{10}\sqrt{6}\,MV_t u_3\,,$$

$$\left\{\frac{\mathrm{d}^2}{\mathrm{d}r^2}+\frac{ME}{2}-\frac{12}{r^2}-M\left(V_c-\frac{8}{10}\,V_t\right)\right\}u_3=-\frac{12}{10}\sqrt{6}\,MV_t u_1\,,$$

dans lesquelles, puisqu'il s'agit d'étudier uniquement l'effet du couplage, nous avons négligé le potentiel de Coulomb petit devant les autres termes. Le calcul mené pour $\lambda = 5{,}8$ donne en l'absence de couplage $K_1^{(2)} = 8°{,}3$. L'introduction du couplage donne $K_\alpha^{(2)} = 8°{,}6$ (donc une modification négligeable), $K_\gamma^{(2)} = 0°{,}0$ et un coefficient du mélange ($\lim_{r\to\infty}(-u_3/u_1)$) de 0,049. La correction apportée à la section efficace (12) est de $0{,}8\times[(3\cos^2\theta-1)/2]$ millibarns/stéradian, donc très petite comme on pouvait s'y attendre.

(12) L'expression de la distribution angulaire tenant compte du couplage P-F donnée par S. A. KUSHNERIUK et M. A. PRESTON (*Proc. Phys. Soc.*, **64**, 8-A, 712) a été revisée par M. GOURDIN (communication privée).

3. – Corrections non adiabatiques au potentiels.

Le potentiel (1) provient de la réduction de l'interaction nucléon-nucléon calculée par la théorie du méson pseudoscalaire. Cette interaction possède en réalité une forme non locale, et est équivalente à un potentiel dépendant des vitesses ([13]). Par ailleurs, elle dépend de l'énergie du système; cette dépendance provient de ce que la méthode de calcul s'écarte de la théorie des perturbations et inclut des corrections non adiabatiques. On peut espérer tenir compte de ces corrections en remplaçant l'interaction non locale par un potentiel dépendant de l'énergie. Le domaine de validité de cette approximation n'est pas très clair aux petites distances mais nous escomptons obtenir, de cette manière, un ordre de grandeur des modifications apportées aux sections efficaces. Ce potentiel s'écrit

$$V = (\tau_1 \cdot \tau_2)\,\frac{G^2}{4\pi}\left(\frac{1}{2M}\right)^2 (\sigma_1 \cdot \nabla)(\sigma_2 \cdot \nabla)\,U_2 - 3\lambda\left(\frac{G^2}{4\pi}\right)^2 U_4 ,$$

où

$$U_2 = \frac{2}{\pi r}\int \frac{\sin(kr)k\,\mathrm{d}k}{\omega_k(\omega_k - \varepsilon)} \quad \text{avec} \quad \omega_k = \sqrt{k^2+1} ,$$

$$U_4 = \left(\frac{2}{\pi}\right)^2 \frac{1}{r^2}\int \frac{\sin(kr)\sin(k'r)k\;\mathrm{d}k\;k'\,\mathrm{d}k'}{\omega_k\omega_{k'}(\omega_k + \omega_{k'} - \varepsilon)} .$$

Ces deux intégrales sont développables en fonction de ε, énergie cinétique dans le système barycentrique: nous négligerons les termes d'ordre supérieur en ε, ce qui n'a pas beaucoup d'importance puisque nous cherchons seulement un ordre de grandeur

$$U_2 = \frac{e^{-\alpha r}}{r} + \varepsilon\left(\frac{2}{\pi}\right)k_0(r) + \frac{\varepsilon^3}{3}\,r\,\frac{2}{\pi}\,k_1(r) \quad \text{où} \quad \alpha = \sqrt{1-\varepsilon^2} ,$$

$$U_4 = \frac{2}{\pi}\,\frac{k_1(2r)}{r^2} + \varepsilon\left(\frac{2}{\pi}\right)^2\left[k_1^2(r) - k_0^2(r)\right] .$$

Dans la limite $\varepsilon = 0$ on retrouve le potentiel (1).

Tableau II.

E	K_0	$K_1^{(0)}$	$K_1^{(1)}$	$K_1^{(2)}$	K_2
18 MeV	52°,2	5°,75	1°,25	3°,8	0°,2
32 MeV	50°,4	11°,9	4°,7	6°,8	0°,5

([13]) J. A. Wheeler: *Phys. Rev.*, **50**, 643 (1936).

Les modifications apportées au potentiel étant importantes, nous avons été obligés, pour avoir un accord approché à 90° pour 18,3 et 32 MeV, de modifier les valeurs de λ et de $G^2/4\pi$. Nous avons tracé (fig. 2) les distributions angulaires calculées pour $\lambda = 20$, $G^2/4\pi = 2{,}55$ qui, malgré les déphasages assez différents (tableau II) sont très voisines de celles du § 2.

4. – Conclusion.

Nous voyons donc que l'accord assez satisfaisant obtenu pour les expériences aux faibles énergies est confirmé par le présent travail en ce qui concerne la diffusion à 18,3 MeV. Au contraire, à 32 MeV un accord satisfaisant avec l'expérience n'a pas pu être obtenu. La diffusion aux énergies intermédiaires fournit, en effet, un test beaucoup plus critique pour l'étude d'un potentiel. Il est très probable que le désaccord enregistré à 32 MeV provient surtout d'une simplification excessive de l'interaction aux courtes distances et que l'étude plus détaillée des termes non locaux serait profitable.

Les auteurs tiennent, en terminant, à exprimer leur reconnaissance pour l'hospitalité dont ils ont bénéficié au Laboratoire de l'École Normale Supérieure et à remercier Monsieur M. Lévy pour ses conseils qui leur ont été précieux et Monsieur M. Gourdin qui leur a communiqué ses travaux avant publication.

RIASSUNTO (*)

Lo scattering proton-proton è stato studiato alle energie intermedie col potenziale dedotto dalla teoria *PS-PS*. È stata esaminata la validità dell'approssimazione di Born negli stati *P* e *D*, e l'influenza dell'accoppiamento *P-F* e delle correzioni non perturbative apportate al potenziale. Dal confronto con l'esperienza risulta un buon accordo a 18,3 MeV, ma un netto disaccordo a 32 MeV.

(*) *Traduzione a cura della Redazione.*

Geomagnetic Effects of the μ Meson Component of Cosmic Radiation at Sea Level.

I. F. Quercia and B. Rispoli

Istituto di Fisica dell'Università - Roma
Istituto Nazionale di Fisica Nucleare - Sezione di Roma

(ricevuto il 22 Luglio 1954)

Summary. — In order to investigate processes of creation of mesons by primary radiation and the hypothetical presence of negative particles in the primary radiation, two experiments have been carried out at high latitude (Rome, 42°) and low latitude (Bombay, 9°): 1) « charge excess experiment »; 2) « absorption spectrum experiment » under water and in the open air. The East-West asymmetry, the latitude effect, the charge excess have been studied as a function of zenithal angle. Some of our conclusions are the following: *a*) the measured negative excess in the Eastern direction can be explained without introducing the hypothesis of negative primary particles; *b*) the energy dependence of the positive excess is not in contradiction with Heitler's theory; *c*) the latitude effect is about 15% in the vertical direction for mesons of energy greater than 0.5 GeV and seems to increase in the Eastern direction, and to decrease in the Western direction with increase of zenithal angle; *d*) the ratio between the energy of the created mesons and the energy of the protons is of the order of 0.2.

1. – Introduction.

In a previous paper [1] we have summarised the results of some experiments on positive and negative μ-mesons performed in the past years in different conditions. The experiments were designed in order to get some information about the processes of creation of mesons by primary radiation and in order to investigate the presence of negative particles in the primary cosmic radiation.

[1] I. F. Quercia and B. Rispoli: *Nuovo Cimento*, **10**, 1142 (1953).

We have found indeed that in the Eeastern direction the ratio ε between positive and negative particles in the primary cosmic radiation decreases rapidly with increasing zenithal angle and becomes less than unity at some angle which depends on latitude, altitude, and the energy of the recorded mesons; in Rome, at sea level, we have found that for mesons of energy greater than 0.5 GeV this angle is approximately 50° and similar results have been found by other authors [2].

The observed excess of negative particles at some Eastern direction has been explained according to our calculations [1,3], by taking into account the effect of Earth's magnetic field on meson trajectories through the atmosphere; however, as the question of primary negative particles is of the greatest interest, we have thought it worth while to complete our experiments with a new set of measurements at low latitude. On account of the quite different value of the Earth's magnetic field a different energy cut-off for primary radiation and a different curvature of the meson trajectories are expected at low latitude; hence the results of the experiments at low latitude permit us to test in different conditions the reliability of our theory.

In this paper we shall describe:

1) Experimental results of measurements performed in Bombay (India) at various zenithal and azimuthal directions, with the same apparatus described in [1] as the « second experiment ». This experiment will be indicated in the following as « charge excess experiment ».

2) Experimental results of an experiment (« absorption spectrum experiment ») designed in order to get information on the absorption spectrum under water of the penetrating component of cosmic radiation. Measurements have been carried out at lake Albano (near Rome), in Rome and in Bombay.

The results of the present research can be examined: *a*) from the geophysical point of view, *b*) from the nuclear point of view.

The zenithal and azimuthal distributions, the East-West asymmetry and the latitude effect have been measured as function of the zenithal angle and the results have been correlated with the geomagnetic energy cut-off of the primary component. Charge excess at various zenithal and azimuthal angles has been measured, and by comparison with theory some information about μ-meson creation processes and about the nature of the primary component can be obtained.

[2] G. Groetzinger and G. W. McClure: *Phys. Rev.*, **77**, 777 (1950).
[3] I. F. Quercia, B. Rispoli and S. Sciuti: *Nuovo Cimento*, **7**, 715 (1950).

2. – Charge Excess Experiment.

The apparatus shown in Fig. 1 has been described in some detail in (1) as the « second experiment ». The two iron blocks were magnetized by a stabilized direct current and during the running of the experiment the magnetic field intensity was 15 000 gauss. The counters of the sets A, B, C were all metallic, with brass wall of 1 mm thick, $2 \cdot 40$ cm² sensitive area; the counters of the set D had the same wall thickness, but a sensitive area of $4 \cdot 96$ cm² and worked all in parallel (4).

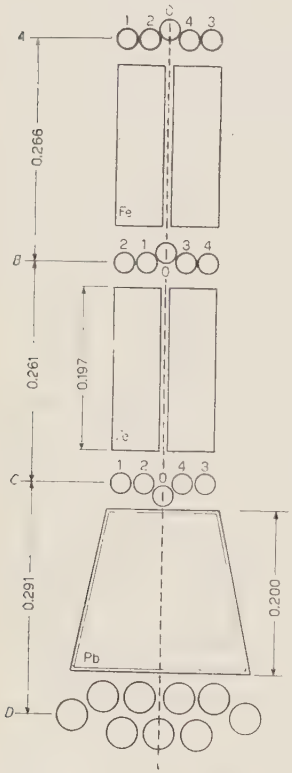

Fig. 1. - Experimental arrangement used for charge excess experiment (1st experiment).

Because of the magnetic field in the iron, the symmetrical telescopes 1 and 3 (i.e. 3-fold coincidences $(A_1B_1C_1)$, $(A_3B_3C_3)$ and the corresponding 4-fold) refer to particles of one sign, and telescopes 2 and 4 refer to particles of opposite sign. Counting rates per hour of 3-fold and 4-fold coincidences recorded with these telescopes will be indicated as $M_3^{\pm}$, $M_4^{\pm}$ according to the sign of the particles.

Pulses from the three central counters of each set (i.e. 0, 2, 4 for A and C, 0, 1, 3 for B) were mixed in order to obtain a « central » 3-fold coincidence $(A_{024}, B_{013}, C_{024})$ and a 4-fold coincidence $(A_{024}, B_{013}, C_{024}, D)$ whose counting rates per minute will be indicated by $N_3^{\pm}$, $N_4^{\pm}$. By means of anticoincidence circuits no counts were recorded in any channels when more than one counter in each set was triggered at the same time.

The frame supporting the iron blocks, lead absorber and counter telescopes can be tilted about a horizontal axis and rotated about a vertical axis. The direction of the main axis of the telescopes in the zenithal direction was measured with an inclinometer with an accuracy of about 0.5 degree.

Measurements have been taken in Bombay (India: geomagnetic latitude $\lambda_2 = 10^0$ North; longitude $\varphi_2 = 143^0\,30'$ East) in the open air, at zenithal

(4) Unfortunately during the running of the measurements in Bombay, some of the counters D were replaced by counters of smaller length; therefore the efficiency of 4-fold was reduced and we could not compare the 4-fold counting rates measured in Rome and in Bombay.

directions 0°, 45°, 60° to the vertical and in the azimuthal directions East, West and South. Zenithal and azimuthal directions and the direction of the magnetic field in iron blocks were frequently changed at random during the course of the measurements.

The meaning of the measured counting rates has been already discussed in § 4 of reference (1). Here we shall summarise the results of this discussion:

a) Counting rates $M_3^{\pm}$ and $M_4^{\pm}$ are mostly due to μ-mesons of the sign selected by the apparatus; spurious events are negligible.

b) Energy ranges of the recorded μ-mesons are: 0.5 ÷ 1.9 GeV for $M_3^{\pm}$ and 0.75 ÷ 1.9 GeV for $M_4^{\pm}$. The calculated mean energy is about 0.9 GeV in vertical direction, and not far from this value in other directions.

c) The « central » coincidences are due to particles of range greater than 314.4 g/cm² of iron + 4.5 g/cm² of brass + 266 g/cm² of lead for the fourfold $N_4^{\pm}$ coincidences.

d) « Central coincidences » are due to μ-mesons of energy greater than 0.5 GeV for 3-fold and greater than 0.75 GeV for 4-fold coincidences, and to an unknown contribution of other penetrating charged particles reaching sea level.

e) In the case of « central coincidences » the magnetic lenses cannot distinguish between particles of opposite charge, because particles of sufficiently high momentum can trigger the coincidence circuit independently of their charge in spite of the direction of the magnetic field inside the iron blocks. Therefore the ratios N^+/N cannot be taken as a measurement of the ratio of positive to negative particles. On the contrary however, particles stopped in the lead absorber, because of their low momentum, are completely identified by the magnetic field according to their charge; consequently the ratio $(N_3^+ - N_4^+)/(N_3^- - N_4^-)$ can be assumed to be the ratio of positive to negative particles in the energy range considered.

In Tables I, II, III are summarized the results for the « central coincidences » $N_3^{\pm}$, $N_4^{\pm}$ and their differences $N_3^{\pm} - N_4^{\pm}$ in Bombay.

Counting rates recorded in Bombay with 3-fold and 4-fold M-coincidences are given in Tables IV, V.

In these tables ε indicates the ratio between the counting rates recorded with magnetic lenses converging positive and negative particles. In the last column of the tables are indicated the average values $\frac{1}{2}[(+) + (-)]$ of the positive and negative counting rates. Statistical errors are indicated.

In Table IV are given the ratios between counting rates (average E-W) recorded

TABLE I. – 3-*fold* « *central coincidences* » *in Bombay.*

Zenith	Azimuth	N_3^+	N_3^-	ε	N_3
0°	—	5.41 ± 0.05	4.94 ± 0.04	1.10 ± 0.01	5.18 ± 0.03
45°	E	2.30 ± 0,03	2.35 ± 0.04	0.98 ± 0.02	2.32 ± 0.03
	W	2.87 ± 0.02	2.41 ± 0.02	1.19 ± 0.01	2.64 ± 0.01
	EW	2.59 ± 0.02	2.38 ± 0.02	1.09 ± 0.01	2.49 ± 0.01
	S	2.77 ± 0.02	2.54 ± 0.02	1.09 ± 0.01	2.65 ± 0.01
60°	E	1.033 ± 0.015	1.092 ± 0.013	0.94 ± 0.02	1.063 ± 0.010
	W	1.405 ± 0.013	1.198 ± 0.015	1.18 ± 0.02	1.302 ± 0.010
	EW	1.219 ± 0.010	1.145 ± 0.010	1.06 ± 0.01	1.182 ± 0.007
	S	1.177 ± 0.020	1.217 ± 0.013	0.97 ± 0.02	1.197 ± 0.011

TABLE II. – 4-*fold* « *central coincidences* » *in Bombay.*

Zenith	Azimuth	N_4^+	N_4^-	ε	N_4
0°	—	4.49 ± 0.04	4.14 ± 0.04	1.08 ± 0.01	4.32 ± 0.03
45°	E	1.99 ± 0.03	1.98 ± 0.04	1.01 ± 0.03	1.985 ± 0.025
	W	2.44 ± 0.02	2.12 ± 0.02	1.15 ± 0.01	2.28 ± 0.01
	EW	2.22 ± 0.02	2.05 ± 0.02	1.08 ± 0.01	2.14 ± 0.01
	S	2.43 ± 0.02	2.29 ± 0.02	1.06 ± 0.01	2.36 ± 0.01
60°	E	0.873 ± 0.013	0.933 ± 0.012	0.94 ± 0.01	0.903 ± 0.009
	W	1.108 ± 0.013	0.987 ± 0.013	1.12 ± 0.02	1.048 ± 0.009
	EW	0.991 ± 0.009	0.920 ± 0.009	1.07 ± 0.01	0.955 ± 0.006
	S	0.960 ± 0.019	0.992 ± 0.015	0.97 ± 0.02	0.976 ± 0.012

TABLE III. – *Differences between* 3-*fold and* 4-*fold* « *central coincidences* » *in Bombay.*

Zenith	Azimuth	$N_3^+ - N_4^+$	$N_3^- - N_4^-$	ε	$N_3 - N_4$
0°	—	0.933 ± 0.020	0.867 ± 0.017	1.08 ± 0.03	0.900 ± 0.013
45°	E	0.308 ± 0.011	0.368 ± 0.016	0.84 ± 0.05	0.388 ± 0.010
	W	0.430 ± 0.010	0.332 ± 0.010	1.30 ± 0.05	0.381 ± 0.007
	EW	0.369 ± 0.007	0.350 ± 0.008	1,05 ± 0.03	0.360 ± 0.005
	S	0.342 ± 0.080	0.322 ± 0.008	1,06 ± 0.04	0.333 ± 0.006
60°	E	0.166 ± 0.005	0.168 ± 0.005	0.98 ± 0.04	0.167 ± 0.004
	W	0.265 ± 0.007	0.208 ± 0.007	1.27 ± 0.05	0.237 ± 0.005
	EW	0.216 ± 0.004	0.188 ± 0.004	1.15 ± 0.03	0.202 ± 0.003
	S	0.213 ± 0.009	0.229 ± 0.009	0.93 ± 0.06	0.221 ± 0.006

TABLE IV. – M_3 *coincidences in Bombay.*

Zenith	Azimuth	M_3^+	M_3^-	ε	M_3
0°	—	6.09 ± 0.26	5.12 ± 0.24	1.19 ± 0.07	5.61 ± 0.16
45°	E	1.59 ± 0.11	1.99 ± 0.12	0.80 ± 0.07	1.79 ± 0.08
	W	2.80 ± 0.15	2.03 ± 0.12	1.38 ± 0.11	2.41 ± 0.19
	EW	2.20 ± 0.09	2.01 ± 0.08	1.09 ± 0.06	2.11 ± 0.06
	S	2.83 ± 0.17	2.43 ± 0.17	1.16 ± 0.08	2.63 ± 01.2
60°	E	0.41 ± 0.04	0.77 ± 0.06	0.53 ± 0.08	0.59 ± 0.03
	W	1.47 ± 0.08	0.64 ± 0.06	2.30 ± 0.25	1.09 ± 0.05
	EW	0.94 ± 0.04	0.71 ± 0.04	1.32 ± 0.09	0.83 ± 0.03
	S	0.79 ± 0.09	0.67 ± 0.09	1.18 ± 0.21	0.73 ± 0.06

TABLE V. – M_4 *Coincidences in Bombay.*

Zenith	Azimuth	M_4^+	M_4^-	ε	M_4
0°	—	3.65 ± 0.21	3.32 ± 0.20	1.10 ± 0.09	3.48 ± 0.15
45°	E	0.96 ± 0.08	1.35 ± 0.10	0.71 ± 0.08	1.15 ± 0.06
	W	1.91 ± 0.12	1.17 ± 0.09	1.63 ± 0.16	1.54 ± 0.08
	EW	1.84 ± 0.07	1.26 ± 0.07	1.46 ± 0.10	1.55 ± 0.05
	S	1.79 ± 0.13	1.62 ± 0.13	1.10 ± 0.09	1.70 ± 0.09
60°	E	0.26 ± 0.03	0.44 ± 0.04	0.59 ± 0.09	0.35 ± 0.02
	W	0.98 ± 0.07	0.39 ± 0.04	2.48 ± 0.31	0.69 ± 0.03
	EW	0.62 ± 0.03	0.42 ± 0.03	1.48 ± 0.13	0.52 ± 0.02
	S	0.62 ± 0.08	0.53 ± 0.08	1.17 ± 0.23	0.58 ± 0.06

TABLE VI. – *Ratios of counting rates for 3-fold coincidences* N_3 *and* M_3, *measured in Rome* (λ_1) *and in Bombay* (λ_2).

Zenith	$\frac{N_3^+(\lambda_1)}{N_3^+(\lambda_2)}$	$\frac{N_3^-(\lambda_1)}{N_3^-(\lambda_2)}$	$\frac{N_3(\lambda_1)}{N_3(\lambda_2)}$	$\frac{M_3^+(\lambda_1)}{M_3^+(\lambda_2)}$	$\frac{M_3^-(\lambda_1)}{M_3^-(\lambda_2)}$	$\frac{M_3(\lambda_1)}{M_3(\lambda_2)}$
0°	1.210 ± 0.014	1.190 ± 0.017	1.200 ± 0.010	1.61 ± 0.08	1.50 ± 0.08	1.56 ± 0.06
45°	1.216 ± 0.012	1.207 ± 0.013	1.209 ± 0.080	1.58 ± 0.08	1.45 ± 0.08	1.51 ± 0.06
60°	1.209 ± 0.013	1.179 ± 0.014	1.191 ± 0.011	1.50 ± 0.08	1.65 ± 0.01	1.56 ± 0.08

in Rome (geomagnetic latitude $\lambda_1 = 42^\circ$ North, longitude $\varphi_1 = 143^\circ\ 30'$ East) for 3-fold coincidences ([5]). Similar ratios for N_4, M_4 and $N_3 - N_4$, $M_3 - M_4$ have not been considered because of the low efficiency of set D in some measurements in Bombay ([4]).

3. – Absorption Spectrum Experiment.

A cross section of the apparatus used for the absorption spectrum measurements, is shown in Fig. 2. Coincidences between pulses of each three counters lying in a straight line are recorded; in this way we obtain 13 3-fold counter telescopes working simultaneously, each pointing in a direction shifted 10° with respect to the preceding one. When the central telescope points towards the zenith, zenithal distributions up to 60° are measured in steps of 10° in the two opposite azimuthal directions. All the counters were of the metallic type, wall thickness 1 mm brass, sensitive area $4 \cdot 40$ cm^2; the distance between the axis of extreme counters of each telescope was 57.2 cm. The product area $\times$ solid angle calculated for each telescope was 6.51 sterad cm^2, taking into account the counter's boundaries, and an integral zenithal distribution following the $\cos^2 \theta$ law.

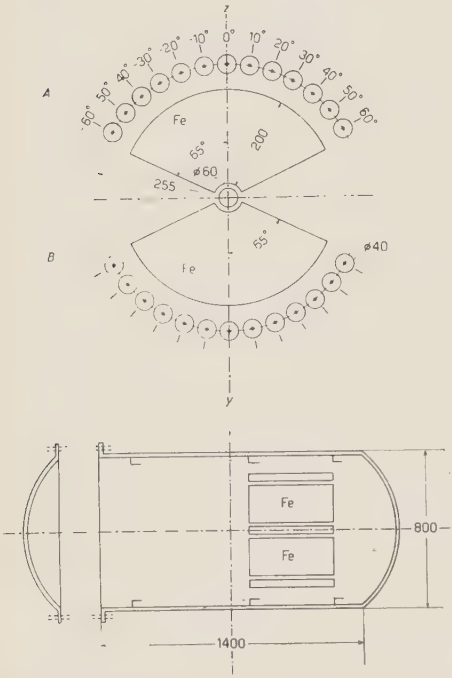

Fig. 2. Experimental arrangement used for absorption spectrum experiment (2nd experiment).

Measurements have been performed with and without the iron absorbers Σ between counters. As shown in Fig. 2 each absorber was 20 cm thick. The whole apparatus was contained in a cylindrical iron tank 8 mm thick.

The watertight tank was lowered under water by means of a crane supported by two small boats. Data collected by the telescopes were recorded

([5]) These ratios have been deduced from preceding tables and from Table III and VI of reference ([1]).

by an apparatus connected by a multiwire cable to the tank under water. The zenithal position of telescopes was continuously monitored by an electronic device with an accuracy of about 0.5 degree. The azimuthal position of the apparatus was indicated by a long alluminium pipe connected to the tank, with an accuracy of about 5 degrees.

Measurements have been performed in Rome under a thin roof and at lake Albano (near Rome; geomagnetic latitude $\lambda_1 = 42^\circ$, longitude $\varphi_1 = 93^\circ$, altitude 215 m above sea level) under 0, 10, 20 metres of water and in Bombay (India; geomagnetic latitude $\lambda_2 = 10^\circ$, longitude $\varphi_2 = 143^\circ\,30'$, sea level) in the open air.

In Table VII are summarized the experimental results obtained in Rome without absorbers Σ of iron. The total thickness of matter crossed by particles during these measurements was about 16.5 g/cm² of iron equivalent, i.e. for μ-mesons an energy cut-off of 48 MeV. I_E^0, I_W^0 represent the counting rates per minute in Eastern and Western directions and $I^0 = \frac{1}{2}(I_E^0 - I_W^0)$ the average values. Reported counting rates are the averages of the counting rates measured in each zenithal direction by different telescopes obtained by tilting the apparatus about a horizontal axis in steps of 10°. In the table statistical errors are indicated together with standard deviations (in brackets) in the cases where we got more than three different measurements.

By comparison of the counting rates obtained with different telescopes pointing in the same direction it was possible to draw the conclusion that differences between the solid angles subtended by the various telescopes never exceed $3 \pm 2\%$.

In Table VIII are summarized measurements performed at lake Albano at various depths with absorbers Σ (iron thickness 325 g/cm²). The energy cut-off under water at various zenithal angles is indicated in the table for μ-mesons. At 0 depth of water the energy cut-off for all channels is 530 MeV (6).

In Table IX are given the measurements taken in Bombay in the open air with and without absorbers Σ. Indicated errors are the bigger of statistical errors and standard deviations.

During the running of all the measurements, the apparatus has been rotated frequently around a vertical axis, so that reported counting rates observed in Eastern and Western directions are computed by averaging data collected by two symmetrical telescopes. In the telescopes the same counters have been used during measurements in Rome, lake Albano and Bombay.

Spurious events, like side showers, can be evaluated from counting rates at 90°. These counting rates measured without absorbers of iron in the open

(6) If the energy cut-off is calculated by taking into account inclined trajectories in the counters' plane the energy cut-off is 550 MeV.

TABLE VII. – *Experimental results obtained in Rome without absorbers Σ.*

Zenith	I^0_E	I^0_W	I^0
0°	3.76 ± 0.04 (0.07)	3.76 ± 0.04 (0.07)	3.76 ± 0.03 (0.05)
10°	3.51 ± 0.03 (0.09)	3.38 ± 0.03 (0.13)	3.45 ± 0.02 (0.08)
20°	3.13 ± 0.04 (0.06)	3.03 ± 0.03 (0.11)	3.08 ± 0.02 (0.06)
30°	2.58 ± 0.03 (0.03)	2.52 ± 0.03 (0.09)	2.55 ± 0.02 (0.05)
40°	1.94 ± 0.04 (0.22)	1.88 ± 0.04 (0.03)	1.91 ± 0.03 (0.11)
50°	1.34 ± 0.04 (—)	1.34 ± 0.03 (0.04)	1.34 ± 0.03 (0.17)
60°	0.84 ± 0.03 (—)	0.76 ± 0.03 (—)	0.80 ± 0.02 (—)
70°	0.33 ± 0.01 (0.04)	0.35 ± 0.01 (0.04)	0.342 ± 0.009 (0.02)
80°	0.15 ± 0.01 (—)	0.13 ± 0.01 (—)	0.140 ± 0.009 (—)
90°	0.050 ± 0.007 (—)	0.048 ± 0.008 (—)	0.049 ± 0.005 (—)

TABLE VIII. – *Measurements performed at Lake Albano with absorbers Σ.*

Thickness m of H_2O	Energy cut-off GeV	Zenith	I_E	I_W	I
0 m	0.53	0°	2.83 ± 0.02 (0.04)	2.83 ± 0.01 (0.04)	2.83 ± 0.01 (0.03)
	»	10°	2.79 ± 0.03 (0.11)	2.55 ± 0.02 (0.07)	2.67 ± 0.02 (0.06)
	»	20°	2.34 ± 0.02 (0.16)	2.47 ± 0.02 (0.06)	2.41 ± 0.01 (0.09)
	»	30°	2.10 ± 0.01 (0.09)	2.11 ± 0.01 (0.08)	2.105 ± 0.009 (0.06)
	»	40°	—	1.60 ± 0.01 (0.12)	—
	»	50°	1.15 ± 0.01 (0.08)	1.31 ± 0.01 (0.19)	1.230 ± 0.009 (0.10)
	»	60°	0.72 ± 0.01 (0.04)	0.74 ± 0.01 (0.03)	0.730 ± 0.007 (0.03)
10 m	2.6	0°	1.38 ± 0.02	1.38 ± 0.02	1.38 ± 0.01
	2.7	10°	1.35 ± 0.02	1.28 ± 0.05	1.32 ± 0.03
	2.8	20°	1.21 ± 0.01	1.23 ± 0.01	1.22 ± 0.009
	3.0	30°	1.07 ± 0.01	1.09 ± 0.02	1.08 ± 0.01
	3.4	40°	0.82 ± 0.01	0.96 ± 0.02	0.89 ± 0.01
	4.0	50°	0.60 ± 0.01	0.89 ± 0.04	0.74 ± 0.02
	5.0	60°	0.37 ± 0.01	0.39 ± 0.01	0.379 ± 0.009
20 m	5.0	0°	0.671 ± 0.035	0.671 ± 0.035	0.671 ± 0.025
	5.1	10°	0.675 ± 0.016	0.654 ± 0.010	0.665 ± 0.010
	5.3	20°	0.652 ± 0.008	0.653 ± 0.013	0.653 ± 0.008
	5.7	30°	0.583 ± 0.013	0.609 ± 0.043	0.596 ± 0.023
	6.5	40°	0.435 ± 0.012	0.475 ± 0.016	0.455 ± 0.010
	7.8	50°	0.308 ± 0.007	0.362 ± 0.010	0.335 ± 0.006
	10.5	60°	0.206 ± 0.006	0.199 ± 0.006	0.203 ± 0.004

air in Rome and in Bombay, do not exceed statistical errors; therefore it is reasonable to neglect these events for the measurements taken in the open air.

Absolute intensities can be obtained by dividing referred counting rates by the calculated solid angle which was found to be 6.51 sterad cm². These intensities under different thicknesses of water and given in Table X together with ROSSI's data (7), are the energy cut-off.

TABLE IX. – *Experimental results obtained in Bombay in the open air.*

Zenith	I_E^0	I_E	$I_E^0 - I_E$	I_W^0	I_W	$I_W^0 - I_W$	$I_E^{0'}$	$I_W^{0'}$
0°	3.26 ± 0.07	2.47 ± 0.02	0.79 ± 0.08	3.26 ± 0.07	2.47 ± 0102	0.79 ± 0.08	3.18 ± 0.02	3.18 ± 0.02
10°	3.26 ± 0.07	2.27 ± 0.02	0.68 ± 0.05	3.11 ± 0.04	2.38 ± 0.03	0.73 ± 0.05	2.98 ± 0102	3.13 ± 0.02
20°	2.62 ± 0.03	2.06 ± 0.02	0.56 ± 0.04	2.92 ± 0.04	—	—	2.60 ± 0.02	2.61 ± 0.04
30°	2.18 ± 0.02	1.73 ± 0.02	0.46 ± 0.03	2.51 ± 0.02	2.03 ± 0.02	0.48 ± 0.03	2.60 ± 0.02	2.61 ± 0.04
40°	1.66 ± 0.02	1.33 ± 0.01	0.33 ± 0.02	1.96 ± 0.04	1.63 ± 0.02	0.33 ± 0.04	2.16 ± 0.02	2.50 ± 0.02
50°	1.02 ± 0.03	0.92 ± 0.01	0.10 ± 0.03	1.23 ± 0.03	0.84 ± 0.02	0.39 ± 0.04	1.62 ± 0.02	1.97 ± 0.05
60°	0.70 ± 0.01	0.57 ± 0.01	0.13 ± 0.02	0.82 ± 0.01	0.75 ± 0.01	0.07 ± 0.02	0.68 ± 0.01	0.82 ± 0.03
70°	—	—	—	—	—	—	0.337 ± 0.006	0.47 ± 0.03
80°	—	—	—	—	—	—	0.119 ± 0.005	0.12 ± 0.01
90°	—	—	—	—	—	—	0.045 ± 0.004	0.039 ± 0.007

I, I^0 indicate respectively the counting rates obtained with and without the absorbers, $I^0 - I$ their difference; $I^{0'}$ the counting rates obtained by tilting the apparatus about a horizontal axis and averaging counting rates of various telescopes pointing in the same direction.

TABLE X. – *Absolute intensity as function of water thickness.*

H_2O Thickness in meters	0	10	20
Energy cut-off for μ-mesons GeV	0.55	2.65	5.00
Absolute intensity (present work) $10^3 \cdot cm^{-2}$ sterad^{-1} s^{-1}	7.25 ± 0.01	3.53 ± 0.05	1.72 ± 0.09
Rossi's data in the same units	7.25	3.50	1.80

The integral spectrum given by ROSSI is shown in Fig. 3; in the same figure are shown experimental points caiculated from measurements of EHMERT (8), and WILSON (9) and experimental results of the present work which are in fairly good agreement with preceding ones. It should be noted that for computing the air thickness equivalent to a given thickness of water, we have used WICK's nomograms (10) and for calculating the air equivalent of a given

(7) B. ROSSI: *Rev. Mod. Phys.*, **20**, 537 (1948).
(8) A. EHMERT: *Zeits. f. Phys.*, **106**, 751 (1937).
(9) V. C. WILSON: *Phys. Rev.*, **53**, 337 (1938).
(10) G. C. WICK: *Nuovo Cimento*, **1**, 310 (1943).

thickness of rock (used as absorbers in Wilson's experiment), we have use data calculated by MANDÒ. ([11]).

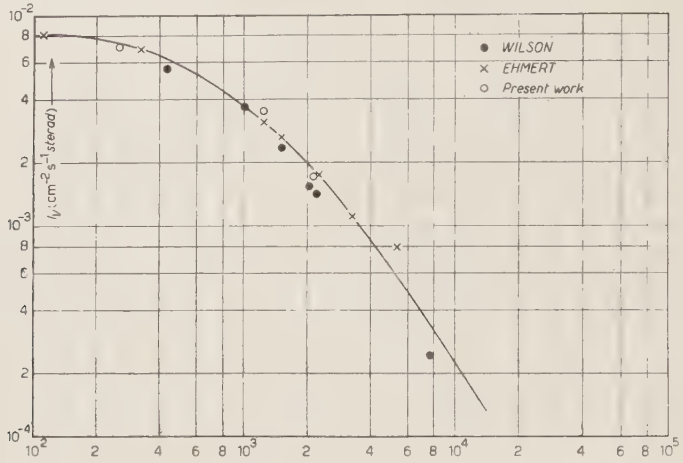

Fig. 3. – Integral spectrum of the penetrating component at sea level.

4. – Theoretical Zenithal and Azimuthal Distributions.

In a previous paper (3) we have calculated the differential μ-meson spectrum as a function of the altitude z of observation and zenithal direction θ and found it to be for positive and negative μ-mesons:

$$n^{\pm}(E, \theta, z)\,\mathrm{d}E = \left[\varphi_\alpha(E, \theta, z) \pm \frac{\nu}{2}\,\varphi_\beta(E, \theta, z)\right]\mathrm{d}E\,, \tag{1}$$

where

$$\varphi = \frac{1}{\varrho}\left[\left(\frac{E}{\varrho x_0 W}\right)^{b/W} \cdot W^{-\gamma} \cdot \Gamma\left(1 + \frac{b}{W}\right)\right]; \qquad (\varrho = \alpha, \beta)\,.$$

E is the meson kinetic energy at the top of the apparatus,

W the energy which a meson would have at the top of the atmosphere; therefore if j is the energy loss per g/cm² of air, X the thickness of the atmosphere in g/cm², h the thickness of homogeneous atmosphere and z the altitude in the same units as h, W can be written as:

$$W = E + jX \sec\theta \cdot \exp\left[-z/h\right],$$

α [1] is the absorption path of the nucleonic component through the atmosphere (it has been assumed equal to 125 g/cm²),

([11]) M. MANDÒ: *Nuovo Cimento*, **9**, 522 (1952).

β^{-1} is the collision path of nucleonic component through the atmosphere (it has been assumed equal to 60 g/cm²),

x_0 is the thickness of air (in g/cm²) crossed by a meson coming from the generation layer,

$b = (\mu c^2 h/\tau_0 c) \sec\theta = 1.24 \sec\theta$ where μ_0 and τ_0 are the mass and the mean life at rest of the μ-meson,

γ is the assumed exponent of the power spectrum of primary radiation (it has been assumed constant and equal to 2.2),

ν is a parameter whose meaning will be seen in the following.

For calculating this spectrum we have used CALDIROLA's [12] theory which assumes the following hypothesis:

1) The primary radiation is protonic.

2) The differential energy spectrum of primary protons is assumed to be a power law with a constant exponent γ.

3) According to Heitler's theory, plural production of mesons is assumed; i.e. in each collision between nucleons a single meson is created according to the following picture:

$$\begin{array}{ll} 1) & \\ 2) & \mathrm{P} + \mathrm{P} = \begin{cases} \mathrm{P} + \mathrm{P} + \pi^0 \\ \mathrm{P} + \mathrm{N} + \pi^+ \end{cases} \\ 3) & \\ 4) & \mathrm{N} + \mathrm{N} = \begin{cases} \mathrm{N} + \mathrm{N} + \pi^0 \\ \mathrm{P} + \mathrm{N} + \pi^- \end{cases} \\ 5) & \\ 6) & \mathrm{N} + \mathrm{P} = \begin{cases} \mathrm{P} + \mathrm{N} + \pi^0 \\ \mathrm{P} + \mathrm{P} + \pi^- \end{cases} \\ 7) & \mathrm{P} + \mathrm{N} = \mathrm{N} + \mathrm{N} + \pi^+ . \end{array}$$

4) The probabilities $u_1, u_2, \ldots, u_7$ of the processes are independent of energy.

5) According to the symmetrical theory of nuclear forces, we have assumed that $u_2 = u_4$ and $u_6 = u_7$. Furthermore the comparison between theory and experimental results indicates that a satisfactory agreement is obtained by assuming:

$$u_1 = u_2 = u_3 = u_4 = \tfrac{1}{2}$$

$$u_5 = u_6 = u_7 = \tfrac{1}{3}$$

[12] P. CALDIROLA: *Nuovo Cimento*, **6**, 565 (1949).

and consequently the parameter ν is found to be:

$$\nu = \frac{2u_2}{u_2 + u_7} = \frac{6}{7} = 0{,}86 \ .$$

6) The fractional energy f transferred from protons to the created mesons is independent of the energy $\mathcal{E}$ of the proton; therefore if W indicates the energy (at creation) of a meson generated by a proton of energy $\mathcal{E}$, we can write:

$$f = \frac{W}{\mathcal{E}} = \text{const} \ . \tag{2}$$

7) The East-West effect on primary radiation, as well as the curvature of the mesons trajectories in the Earth's magnetic field are neglected.

This last effect is quite negligible in the North-South plane but it becomes important in the East-West plane, as shown by our experimental results. Trajectories of positive mesons coming from East (and negative from West) are indeed curved in such a way as to be longer than trajectories of mesons having opposite charge. This effect has been investigated by putting in the formulas instead of the zenithal angle θ, an angle

$$\theta_> = \theta + \Delta$$

for positive mesons coming from East (and negative from West) and an angle

$$\theta_< = \theta - \Delta$$

for negative mesons coming from East (and positive from West), Δ being the angle of deviation of the meson trajectories due to the horizontal component of the Earth's magnetic field. Δ is a function of the meson energy of the direction of observation θ, of the latitude λ and altitude z where the mesons are observed; if it is assumed that all mesons are generated under 100 g/cm^2 of atmosphere Δ is equal to

$$\Delta(E, \theta, \lambda, z) = \frac{\Lambda(\lambda)}{W \cos\theta} \ln \left(\frac{x_0 \cos\theta}{100} \frac{W}{E} \right) ,$$

where $\Lambda(\lambda)$ is a constant which contains the value of the Earth's magnetic field at the latitude λ, W the energy at creation level, E the energy of mesons at observation level.

Hereafter an index $>$ or $<$ will indicate that an angle $\theta_>$ or $\theta_<$ has been considered instead of θ. If we call $e_0^{\pm}(E, z, \theta, \lambda)$, $w_0^{\pm}(E, z, \theta, \lambda)$ the differential spectra of positive and negative mesons coming from East and West (the index $_0$ will denote that the effect of the energy cut-off of the primary radiation has

been neglected, and $e_0(E, z, \theta, \lambda)$, $w_0(E, z, \theta, \lambda)$ the total meson spectrum, i.e.

$$e_0 = \tfrac{1}{2}(e_0^+ + e_0^-) , \qquad w_0 = \tfrac{1}{2}(w_0^+ + w_0^-) ;$$

from equation (1) and the preceding discussion, we get the following expressions:

$$e_0^+ (E, z, \theta, \lambda) = \varphi_{\alpha>} + \frac{\nu}{2}\varphi_{\beta>} ,$$

$$e_0^- (E, z, \lambda, \theta) = \varphi_{\alpha<} - \frac{\nu}{2}\varphi_{\beta<} ,$$

$$w_0^+(E, z, \theta, \lambda) = \varphi_{\alpha<} + \frac{\nu}{2}\varphi_{\beta<} ,$$

$$w_0^-(E, z, \theta, \lambda) = \varphi_{\alpha>} - \frac{\nu}{2}\varphi_{\beta>} .$$

$$e_0 (E, z, \theta, \lambda) = \Phi_\alpha \left(1 - \frac{1}{2} A_0\right) ,$$

$$w_0 (E, z, \theta, \lambda) = \Phi_\alpha \left(1 + \frac{1}{2} A_0\right) ,$$

where Φ_α is given by:

$$\Phi_\alpha = \tfrac{1}{2}(\varphi_{\alpha>} + \varphi_{\alpha<})$$

and

$$A_0 = \frac{\nu}{2}\frac{\varphi_{\beta>} - \varphi_{\beta<}}{\Phi_\alpha} = 2\,\frac{w_0 - e_0}{w_0 + e_0} \tag{3}$$

represent the asymmetry due to the curvature of the meson trajectories through the atmosphere: this function has been calculated for the Bombay latitude and plotted in Fig. 4.

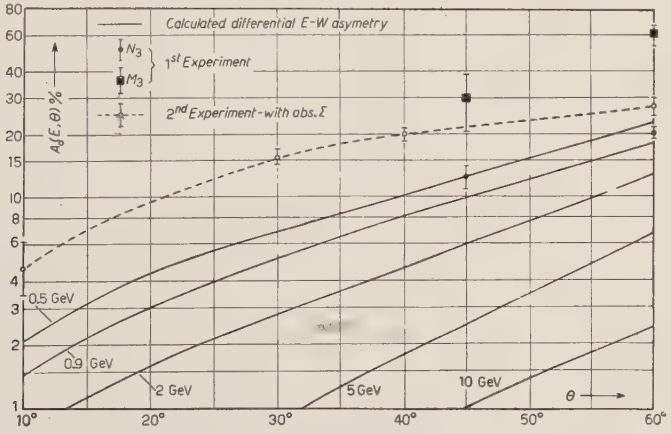

Fig. 4. – Asymmetry $A_0(E, \theta)$ at Bombay latitude.

5. – East-West Asymmetry.

In the same Fig. 4 in which is plotted the function A_0 defined by (3), we have plotted the experimental results of the asymmetry defined by the expression:

$$A_{exp} = 2 \frac{I_W - I_E}{I_W + I_E}$$

obtained from the N_3 and M_3 counting rates of the « charge excess experiment » and from the I counting rates of the « absorption spectrum experiment » at 0 depth with the absorbers Σ. N_3 and I both refer to mesons of energy greater than 0.5 GeV, while M_3 refers to mesons having average energy of about 0.9 GeV. A_{exp} for both experiments as well as the calculated integral of the function A_0 are given in Table XI.

TABLE XI.

Zenith	Calculated integral asymmetry	Charge excess experiment					Absorpt. spectrum experiment	
		N_3	N_4	$(N_3 - N_4)$	M_3	M_4	With absorbers	Without absorbers
Energy (GeV)	$\geqslant 0.5$	$\geqslant 0.5$	$\geqslant 0.75$	$0.5 \div 0.75$	$0.5 \div 1.9$	$0.75 \div 1.9$	$\geqslant 0.5$	$\geqslant 0.05$
10°	0.6	—	—	—	—	—	4.7 ± 1.5	5.4 ± 2.0
20°	1.1	—	—	—	—	—	—	10.9 ± 1.7
30°	1.8	—	—	—	—	—	10.0 ± 1.2	13.7 ± 1.3
40°	2.9	—	—	—	—	—	20.1 ± 1.6	16.3 ± 2.6
45°	3.5	12.7 ± 1.5	13.2 ± 1.0	12.2 ± 3.6	29.8 ± 9.2	28.7 ± 7.3	—	–
50°	4.1	—	—	—	—	—	—	18.9 ± 4.0
60°	6.7	20.3 ± 1.3	14.8 ± 0.9	34.5 ± 3.5	59.5 ± 6.0	61.5 ± 9.9	27.7 ± 2.5	15.7 ± 2.4

The experimental results lead to the following conclusions:

1) The E-W asymmetry increases with increasing zenithal angle;

2) The effect is greater in differential channels than in integral ones;

3) In the « absorption spectrum experiment » higher values of the effect are obtained when absorbers Σ are included;

4) A discrepancy has been found between the effects deduced from M counting rates and $N_3 - N_4$ counting rates.

5) The experimental values A_{exp} are higher than the asymmetry A_0 calculated by disregarding the primary asymmetry.

The effects 1), 2) were expected and quite obvious.

The effect 3) is understood by taking into account that, because of the incoherent scattering suffered during the crossing of the atmosphere, a very low asymmetry must be expected for slow particles which are stopped in the absorbers Σ.

On the contrary the effect 4) was unexpected and we cannot explain it. As a matter of fact counting rates M and $N_3 - N_4$ refer to different events: *a*) counting rates M are due to μ-mesons (or particles of similar mass) whose energy lies in the indicated range, heavier particles being excluded because, on account of the high momentum required for crossing the apparatus, they are not appreciably deviated by magnetic field; *b*) counting rates $N_3 - N_4$ are instead due to all particles crossing the magnetized iron blocks and stopped in the lead absorber. However, if, according to the usual picture of cosmic rays at sea level, it is assumed that about 90% of particles recorded by N_3-N_4 are μ-mesons (the rest being probably protons), the E-W asymmetry measured in this channel should not be different from the asymmetry measured by M-coincidences. However, on account of the low efficiency of set D (4) we do not believe it worth while to consider this discrepancy.

The effect 5) is to be expected because of the asymmetry due to the low energy cut-off of the primary radiation. We shall consider it reasonable to assume that the measured asymmetry is the sum of the asymmetry A_0 due to the curvature of the meson trajectories in the atmosphere and the asymmetry due to the low energy cut-off of the primary radiation. Consequently if A_P indicates the primary asymmetry we should have:

$$A_P = A_{exp} - A_0 .$$

This comparison has been done between the experimental asymmetry measured by N_3 counting rates, i.e. for mesons of energy greater than 0.5 GeV and the integrated values of the function $A_0(E, \theta)$ which are given in Table XI, and $A_P(\theta)$ has been found to be 9.2% at 45° and 13.6% at 60°. It must be observed that these values refer to the asymmetry of all protons whose energy is greater than the energy $\mathcal{E}^*(\theta)$ required for generating mesons which can cross the atmosphere and reach the apparatus with a given zenithal angle

and an energy greater than 0.5 GeV. The energy $\mathcal{E}^*(\theta)$ can be calculated for $\theta = 45^\circ$ and $\theta = 60^\circ$ according to the following argument.

If a primary asymmetry A_p has been found, it means that the energy cut-off $\mathcal{E}_E(\theta)$ in a given zenithal Eastern direction due to the Earth's magnetic field acting on primary protons, is bigger than the above defined cut-off $\mathcal{E}^*(\theta)$. Therefore, as the ratios I_W/I_E between counting rates for a given zenithal angle in Western and Eastern directions are respectively 1.10 at 45° and 1.14 at 60°, we have forced to admit that $\mathcal{E}_E > \mathcal{E}^*$ for $\theta \geqslant 45^\circ$. On the other hand, if we suppose that $\mathcal{E}^* > \mathcal{E}_W$ as a consequence of our assumptions (above specified in § 4) the integral ratio $a = I_W/I_E$ should be given by:

$$a(\theta) = \left[\frac{\mathcal{E}^*(\theta)}{\mathcal{E}_E(\theta)}\right]^{1-\gamma}.$$

Now, the cut-off energies are known having been calculated by LEMAITRE, VALLARTA and recently resumed by ALPHER [13]; therefore the knowledge of the ratio a and the energy cut-off in the Eastern direction (23 GeV for $\theta = 45^\circ$ and 28 for $\theta = 60^\circ$) leads to the knowledge of $\mathcal{E}^*$ which is found to be 21.8 for $\theta = 45^\circ$ and 25.1 GeV for $\theta = 60^\circ$ [14].

This result can be easily used for calculating the fractional energy f (defined by (2)) transferred from protons to created mesons; by calculating the minimum energy W required for a meson at creation in order to reach our apparatus (at sea level) with an energy greater than 0.5 GeV with a given zenithal direction, the ratio $f = W/\mathcal{E}^*$ comes to be 15% and 16% in the two cases investigated. This result shows that f can be considered independent of energy and this can be taken as an « a posteriori » justification of the hypothesis assumed in the calculations.

6. – Zenithal Distributions.

In Fig. 5 are given the zenithal distributions obtained at Lake Albano at various depths, and the theoretical zenithal distributions calculated by integrating expressions (1). The agreement can be considered satisfactory for 0 m and 10 m water, but at large angles and under 20 m of water the theory seems to be inadequate; however in these conditions the unknown contribution of showers cannot be considered negligible.

---

[13] R. A. ALPHER: *Journ. Geophys.*, **55**, 347 (1950).

[14] These calculations have been performed by assuming, as above indicated, the exponent of the primary radiation equal to 2.2.

Zenithal distributions obtained in Rome and Bombay with and without absorber Σ are given in Figg. 6 and 7. No appreciable E-W asymmetry has been found at high latitude; therefore the curves plotted in Figg. 6 and 7

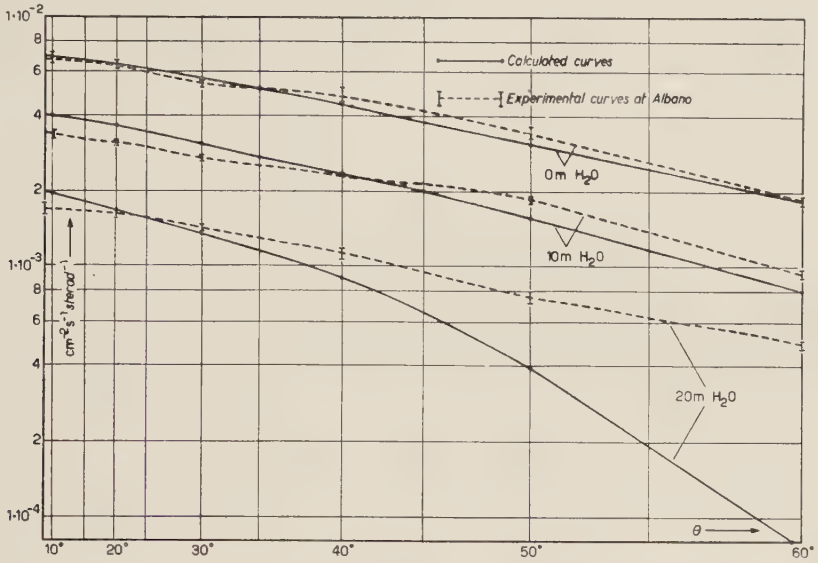

Fig. 5. – Theoretical and experimental distributions obtained at Lake Albano at various depths.

represent the average intensity $I = \frac{1}{2}(I_E + I_W)$. On the contrary measurements performed in Bombay show an East-West asymmetry which depends on zenithal angle. Moreover the comparison between Rome and Bombay

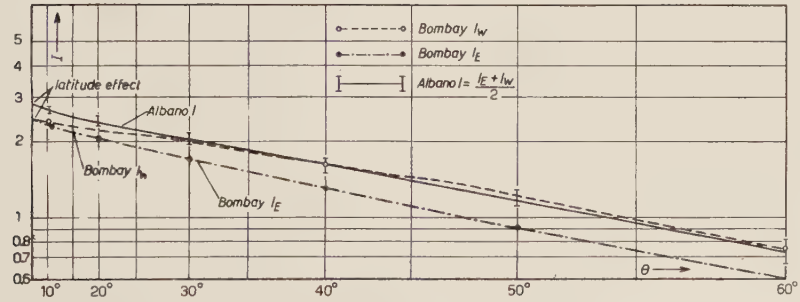

Fig. 6. – Zenithal distributions obtained in Rome and Bombay with absorber.

data shows a latitude effect of about 15% in the vertical direction decreasing towards the west, and becoming negligible at about 30° West. It must be emphasized that *absolute* counting rates measured in the Western direction

in Bombay are in very good agreement with the absolute counting rates averaged in the E-W plane measured in Rome.

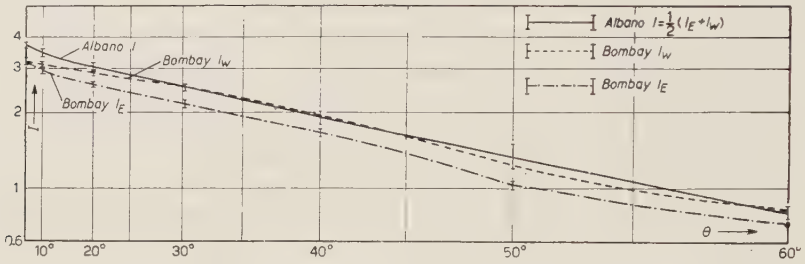

Fig. 7. – Zenithal distributions obtained in Rome and Bombay without absorber.

The zenithal distributions in Rome and Lake Albano follow approximately the law:

$$I(\theta) = I_0 \cos^2 \theta \,. \tag{4}$$

On the contrary the zenithal distribution in the eastern direction at Bombay does not follow this law, because of the energy cut-off of the primary radiation.

In Table XII are given the ratios of the intensities recorded by the « charge excess experiment » at 45° and 60°, to the intensities measured in the vertical

TABLE XII. – *Relative intensities measured in Rome and in Bombay by the « charge excess experiment ».*

Zenith	Azimuth	Latitude	Energy GeV				
			$\geqslant 0.53$	$\geqslant 0.75$	$0.53 \div 0.75$	$0.53 \div 1.9$	$0.75 \div 1.9$
45°	S	Rome	0.522 ± 0.004	—	—	0.375 ± 0.012	0.352 ± 0.013
		Bombay	0.511 ± 0.003	0.546 ± 0.004	0.370 ± 0.008	0.469 ± 0.025	0.189 ± 0.032
	EW	Rome	0.484 ± 0.004	0.505 ± 0.003	0.350 ± 0.008	0.365 ± 0.012	0.377 ± 0.017
		Bombay	0.481 ± 0.003	0.495 ± 0.004	0.400 ± 0.008	0.376 ± 0.001	0.445 ± 0.024
60°	S	Bombay	0.231 ± 0.003	0.226 ± 0.003	0.246 ± 0.008	0.130 ± 0.011	0.167 ± 0.009
	EW	Rome	0.227 ± 0.002	0.241 ± 0.002	0.133 ± 0.003	0.148 ± 0.006	0.166 ± 0.008
		Bombay	0.228 ± 0.002	0.221 ± 0.002	0.224 ± 0.004	0.148 ± 0.007	0.149 ± 0.017

The figures indicated in the table are the ratios $I(\theta)/I(0)$. EW indicates the averaged values in the East-West plane, and S in Southern direction. All values refer to the total component (positive+negative μ-mesons).

direction in Bombay, and in Rome. The comparison between the Rome and Bombay data shows a very good agreement for N_3 and M_3 coincidences, but for 4-fold coincidences we find a discrepancy probably due to the low efficiency of the set D of counters (4). As was pointed out in reference (1), the zenithal distribution of M component does not follow the equation (4) because of the rapidly decreasing intensity at small angles.

7. – Charge Excess.

In Fig. 8 are plotted against zenithal angle in the East-West plane the counting rates $M_3^{\pm}$ of positive and negative mesons. By comparing this distribution with the distribution obtained with the same apparatus in Rome and given in Fig. 7 of reference (1), one observes that positive counting rates become equal to negative counting rates (i.e. $\varepsilon = 1$) at an angle $\theta \sim 30°$ whereas in Rome we

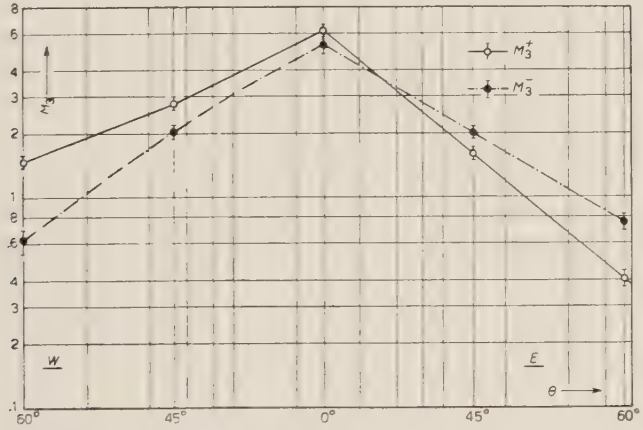

Fig. 8. – Zenithal distribution in E-W plane of positive and negative μ-mesons (mean energy 0.9 GeV).

have found $\theta \sim 50°$. We expected to find this effect because the horizontal component of the Earth's magnetic field increases with decreasing latitude and consequently the bending of the mesons trajectories is bigger at low latitudes.

As Fig. 8 shows, the positive to negative ratio ε is a function of zenith and azimuth angle on account of the curvature of the meson trajectories in the atmosphere; therefore the ratio ε at a given zenith and azimuth depends on the positive to negative ratio at creation, but it is also affected by the differences introduced on the positive and negative intensities by the different

energy loss and decay probability along asimmetrycal trjectories. Consequently in order to get some information about the positive excess unaffected (in first approximation) by the curvature of the trajectories, we will compare the intensities of positive and negative mesons which have travelled through the atmosphere along symmetrical trajectories.

If A is the total East-West asymmetry due both to the energy cut-off of the primaries and to the curvature of trajectories, the differential meson spectra $w^{\pm}$, $e^{\pm}$ in the Western and Eastern directions can be approximately written

$$w^{\pm}(E, \theta) \cong s^{\pm}(E, \theta)[1 + \tfrac{1}{2}A(E, \theta)]$$

$$e^{\pm}(E, \theta) \cong s^{\pm}(E, \theta)[1 - \tfrac{1}{2}A(E, \theta)],$$

where $s^{\pm}(E, \theta)$ indicates the differential spectra of positive and negative mesons in the Southern direction given by expression (1); hence the ratios w^{+}/e^{-}, e^{+}/w^{-} become

$$(5) \qquad \begin{cases} \dfrac{w^{+}(E, \theta)}{e^{-}(E, \theta)} = \eta(E, \theta) \cdot a(E, \theta)\,, \\ \dfrac{e^{+}(E, \theta)}{w^{-}(E, \theta)} = \dfrac{\eta(E, \theta)}{a(E, \theta)} \end{cases}$$

where

$$a(E, \theta) = \frac{1 + \frac{1}{2}A(E, \theta)}{1 - \frac{1}{2}A(E, \theta)}$$

and

$$\eta = \frac{s^{+}(E, \theta)}{s^{-}(E, \theta)}$$

represents the theoretical positive to negative ratio in the Southern direction and hence unaffected by geomagnetic effects. From equation (1) η can be easily derived and found to be:

$$\eta = \frac{1 + \frac{\nu}{2}\frac{\varphi_\beta}{\varphi_\alpha}}{1 - \frac{\nu}{2}\frac{\varphi_\beta}{\varphi_\alpha}} = \frac{1 + \frac{\nu}{2}\left(\frac{\alpha}{\beta}\right)^{1+b/W}}{1 - \frac{\nu}{2}\left(\frac{\alpha}{\beta}\right)^{1+b/W}}.$$

In addition we would like to observe that the ratios w^{+}/e^{-}, e^{+}/w^{-} represent respectively the positive to negative ratios measured in directions $\theta_{<}$, $\theta_{>}$; therefore they will indicated as $\varepsilon_{<}$, $\varepsilon_{>}$. The experimental values of $\varepsilon_{<}$, $\varepsilon_{>}$ together with the positive to negative ratio $\varepsilon_{\leq}$ measured in the Southern di-

rection, and theoretical value of the function η calculated for the mean energy 0.9 GeV of the recorded mesons, are given in Table XIII; the figures in brackets

TABLE XIII. – *Experimental values ε and calculated values η of the positive to negative ratio.*

Zenith	M_3 Coincidences			M_4 Coincidences			η
	$\varepsilon_< = M_W^+/M_E^-$	$\varepsilon_> = M_E^+/M_W^-$	$\varepsilon_S = M_S^+/M_S^-$	$\varepsilon_<$	$\varepsilon_>$	ε_S	
0°	—	—	1.19±0.07 (1.24)	—	—	1.10±0.08 (1.18)	1.35
45°	1.40±0.10 (1.51)	0.79±0.08 (0.73)	1.12±0.08 (1.20)	1.41±0.15 (1.60)	0.82±0.09 0(.58)	1.10±0.09 (1.14)	1.34
60°	1.90±0.20 (2.14)	0.64±0.10 (.053)	1.18±0.21 (1.23)	2.23±0.28 (2.85)	0.67±0.12 (0.46)	1.17±0.23 (1.24)	1.33

represent the ratios obtained from experimental data corrected for knock-on electron contribution. In reference (1) it was indeed pointed out that μ-mesons of energy greater than 1.9 GeV which are weakly deflected by the magnetic field, can give a spurious M coincidence on account of a secondary knock-on electron; assuming a $\cos^2\theta$ law for the zenithal distribution of μ-mesons the contribution given to M_3 coincidences by these events has been calculated and given in Table X of reference (1); but if a $\cos^3\theta$ law is assumed, as suggested by experimental results, this contribution is found to be 1.20 counts per hour in the vertical direction, 0.42 at 45° and 0.15 at 60°.

Let us observe now that, as equations (5) show, η is the geometrical mean between the ratios $\varepsilon_< = w^+/e^-$ and $\varepsilon_> = e^+/w^-$; consequently the asymmetry $a(E, \theta)$ should be calculable from:

$$a = \frac{\varepsilon_<}{\eta} = \frac{\eta}{\varepsilon_>} .$$

In Table XIV are given the experimental ratios $\varepsilon_</\varepsilon_S$, $\varepsilon_S/\varepsilon_>$, which, according to the preceding argument should be both equal to a; by averaging all 4 experi-

TABLE XIV. – *Asymmetry deduced from experimental ratios* $\varepsilon_</\varepsilon_S$; $\varepsilon_S/\varepsilon_>$.

Zenith	M_3 Coincidences		M_4 Coincidences		a ($\bar{E} \cong 0.9$)	100 A ($\bar{E} \cong 0.9$)
	$\varepsilon_</\varepsilon_S$	$\varepsilon_S/\varepsilon_>$	$\varepsilon_</\varepsilon_S$	$\varepsilon_S/\varepsilon_>$		
45°	1.25±0.13	1.42±0.17	1.28±0.17	1.34±0.18	1.32±0.04	27.7±6.1
60°	1.61±0.34	1.84±0.44	1.91±0.44	1.74±0.38	1.77±0.07	55.5±3.5

mental values obtained, we have calculated the values of the functions a, A which are indicated in the last columns.

From data collected in this experiment in Bombay, the following conclusions can be drawn:

1) the positive to negative ratio, according to our theory, was expected to be greater than the measured values;

2) the measured negative excess in the Eastern direction can be explained without introducing the hypothesis of negative primary particles;

3) on account of statistical errors no definite conclusion can be deduced from experimental data about the energy and zenithal dependence of the positive excess; however our data cannot be considered in disagreement with the theory, which is deduced from HEITLER's assumptions, notwithstanding the discrepancy pointed out in 1);

4) by subtracting the asymmetry A_0 defined by equation (3) from experimental values A given by table XIV, we have deduced that the asymmetry A_p of primary protons responsible of the recorded mesons is about 17% for $\theta = 45^\circ$ and 37% for $\theta = 60^\circ$. These values are not in contradiction with the values 9°_0 and 14°_0 given in § 5 because these last data refer to protons responsible for mesons which reach the apparatus with an energy greater than 0.5 GeV while preceding ones refer to mesons whose energy lies between 0.5 and 1.9 GeV (mean energy 0.9 GeV).

8. – Latitude Effect.

As is well known, the intensity of cosmic radiation depends on the latitude and longitude of the observation station. The longitude effect being very small, will be neglected in the following discussion; the latitude effect is correlated with the geomagnetic latitude ([15]) as was first shown by COMPTON ([16]) and measured by MILLIKAN and NEHER ([17]).

Usually the latitude effect measured between two stations of latitude λ_1, λ_2 with $\lambda_1 > \lambda_2$, is defined by

$$\varepsilon = \frac{I(\lambda_2) - I(\lambda_1)}{I(\lambda_1)} .$$

([15]) The geomagnetic latitude is given by:

$$\lambda = \arcsin [\cos \Omega \cdot \cos 78.5^\circ \cdot \cos (A - 69.0^\circ) + \sin \Omega \sin 78.5^\circ]$$

where A is the geographical latitude and Ω the geographical Western longitude.

([16]) A. H. COMPTON: *Phys. Rev.*, **43**, 387 (1933).

([17]) R. A. MILLIKAN and H. V. NEHER: *Phys. Rev.*, **43**, 6661 (1933); **47**, 205 (1935); **50**, 15 (1936); *Proc. Nat. Accad. Sci.*, **21**, 313 (1935); *Science*, **82**, 574 (1935).

where $I(\lambda_1)$, $I(\lambda_2)$ indicate the intensity of cosmic radiation at the two latitudes λ_1, λ_2. As the researches of MILLIKAN and NEHER have well established, the effect ζ increases by increasing λ_1 and decreasing λ_2 up to $\lambda_1 = 45^\circ$ and does not increase further for $\lambda_1 > 45^\circ$. These authors found by means of an experiment performed with an ionization chamber of 15 cm diameter surrounded by 10 cm lead, that the latitude effect has its maximum value in the Indian Ocean (for $\lambda_1 \geqslant 45^\circ$) and is equal to about 12%.

For this reason we planned to perform the present research in Bombay (India), whose geomagnetic latitude is about 9° with the aim of comparing data collected there with data collected in Rome (latitude 42°) which is near the « knee » of the latitude effect. It should be observed that measurements performed in the past years by MILLIKAN and NEHER are not directly correlated with ours because these authors measured the total cosmic radiation coming from the whole upper hemisphere but filtered by 10 cm lead, while we have measured latitude effects as a function of energy, zenith and azimuth, and separately for positive and negative μ-mesons.

The latitude effects ζ which can be deduced from our experiments are given in Table XV; from these data the following conclusions can be drawn:

1) in the vertical direction for mesons of energy greater than 0.5 GeV by averaging data of both experiments we have found a latitude effect equal to $15.2 \pm 1.2\%$ (the same has been found for the total component, i.e. the « absorption spectrum experiment » data without absorbers), while for mesons of energy between 0.5 and 1.9 GeV the effect is 35.8 ± 2.4;

2) the latitude effect measured in the Eastern directions is always larger than the effect measured in the Western directions;

3) the latitude effect in the Eastern direction increases with increasing zenithal angle;

4) the latitude effect in the Western direction decreases with increasing zenithal angle and vanishes at some angle which depends on the energy;

5) the effect averaged in the East-West plane is rougly independent of zenithal angle;

6) the latitude effect decreases with increasing energy; as is shown by the fact that in differential channels the effect is much bigger;

7) for angles smaller than 60° the effect measured on positive mesons seems to be a little larger than the effect measured on negative mesons; for $\vartheta = 60^\circ$ this effect is emphasized in the Eastern direction, whereas the latitude effect of positive mesons in the Western direction vanishes.

TABLE XV. – *Latitude effects* ζ.

« Charge excess experiment »								« Absorpt. spectrum experiment »	
Energy		0.5÷1.9			⩾0.5			⩾0.5	⩾0.05
Zenith	Azimuth	M_3^+	M_3^-	M_3	N_3^+	N_3^-	N_3	With abs. Σ	Without abs. Σ
0°	—	37.7±3.1	33.2±3.6	35.8±2.4	17.4±0.7	15.9±1.4	16.7±0.7	12.8±1.9	15.5±1.
10°	E	—	—	—	—	—	—	18.6±4.5	15.9±1.
	W	—	—	—	—	—	—	6.7±1.4	7.4±1.
	EW	—	—	—	—	—	—	12.7±1.1	11.3±0.
20°	E	—	—	—	—	—	—	12.0±7.5	16.5±0.
	W	—	—	—	—	—	—	—	13.9±1.
	EW	—	—	—	—	—	—	—	15.3±0.
30°	E	—	—	—	—	—	—	17.6±1.2	15.5±1
	W	—	—	—	—	—	—	3.5±1.1	—8.0±1
	EW	—	—	—	—	—	—	10.7±0.6	8.6±0.
40°	E	—	—	—	—	—	—	—	14.5±2
	W	—	—	—	—	—	—	—1.8±1.3	—4.5±3
	EW	—	—	—	—	—	—	—	5.8±2
45°	E	49.6±3.1	37.2±4.7	44.2±3.1	24.8±1.2	21.1±1.3	23.1±1.2	—	—
	W	23.9±5.2	22.6±6.0	23.4±4.6	10.8±0.8	12.8±1.0	11.6±0.8	—	—
	EW	37.7±3.1	33.2±3.6	33.6±2.6	17.4±0.7	17.4±0.7	17.4±0.7	—	—
50°	E	—	—	—	—	—	—	20.0±1.9	13.7±3
	W	—	—	—	—	—	—	—	—2.1±3
	EW	—	—	—	—	—	—	—	6.7±2
60°	E	65.4 ±4.0	42.3±6.3	53.7±3.3	24.2±1.2	24.2±1.2	24.2±0.6	21.3±1.3	16.5±4
	W	—0.04±0.04	27.1±8.5	8.8±2.0	10.7±1.7	4.9±0.9	7.4±0.9	—1.2±1.9	—8.1±5
	EW	23.2 ± 3.6	39.2±3.7	35.8±3.3	17.4±0.7	14.9±1.1	15.9±0.7	9.6±1.6	6.3±3

All the effects indicated in 2), 3), 4), 5), 6) can be easily explained by considering the energy cut-off for primary protons in the Eastern and Western directions at the two latitudes, which have been deduced from ALPHER's paper [13] and given in Table XVI.

The energy cut-off $\mathcal{E}_E(\lambda, \theta)$ at Bombay latitude indeed increases in the Eastern direction with increasing zenithal angle while $\mathcal{E}_W(\lambda, \theta)$ decreases. The energy cut-off in the Western direction is so low that we should not expect

TABLE XVI. – *Energy cut-off (in* GeV) *for protons and minimum energy required for creating mesons observable by our apparatus.*

Zenith	Energy cut-off for protons				$\mathcal{E}_E^*(\theta)$	$f_E(\theta)$ %
	$\lambda_1 = 40^\circ$		$\lambda_2 = 10^\circ$			
	East	West	East	West		
15°	5	4.0	15.0	11.8	—	—
30°	5	3.8	17.8	10.0	17.6	14.7
45°	5	3.0	23.0	9.8	18.4	16.9
60°	18	3.0	28.0	9.0	21.2	19.9

any latitude effect for large angles unless we could suppose that a large fraction of the observed μ-mesons might be generated in the low layers of the atmosphere; the « absorption spectrum experiment » confirms this point of view $\zeta_W(\theta)$ vanishing at some angle between 30° and 40°, but the « charge excess experiment » shows $\zeta_W(\theta)$ decreasing with zenithal angle but never vanishing up to 60°.

A similar argument used for calculating the fractional energy f given by protons to mesons from the East-West asymmetry, can now be considered for the latitude effects $\zeta_E(\theta)$ in the Eastern directions. If $\mathcal{E}_W^*(\theta)$ indicates some energy greater than energy cut-off $\mathcal{E}_E(\lambda_1, \theta)$ at latitude λ_1, but lower than the energy cut-off at latitude $\mathcal{E}_E(\lambda_2, \theta)$ for a given zenithal angle we can write the following expression:

$$\left[\frac{\mathcal{E}_E^*(\theta)}{\mathcal{E}_E(\lambda_2, \theta)}\right]^{1-\gamma} = \frac{I_E(\lambda_1, \theta)}{I_E(\lambda_2, \theta)} = \frac{1}{1 - \zeta_E(\theta)},$$

from which have been derived by substituting for $\zeta_E(\theta)$ the experimental values of Table XV, the energies $\mathcal{E}_W^*(\theta)$ indicated in the Table XVI together with the ratios $f = \mathcal{E}^*/W$. These values do not contradict the preceding ones or even values of f deduced from the Rome experiment (1) and from above airplane measurements (3) excepting a value of 40% deduced at 3500 m sea level (1) from North-South asymmetry.

Let us consider now data collected by the « absorption experiment ». In Fig. 9 are plotted against zenith angle, the cut-off energies for protons in the E-W plane at the two latitudes of Rome and Bombay (curves *a* and *b*). In the same figure is plotted — curve *c* — the minimum energy that a meson must have at the creation layer in order to reach sea level (atmospheric cut-off). Because of the fact that in the western direction we did not observe any latitude effect for zenithal angles greater than 30°, we must conclude that mesons

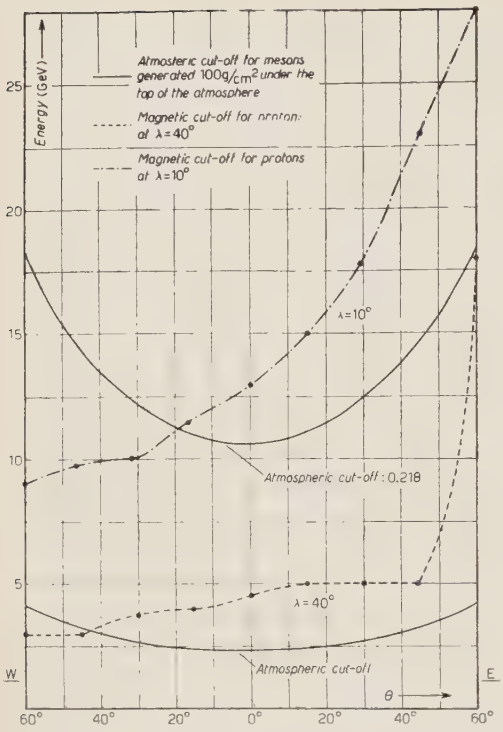

Fig. 9. – Cut-off energies for protons in E-W plane at Rome (curve *a*) and at Bombay (curve *b*); atmospheric cut-off for mesons i.e. minimum energy required for a meson created at the top of the atmosphere to reach our apparatur (curve *a*); atmospheric cut-off for mesons divided by *f*, i.e. minimum energy required by protons for creating mesons which cross our apparatus (curve *d*).

recorded in this direction have been created by protons whose energy is above the geomagnetic cut-off which is 10 GeV (Table XVI.) The atmospheric cut-off for mesons which reach the apparatus with an energy greater than 0.5 GeV and zenithal angle 30° is 2.18 GeV; consequently *f* would be 21.8%; this value is greater than the value obtained in the Eastern direction at 30° but not in contradiction with preceding determinations if one considers that *f* must be considered a mean value of the fractional energy given by protons to mesons which can be modified by the selection of mesons due to the conditions of the experiment. The curve *d*) of Fig. 9 represents the atmopsheric cut-off divided by $f = 0.218$; it is obviously a plot of the minimum energy required by a proton for creating a meson which is able to reach sea level in the given direction. As Fig. 9 shows, curve *d* is everywhere higher than curve *b* which represents the cut-off energy for protons at Rome latitude; on the contrary it is always below curve *a* in the eastern and western directions for angles not exceeding 30° at Bombay latitude. Therefore we must expect finding at the latitude of Bombay an East West asymmetry due to the primary cut-off and no effect should be measurable in Rome. Experimental data reported in Table XI confirm the results of the above discussion.

9. – Conclusions.

The conclusions which can be drawn from the present research, concern: *a*) nuclear effects (production of mesons in nuclear collisions); *b*) geomagnetic

effects (energy cut-off of primaries, curving of meson trajectories in the atmosphere).

Unfortunately the results of our experiments cannot give an answer to important questions of nuclear physics withouth a reliable theory which explains all phenomena in cosmic radiation; however we have developed a theory based on reasonable hypotheses and taking into account nuclear and geomagnetic effects (this simple theory cannot account for all details of cosmic ray phenomena) in order to get an indirect test of the introduced hypotheses by comparison with experimental results. The conclusions which can be drawn are the following.

1) The zenithal distributions agree fairly well with the calculated ones excepting at large angle under 20 m water.

2) The observed negative excess is to be considered as an effect of the Earth's magnetic field on meson trajectories; therefore it can be explained without introducing the presence of negative particles in the primary radiation.

3) The positive excess is roughly independent of zenithal angle as our theory based on HEITLER's assumptions predicts but statistical errors do not allow us to draw any definite conclusion; however it seems reasonable to exclude that a large fraction of recorded mesons might be generated with a large multiplicity.

4) The measured East-West asymmetry cannot be considered as only due to the energy cut-off of the primaries because a large contribution is given by the curving of the meson trajectories. Reasonable values of both asymmetries having been found we may regard as satisfactory the agreement between theory and experiment.

5) The measured latitude effects fit well with preceding measurements. Zenithal and azimuthal dependence of the latitude effects is in a very good agreement with the theoretical energy cut-off for primary protons; hence we may conclude that most of the mesons which cross our apparatus are generated by protons which give to the mesons a fraction of the order of 15-20 % of their energy, according to theoretical calculations.

10. – Acknowledgements.

We are gratefully indebted to the « Genio Militare Italiano » and to « Vigili del Fuoco » who helped us to carry out the measurements, at Lake Albano providing skilled assistance and special materials.

Measurements in Bombay were performed in the « Tata Institute for Fundamental Research ». We are very deeply indebted to Prof. H. J. BHABHA,

Director of the « Tata Institute » for kind hospitality and for help received during the course of our work.

We would like also to express our thanks to Mr. M. GALIANI for his continuous and skilled help and assistance during the preparation and the running of measurements in Italy and in India.

A grant from the « International Union of Pure and Applied Physics » supported part of the expenses for the measurements in Bombay.

RIASSUNTO

Al fine di studiare i processi di creazione dei mesoni da parte della radiazione primaria, e la ipotetica presenza di particelle primarie negative, sono stati effettuati due esperimenti ad alta latitudine (Roma 42°) e bassa latitudine (Bombay 9°). Sono stati misurati in funzione dell'angolo zenitale: 1) l'asimmetria est-ovest; 2) l'effetto di latitudine; 3) l'eccesso di carica. I risultati delle nostre misure indicano: *a*) che l'effetto negativo misurato in direzione est può essere spiegato senza introdurre l'ipotesi di una primaria negativa; *b*) la dipendenza dell'eccesso positivo dall'energia non è in contrasto con la teoria di Heitler; *c*) l'effetto di latitudine è di circa il 15% in direzione verticale per mesoni di energia maggiore di 0,5 GeV, e sembra aumentare in direzione est e diminuire in direzione ovest con l'angolo zenitale; *d*) la frazione di energia ceduta dai protoni ai mesoni all'atto della generazione è dell'ordine del 20%.

A Nuclear Inductor for Measurements of Thermal Relaxation Times in Liquids.

G. Chiarotti, G. Cristiani, L. Giulotto and G. Lanzi

Istituto di Fisica dell'Università - Pavia

(ricevuto il 24 Luglio 1954)

Summary. — A device for measurements of nuclear relaxation times in liquids in the range from 10^{-2} s to the longest observable times is described. Two equivalent methods are used which are based on the record of « in phase » signals due to the total reversal of the nuclear magnetization.

We think it useful to describe an arrangement used by us for measurements of the nuclear relaxation times in pure liquids and in liquids containing paramagnetic gases in solution. Two equivalent methods have been used, which are based on the record of « in phase » signals due to the total reversal of the nuclear magnetization. The experimental results and their discussion will be the object of a later paper.

Several devices suitable for the study of the nuclear paramagnetic resonance have been described by various authors. The original arrangements of Bloch and cow. (1) and Purcell and cow. (2) are well known; other devices have been afterwards described, which generally are used for measurements of nuclear magnetogyric ratios, for the study of structures of nuclear magnetic resonance lines and for the measure of relaxation times.

Our arrangement is proper for measurements of relaxation times in liquids, in the range from 10^{-2} s to the longest observable times and enables us to obtain a good degree of accuracy. It is derived from Bloch's inductor, but presents some remarkable modifications suggested especially by the particular

(1) F. Bloch, W. W. Hansen and M. Packard: *Phys. Rev.*, **70**, 474 (1946).
(2) N. Bloembergen, E. M. Purcell and R. V. Pound: *Phys. Rev.*, **73**, 679 (1948).

methods chosen for the relaxation time measurement. Therefore we shall describe at first the methods used.

1. – The Method Used.

The method so far most frequently used for measurements of thermal relaxation times in liquids and in crystals is the method first used by PURCELL and cow. ([2,3]) which is based on the saturation effect of the nuclear absorption curve in a strong r.f. field. Some other methods have also been used ([4-9]).

The methods used by us may be suitable in the case of liquids for their simplicity. The signals «in phase» due to the total reversal of the magnetization (case of the adiabatic rapid passage), can be observed when T_1 and T_2 are of the same order of magnitude as in liquids, and the condition:

$$\frac{\mathrm{d}H_0}{\mathrm{d}t} \ll \gamma H_1^2 , \tag{1}$$

is verified, where H_0 is the external constant magnetic field, H_1 is the rotating r.f. field and γ is the nuclear magnetogyric ratio. If the interval of time between two successive passages through resonance is comparable with T_1, the magnetization, during this time interval tends to the value M_0 of the Curie formula, without however reaching it. Then the amplitudes of the observed signals depend upon this time interval. If the constant magnetic field is modulated symmetrically with respect to the Larmor field H^* (Fig. 1*a*), the signals corresponding to passages through resonance with increasing and decreasing field follow at equal intervals of time. They result alternatively up and down, depending on the sense of the passage. After a certain number of passages,

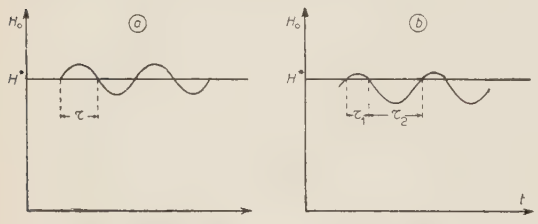

Fig. 1. Symmetrical (*a*) and asymmetrycal (*b*) modulation of the constant magnetic field.

([3]) N. BLOEMBERGEN: *Nuclear Magnetic Relaxation* (The Hague, 1948).
([4]) H. TORREY: *Phys. Rev.*, **75**, 1326 (1949); **76**, 1059 (1949).
([5]) E. HAHN: *Phys. Rev.*, **76**, 461 (1949); **77**, 297 (1950).
([6]) G. E. PAKE: *Am. Journ. Phys.*, **18**, 438, 473 (1950).
([7]) N. F. RAMSEY: *Phys. Rev.*, **83**, 540 (1951).
([8]) R. L. CONGER and P. W. SELWOOD: *Journ. of Ch. Phys.*, **20**, 383 (1952).
([9]) G. CHIAROTTI and L. GIULOTTO: *Nuovo Cimento*, **10**, 54 (1953).

the conditions of Fig. 2 are reached. The amplitudes of the observed signals are proportional to the value M_1 of the magnetization at every passage which depends on the sweep frequency and is given by:

$$M_1 = M_0 \frac{1 - \exp[-\tau/T_1]}{1 + \exp[-\tau/T_1]}, \tag{2}$$

where τ is the time-interval between two successive passages through resonance. Two records with different sweep frequencies, enable us to obtain the

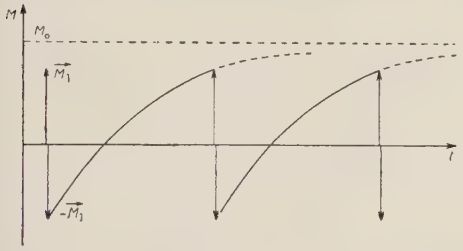

Fig. 2. – Behaviour of the nuclear magnetization as a function of the time in the case of « adiabatic rapid passage » with symmetrical sweep. Signals recorded in these conditions are shown in Fig. 10*a*.

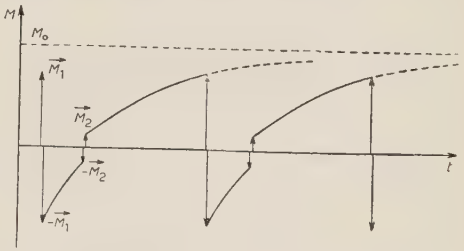

Fig. 3. – Behaviour of the nuclear magnetization as a function of the time in the case of the « adiabatic rapid passage » with asymmetrical sweep. Signals recorded in these conditions are shown in Fig. 10*b*.

relaxation time T_1. In Fig. 10*a* are reproduced three records of pure water signals obtained by symmetrically modulating the constant magnetic field, with sweep periods respectively of 3.45 s, 6.8 s and 28.9 s.

Another method, equivalent to the former, utilizes only one record of signals obtained with resonance field not centered with respect tothe sweep (Fig. 1*b*). In this case the intervals between passages through resonance are not equal, the magnetization M_1 and M_2 we find at resonance with increasing and decreasing H_0 are different and therefore the signals are alternatively of different amplitudes. The amplitudes of the signals are proportional to:

$$\begin{cases} M_1 = M_0 \dfrac{1 + \exp[-(\tau_1 + \tau_2)/T_1] - 2\exp[-\tau_2/T_1]}{1 - \exp[-(\tau_1+\tau_2)/T_1]}, \\ M_2 = M_0 \dfrac{-1 - \exp[-(\tau_1+\tau_2)/T_1] + 2\exp[-\tau_1/T_1]}{1 - \exp[-(\tau_1+\tau_2)/T_1]}. \end{cases} \tag{3}$$

where τ_1 and τ_2 are the time intervals between the passages. This case is illustrated in Fig. 3 and corresponds to the record of Fig. 10*b* obtained by asymmetrically sweeping and with a sweep period of 5.7 s.

To obtain good precision with the first method, it is necessary that one of two sweep periods is of the order of T_1 and the other several times greater. With the second method a proper sweep period is of the order of T_1, or somewhat greater. This method is like that used by CONGER and SELWOOD [8] for measurements of relaxation times in solutions of paramagnetic ions. They used a fixed sweep frequency of 60 Hz and were able therefore to measure thermal relaxation times in a limited range (around 10^{-2} s). We have extended the sweep frequency range from 100Hz to 0, making it possible to determine the relaxation times for pure liquids too.

2. – The Experimental Arrangement.

The block diagram of the experimental arrangement is plotted in Fig. 4. *A* is the r.f. head containing the transmitting and receiving coils placed in the gap of the magnet *B*. The transmitter consists of a commercial standard signal generator *C* followed by a r.f. power amplifier with symmetrical output *D*. The frequency we used for measurements of proton relaxation in liquids is 7 MHz (resonance field 1 650 oersted). *E* is a device to control the amplitude and the phase of the r.f. « leakage » voltage in the receiving coil. The receiver consists of a r.f. amplifier *F* followed by a detector *G* and by a d.c. amplifier *H*. *I* is a symmetrical diode voltmeter which permits us to know the strenght of the r.f. field by measuring the voltage across the transmitting coils. *L* is a r.f. heterodyne voltmeter (Brüel & Kjaer - Type 2002) to measure the voltage across the receiving coil with voltage ranges from 10 V to 10 μV f.s. The signals can be observed on the screen of an oscilloscope *M* and recorded with a cathode ray tube recorder *N* or with a galvanometer recorder *O*, depending on the sweep frequency range. The modulation of the constant field can be

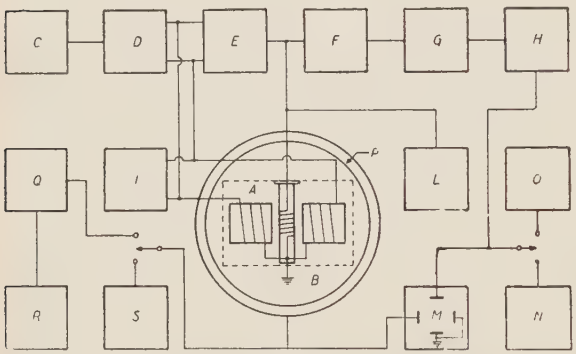

Fig. 4. - Block diagram of the arrangement. *A* r.f. head; *B* magnet; *C* standard signal generator; *D* r.f. power amplifier; *E* r.f. phase shifter; *F* r.f. amplifier; *G* detector; *H* d.c. amplifier; *I* symmetrical diode voltmeter; *L* heterodyne r.f. voltmeter; *M* oscilloscope; *N* C.R.T. recorder; *O* galvanometer recorder; *P*; modulating coil of the magnet; *Q* audio frequency power amplifier; *R* 20 - 1000 Hz beat oscillator; *S* 0-20 Hz generator.

obtained by connecting the modulation coils P to a power amplifier Q driven by a beat oscillator R for frequencies from 20 to 100 Hz or to a particular device S described below for frequencies from 0 to 20 Hz.

In Fig. 5 the r.f. head with the transmitting and receiving coils is plotted. The angle between the transmitting (1, 1) and receiving (2) coils can be regulated around 90°, by means of the screw (3) in order to minimize the coupling. The transmitting coils can be rigidly blocked by means of the screw (4). The r.f. head is fixed against the brass head of the magnet coils. The coils are strongly pressed by brass spacers in order to hamper any vibration. The shields of the r.f. head are split to reduce the Foucault currents caused by the modulation of the constant field. As a result of these precautions the noises caused by the vibrations are practically cut out. The receiving coil is wound on a thin glass tube in which we can easily introduce the sample.

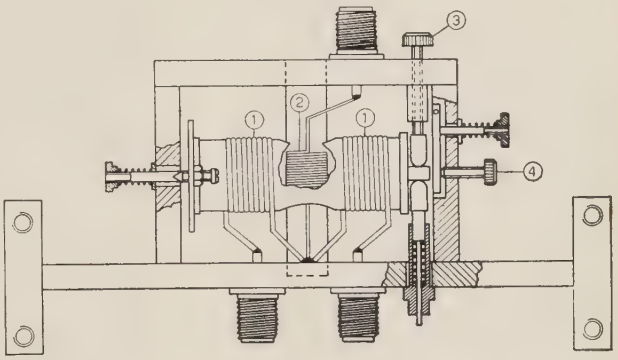

Fig. 5. — r.f. head; for description see text.

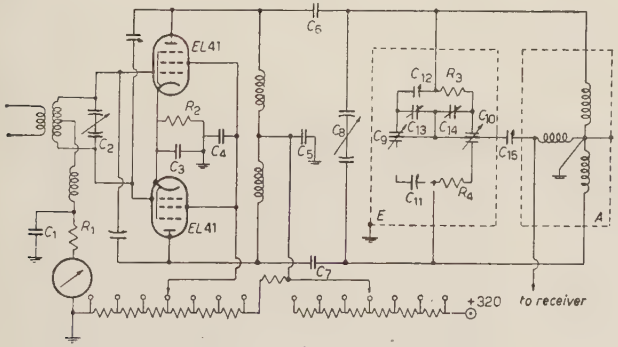

Fig. 6. — Final stage of the r.f. power amplifier with the r.f. head A and the r.f. phase shifter E. C_1, C_3, C_4, C_5, — 10 000 pF; C_2, C_8, — 200 + 200 pF; C_6, C_7 — 2 500 pF; C_9, C_{10} — 50+50 pF; C_{11}, C_{12}— 3 — 30 pF; C_{13}, C_{14}, C_{15} — 2 — 10 pF; R_1 — 25 kΩ; R_2 — 300 Ω; R_3, R_4 — 2 500 Ω.

The pole pieces of the magnet have a diameter of 12 cm and are shaped according to Rose's [10] instructions to improve the field uniformity in the central region. The gap is of 6 cm. The magnet is supplied by a battery of accumulators.

By regulating the screw (3) of the device of Fig. 5, the voltage across the

[10] M. E. Rose: *Phys. Rev.*, **53**, 715 (1938).

receiving coil can be reduced to about 1/100 of the voltage across the transmitting coils. To reduce more accurately the r.f. « leakage » in the receiving coil and to control its phase, the device E of Fig. 4 is used. This is shown in detail in Fig. 6 with the output stage of the r.f. amplifier F of Fig. 4. The working of the device E is easy to understand. The butterfly condensers C_9 and C_{10} serve for rough adjustement, the trimmers C_{13} and C_{14} for a more accurate regulation. Our arrangement does not contain variable resistors which could introduce some noises and it enables one to ground the centre of the transmitting coils. It presents therefore some advantages with respect to stability. Using the device E of Fig. 4, the residual unbalance could be steadily reduced to less than $1/10^6$ of the voltage across the transmitting coils. In these conditions the amplitudes of the nuclear signals can result greater than the residual unbalance. The sign and the shape of the nuclear signals are then altered. Such a case is illustrated in Fig. 10*c*, where two records of the signals of protons in water are reproduced, obtained with the same value of the oscillating field and with the same period of symmetrical sweep. In both records the signals are due to the total reversal of the magnetization. In the lower record the residual unbalance is greater than the amplitudes of the signals: they therefore turn out to be of equal amplitudes and alternatively up and down. In the upper record, the residual unbalance is very small with respect to the amplitudes of the nuclear signals: they are therefore of equal amplitudes and all up.

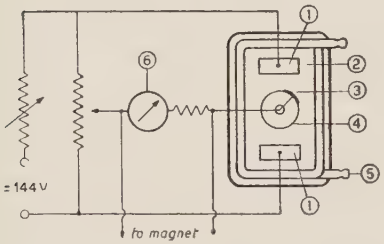

Fig. 7. – 0 — 20 Hz generator. (1) carbon electrodes; (2) aqueous solution of $NaHCO_3$; (3) nickel electrode; (4) rotating glass cylinder; (5) glass tube for cooling; (6) galvanometer.

The other parts of the block diagram of Fig. 4 do not require particular descriptions with the exception of the 0-20 Hz generator S. This is shown in Fig. 7 and consists of a bridge, two sides of which are formed by an electrolytic cell in wich the electrode (3) is a nickel thin plate eccentrically rotating by means of a synchronous motor. The rotation frequency can be varied by means of a system of gears and by a continuous shifting. The galvanometer (6) serves to balance the d.c. component.

The signals of Figg. 8, 9 obtained with a sweep frequency of 50 Hz have been photographed on the oscilloscope screen and give an idea of the behaviour of our device when it is operating in the usual way.

The signals of Fig. 10 have been recorded with the recording galvanometer and are like those we used to measure the relaxation times. Before recording signals of this type we took care that the condition (1) was satisfied. The r.f. field H_1 was measured with the diode voltmeter I calibrated in oersted

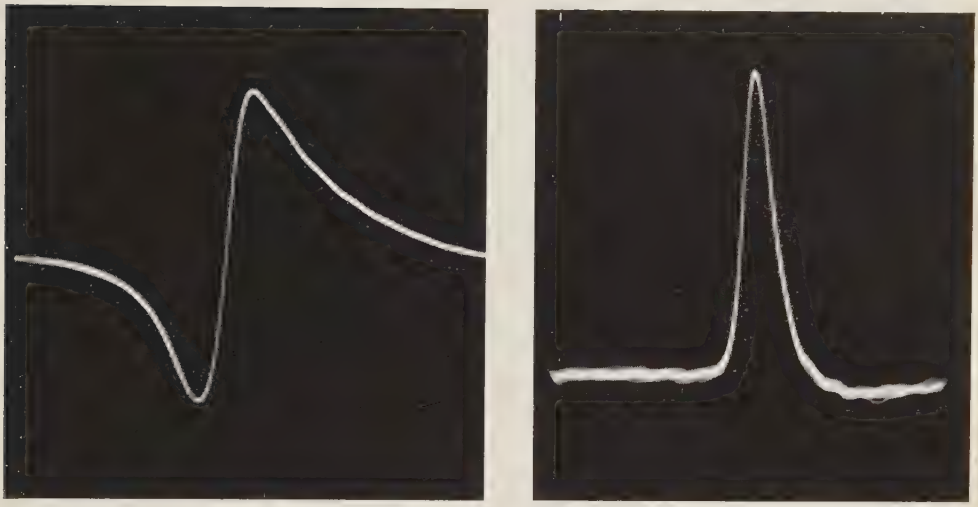

a) *b*)

Fig. 8. – Signals corresponding to « slow passages », obtained with aqueous concentrated solution of ferric nitrate with a sweep frequency of 50 Hz. (*a*) signals « in phase »; (*b*) signals « out of phase ».

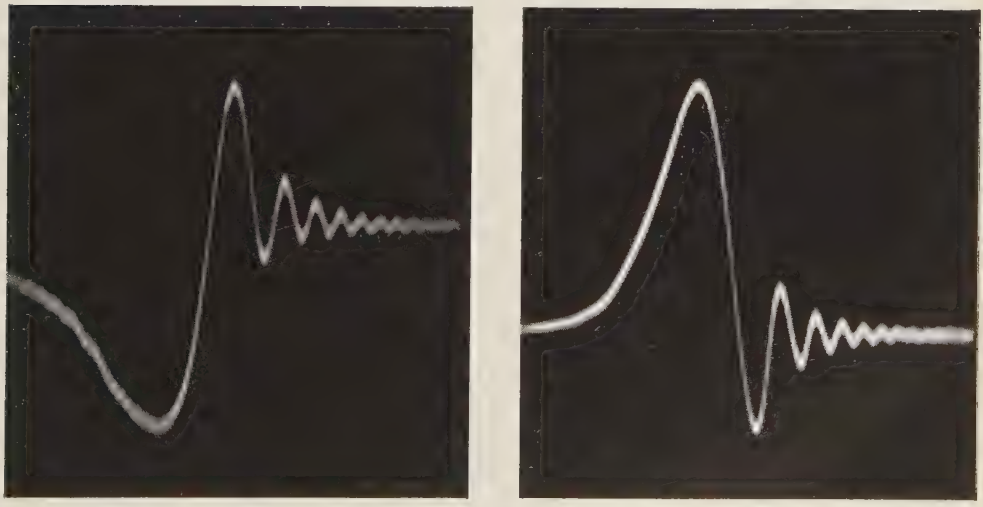

a) *b*)

Fig. 9. – Signals corresponding to « rapid passages » obtained with aqueous diluted solution of copper sulphate with a sweep frequency of 50 Hz. (*a*) signals « in phase »; (*b*) signals « out of phase ».

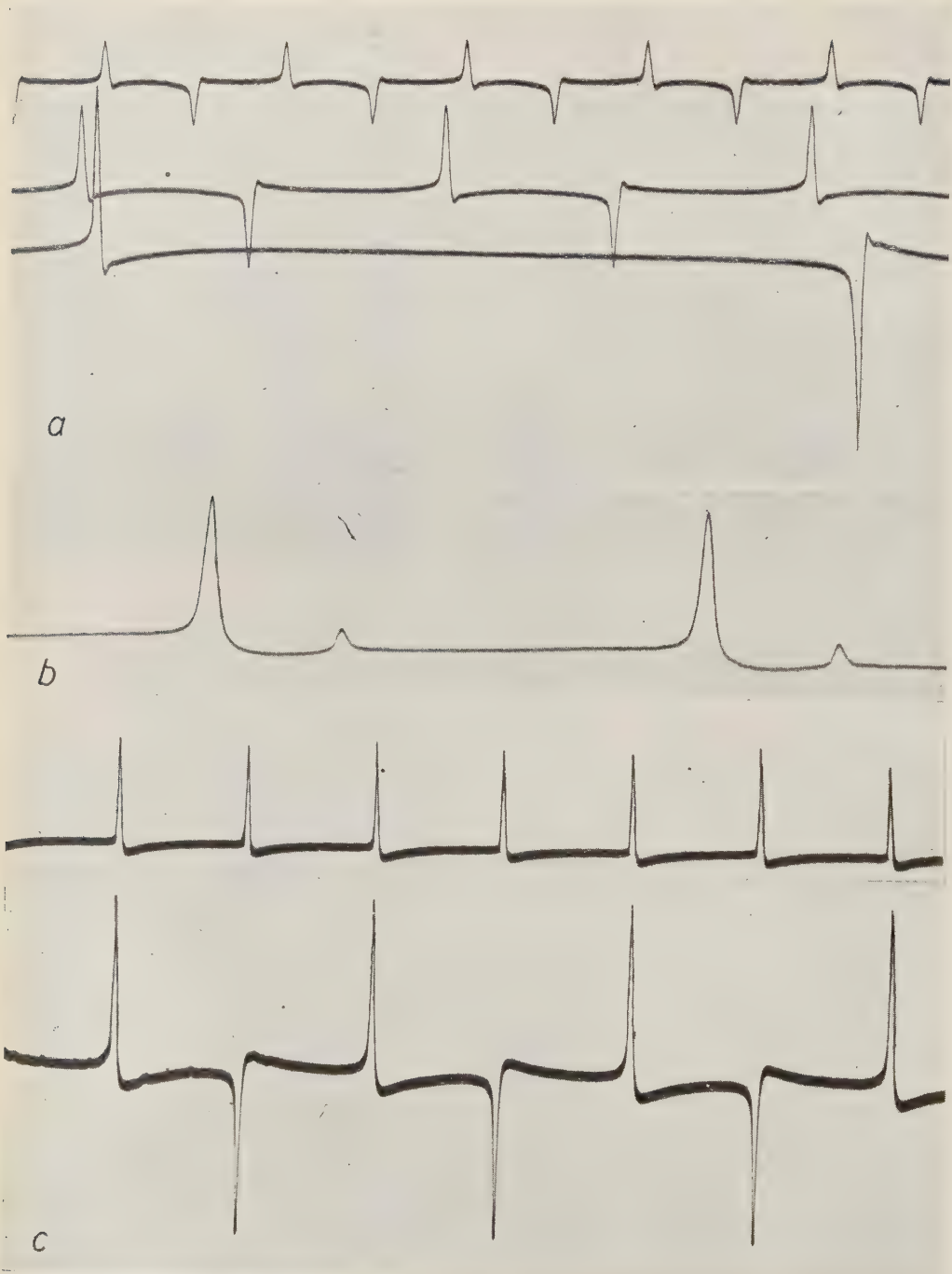

Fig. 10. – Signals « in phase » of the protons of the pure water due to the total reversal of the magnetization. (*a*) signals obtained with symmetrical sweep using sweep periods of 3.45 s, 6.8 s and 28.9 s; (*b*) signals obtained with asymmetrical sweep using sweep period of 5.7 s.; (*c*) upper record: case of the r.f. « leakage » less than the signals; lower record: case the r.f. « leakage » much greater than the signals.

with the same method used in a previous work [9]. The variation of the constant field dH_0/dt was measured by means of a small coil introduced in the field and connected to a vacuum tube voltmeter or to a rapid galvanometer (not indicated in the block diagram of Fig. 4) depending on the range of the sweep frequency.

This work was performed with financial support of the C.N.R. One of us (G. Ch.) would like to thank the C.N.R. for its grant.

RIASSUNTO

Viene descritto un dispositivo per misure di tempi di rilassamento nucleare in liquidi nel range da 10^{-2} s ai più lunghi valori osservabili. Vengono usati due metodi equivalenti basati sulla registrazione dei segnali in fase dovuti al completo capovolgimento della magnetizzazione.

A Cloud Chamber Analysis of Cosmic Radiation at 3500 m. Part B: Results on the Hard and Soft Components.

A. Lovati, A. Mura, C. Succi and G. Tagliaferri

Istituto di Scienze Fisiche dell'Università - Milano
Istituto Nazionale di Fisica Nucleare - Sezione di Milano

(ricevuto il 25 Luglio 1954)

Summary. — A multiplate cloud chamber has been operated at 3500 metres a.s.l., yielding 16000 photographs of random expansions. The present paper is intended to investigate some questions pertaining to the general cosmic ray phenomenology. In particular, the zenith angle dependence of the directional intensities of both hard and soft component is found to follow a squared cosine law. In the range 0.3-2 GeV, the differential energy spectrum of the soft component is shown to be well represented by a power law with exponent — 2.5. The rate of production of nuclear disintegrations in lead and the correlation between the disintegrations and other events are examined.

1. – Introduction.

In a previous publication (1), referred to hereafter as Part A, it was reported about the employing of a randomly operated cloud chamber to carry out an unbiassed analysis of some aspects of cosmic radiation at mountain altitude. Part A was devoted to study the yield of electronic component from nuclear disintegrations in lead. Now the photographs gathered have been examined with the purpose of gaining information on (i) the zenith angle dependence of the directional intensities of the hard and soft components, (ii) the rates of occurrence of nuclear disintegrations and electron-photon showers in lead, (iii) the size distribution of the electronic showers and (iv) the correlation

(1) A. Lovati, A. Mura, G. Tagliaferri and S. Terrani: *Nuovo Cimento*, **9**, 946 (1952).

between the nuclear disintegrations and other events. It will be apparent that we did intend to investigate somewhat about questions pertaining to the general cosmic ray phenomenology: the possibility of investigating this kind of questions was offered to us by the use of an experimental technique well suited to give a truthful picture of the cosmic ray particles and their interactions.

It is hardly necessary to recall that the well-known advantage of avoiding selective recording of the cosmic ray phenomena by the use of the random expansion procedure is counterbalanced by the very reduced rate at which the infrequent events can be collected. Consequently the possibility of attaining by this technique a certain kind of information relies in the first place upon chamber dimensions. The cloud chamber (2) we employed had a sensitive illuminated volume of $60 \times 50 \times 15$ cm^3 and contained 9 lead plates 18 g cm^{-2} thick each.

2. – Determination of the Chamber Collecting Time.

In order to estimate the rates of occurrence of whatever particular event registrared on the photographs, one must determine the chamber collecting time.

Let us consider the sensitive time of the chamber. In our instrument that time could easily be as long as 0.2 s. However the full time of chamber sensitivity cannot be used, if one demands the collecting of tracks moderately distorted. In this case the collecting time must be substantially shorter than the sensitive time and its lenght is determined by the instant of lighting for photography. Anyhow it is observed that the number of tracks actually photographed turns out to be a little lower than expected basing on the delay of flashing the lamps. That is understood as a consequence of some unevenness in chamber operation, mostly for thermal instability. It seems thus convenient to determine *experimentally* an *equivalent collecting time.*

For this purpose the tracks registered on the photographs were divided into three classes: (i) sharp tracks, due to particles that entered the chamber after the end of the expansion; (ii) tracks whose larger breadth suggests they were originated whilst the expansion was taking place and (iii) tracks showing two separate columns of ionization, clearly caused by pre-expansion particles. Only tracks belonging to classes (i) and (ii) were taken into account, both here and in the following.

(2) A. Lovati, A. Mura, G. Tagliaferri and L. Terra: *Nuovo Cimento*, **8**, 713 (1951).

The equivalent collecting time was determined by counting the number of particles crossing all the chamber plates, that is crossing at least 162 g cm^{-2} of lead. The resulting rate was $f = 0.145 \pm 0.010$ penetrating particles per photograph. On the other hand the absolute vertical intensity of penetrating particles in our experimental conditions is known ([3]) to be

$$I_v = 1.60 \cdot 10^{-2} \text{ p.p. cm}^{-2} \text{ sterad}^{-1} \text{ s}^{-1} .$$

Assuming now a squared cosine law ([4]) (see also § 3·1) for the zenith angle dependence of the directional intensity of the hard component, the expected number of penetrating particles crossing the nine chamber plates per second should be (see § 3·2) $F = 1.53$. Hence the mean equivalent collecting time per photograph is given by

$$f/F = 0.145/1.53 = 0.095 \text{ s}$$

and the total collecting time for the 16 000 photographs we gathered turns out to be 1 500 s. The estimated error is of the order of 15%.

3. – Some Results on the Hard Component.

3·1. *Zenith angle dependence of the directional intensity.* – On the average, everyone of the 16 000 photographs shows 0.75 near minimum ionizing particles, which cross two lead plates at least, without being appreciably scattered or undergoing cascade multiplication. These particles can be confidently identified as μ-mesons and protons, which are known to be the main constituents of the hard component at mountain altitude.

The zenith angle dependence of the directional intensity of the hard component was shown several years ago to follow a $\cos^n \theta$ law (θ = zenith angle), with $n = 2$, at least from sea level to mountain height. All the measurements concerned were taken with counter coincidence methods ([4]). Recently, however, BARONI *et al.* ([5]) reported a nuclear plate result according to which for μ-mesons of kinetic energy greater than 40 MeV one should rather assume an exponent $n = 3.5$. We thought therefore of some interest to obtain from our own photographs the angular distribution of the penetrating particles.

In order to compare the *projected* angular distribution given by the photo-

([3]) B. ROSSI: *Rev. Mod. Phys.*, **20**, 537 (1948).
([4]) K. I. GREISEN: *Phys. Rev.*, **61**, 218 (1942).
([5]) G. BARONI, G. CORTINI, A. MILONE, L. SCARSI and G. VANDERHAEGHE: *Nuovo Cimento*, **9**, 867 (1952).

graphs with the distribution functions foreseen by the $\cos^n \theta$ law, we have carried out the following calculation.

Let A and B (Fig. 1) be two horizontal rectangles, having dimensions $2X$ by $2Y$, and placed one above the other at the distance Z. The direction of motion of one particle crossing the two rectangles is individuated by the angles θ_0 and ψ, which are bound to the zenithal angle θ by

$$\cos \theta = \cos \theta_0 \cos \psi \,. \tag{1}$$

The elementary solid angle is given by the expression

$$\mathrm{d}w = \cos \psi \, \mathrm{d}\psi \, \mathrm{d}\theta_0 \,. \tag{2}$$

Assume that the intensity of the incident particles be represented by the law

$$I = I_v \cos^n \theta \,, \tag{3}$$

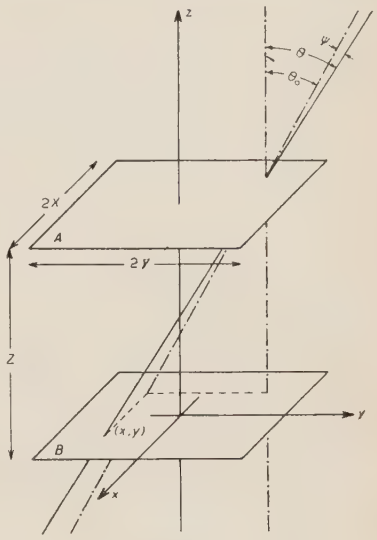

Fig. 1.

I_v being their vertical intensity. Then the total flux of particles through the two rectangles will be

$$\Phi_n = \int\int\int \mathrm{d}x \, \mathrm{d}y \cos \theta I \mathrm{d}w = \int\int\int \mathrm{d}x \, \mathrm{d}y \cos \theta I_v \cos^n \theta \, \mathrm{d}w = \tag{4}$$

$$= I_v \int_{-Y}^{Y} \mathrm{d}y \int_{\theta_1}^{\theta_2} \cos^{n+1} \theta_0 \, \mathrm{d}\theta_0 \int_{-X}^{X} \mathrm{d}x \int_{\psi_1}^{\psi_2} \cos^{n+2} \psi \, \mathrm{d}\psi \,,$$

with

$$\theta_1 = -\operatorname{arctg} \frac{Y+y}{Z} \,, \qquad \theta_2 = \operatorname{arctg} \frac{Y-y}{Z} \,.$$

and

$$\psi_1 = -\operatorname{arctg} \left(\frac{X+x}{Z} \cos \theta_0 \right) , \qquad \psi_2 = \operatorname{arctg} \left(\frac{X-x}{Z} \cos \theta_0 \right) .$$

Re-write now expression (4) inverting the order of integration

$$\Phi_n = 2 I_v \int_{0}^{\operatorname{arctg} 2Y/Z} \cos^{n+1} \theta_0 \, \mathrm{d}\theta_0 \int_{-Y}^{Y - Z \operatorname{tg} \theta_0} \mathrm{d}y \int_{-X}^{X} \mathrm{d}x \int_{\psi_1}^{\psi_2} \cos^{n+2} \psi \, \mathrm{d}\psi \,. \tag{5}$$

Define $N_n(\theta_0)$ the orthogonal projection on the vertical plane yz of the angular distribution function. We have

$$\Phi_n = \int N_n(\theta_0)\mathrm{d}\theta_0 \,. \tag{6}$$

Then

$$N_n(\theta_0) = 2I_v \cos^{n+1}\theta_0 \int_{-Y}^{Y - Z\,\mathrm{tg}\,\theta_0} \mathrm{d}y \int_{-X}^{X} \mathrm{d}x \int_{\psi_1}^{\psi_2} \cos^{n+2}\psi\,\mathrm{d}\psi = \tag{7}$$

$$= 2I_v(2Y - Z\,\mathrm{tg}\,\theta_0)\cos^{n+1}\theta_0 \int_{-X}^{X} \mathrm{d}x \int_{\psi_1}^{\psi_2} \cos^{n+2}\psi\mathrm{d}\psi \,,$$

with the limitation

$$2Y - Z\,\mathrm{tg}\,\theta_0 > 0 \,, \qquad \mathrm{tg}\,\theta_0 < \frac{2Y}{Z} \,. \tag{8}$$

Expression (7) can be easily integrated for two special cases here of interest: $n = 2$ and $n = 4$. We get

$$N_2(\theta_0) = 2I_v(2Y - Z\,\mathrm{tg}\,\theta_0)\cos^3\theta_0 \left\{ (X^2 Z\cos\theta_0)/(4X^2\cos^2\theta_0 + Z^2) + \right. \tag{9}$$

$$\left. + \frac{3}{2} X \,\mathrm{arctg}\left(\frac{2X}{Z}\cos\theta_0\right)\right\} \,,$$

and

$$N_4(\theta_0) = 2I_v(2Y - Z\,\mathrm{tg}\,\theta_0)\cos^5\theta_0 \left\{ \frac{1}{3}\frac{Z}{\cos\theta_0}\cdot[1 - Z^4/(4X^2\cos^2\theta_0 + Z^2)^2]\right\} + \tag{10}$$

$$+ \frac{5}{6}\cos^2\theta_0 N_2(\theta_0) \,.$$

The comparison with the experimental findings is displayed in Fig. 2. The hystogram gives the distribution of the projected zenith angles (6) of 3 000 penetrating particles that cross the first two lead plates, as observed in a group of about 4 000 photographs. The curves are the plots of $N_2(\theta_0)$ and $N_4(\theta_0)$, both calculated for the pertinent values $2X = 15$ cm, $2Y = 36$ cm and $Z = 7$ cm (Z is here the distance between the outer surfaces of the two plates), and nor-

(6) Actually the distribution we see on the photographs is not the true orthogonally projected distribution, because of the cameras being at a finite distance from the cloud chamber and at angles of 10° to its axis. For the present analysis, however, the errors involved are unimportant.

malized to give the right flux of 3 000 particles. One sees that satisfactory agreement is obtained with the $N_2(\theta_0)$ curve, thus favouring the assumption of a $\cos^2\theta$ law. It should be noticed that the minimum kinetic energy for the particles to be included in these statistics was $\sim$ 90 MeV for μ-mesons, and $\sim$ 300 MeV for protons.

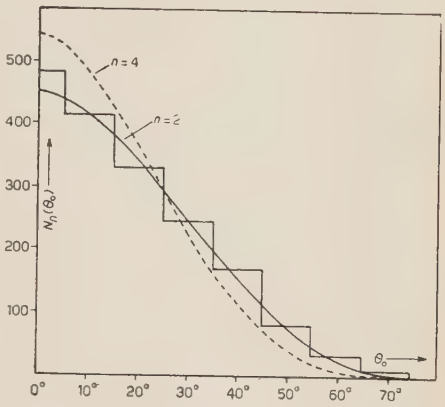

Fig. 2. – Distribution of the projected zenith angles θ_0 for 3 000 penetrating particles crossing the first two lead plates. The curves give the expected values according to a law $I = I_v \cos^n\theta$, with $n=2$ (solid line) and with $n=4$ (broken line).

3·2. *Total flux of penetrating particles.* – To evaluate the equivalent collecting time of the chamber, we needed the total flux of penetrating particles through the nine chamber plates (see § **2**). This was obtained by means of a graphical integration of

$$(6\text{-}bis) \qquad \Phi_2 = \int N_2(\theta_0)\,\mathrm{d}\theta_0\,,$$

after calculating expression (9) for the values $I_v = 1.60$ p.p. cm^{-2} sterad^{-1} s^{-1}, $2X = 15$ cm, $2Y = 36$ cm, $Z = 46$ cm (Z is here the distance between the outer surfaces of the first and last plate).

The resulting flux across the nine plates was $F = 1.53$ p.p. per second.

3·3. *Rate of knock-on electrons production in lead.* – The rate of knock-on electron production in lead was deduced for 3 000 penetrating particles crossing at least the first two plates of the chamber. The events considered were either forward collision electrons whose rather straight path and near minimum ionization indicated an energy greater than about 1 MeV, or electron showers clearly related to the penetrating particles. We found (4.85 $\pm$ 0.05) percent knock-on events per lead plate traversed. This figure is appreciably lower than the one of (7.4 $\pm$ 0.2) percent reported by HAZEN (7) for penetrating particles crossing 3 lead plates 0.6 cm thick each, almost at the same height: it seems difficult to understand the reason of the discrepancy.

It is interesting to compare the rate obtained for the penetrating particles at 3 500 m, where these are known to be a mixture of μ-mesons and protons (here μ-mesons of kinetic energy greater than $\sim$ 90 MeV and protons of kinetic

(7) W. E. HAZEN: *Phy. Rev.*, **64**, 7 (1943).

(8) A. LOVATI, A. MURA and C. SUCCI: *Nuovo Cimento*, **11**, 92 (1954) and references there cited.

energy greater than ~ 300 MeV), and the rate of knock-ons found, with plates of the same thickness, at sea level or at moderate depths undergound ([8]), where the penetrating particles are mostly μ-mesons. The comparison allows to confirm that an appreciable number of protons is present in the beam of penetrating particles at 3500 m and enables to do a rough estimation of the fraction of protons among the penetrating particles: in our experimental conditions a value around 12 percent can be obtained, if we make the reasonable assumption that the rate of production of knock-ons from μ-mesons should be 5.5 percent per lead plate crossed. It is worth noticing that the number of protons with energies > 400 MeV was (7.9 ± 1.5) percent of the p. p. according to GREGORY and TINLOT ([9]), while recently WHITTEMORE and SHUTT ([10]) and MILLER *et al.* ([11]) reported (19 ± 2) and (20 ± 2) percent for the fraction of protons in the ionizing nonelectronic particles, respectively for momenta above 0.3 GeV/c and in the momentum range 0.7-2.0 GeV/c.

4. – Some Results on the Nuclear Disintegrations.

4·1. *Rate of occurrence of nuclear disintegrations.* – In Part A we reported the results concerning the nuclear disintegrations observed in the lead plates: the disintegrations were distributed according to the number of penetrating shower particles ([12]) showing within the chamber. We summarize now those results in Table I.

TABLE I.

Number of p.s.p.	0 or 1	$\geqslant 2$	total	Chamber collecting time
Number of disintegration	594	66	660	
Corrected number of disintegrations (see Part A)	—	—	1760	1500 s

The knowledge of the chamber collecting time enables to evaluate the rates of occurrence, e.g. for day and gram of lead, of the disintegrations produced by cosmic rays at 3500 m a.s.l. (geomagnetic lat. 47° 7′ N). Yet, it

([9]) B. P. GREGORY and J. H. TINLOT: *Phys. Rev.*, **81**, 675 (1951).

([10]) W. L. WHITTEMORE and R. P. SHUTT: *Phys. Rev.*, **86**, 940 (1952).

([11]) C. E. MILLER, J. E. HENDERSON, G. R. GARRISON, D. S. POTTER, W. M. SANDSTROM and J. TODD: *Phys. Rev.*, **94**, 167 (1954).

([12]) We defined a *penetrating shower particle* (p.s.p.) a penetrating particle which could be seen to ionize near the minimum ($\leqslant$ twice the minimum) before and after crossing the plate just close the one where the disintegration took place. The corresponding energies for protons and μ-mesons are at least 270 and 60 MeV respectively.

should be noticed that the total thickness of lead contained within the chamber was of the order of a nuclear interaction lenght and therefore some of the disintegrations observed could have been of secondary origin. No allowance was made for this effect, whose importance was believed of minor concern here.

Let us consider first the rate of occurrence of the disintegrations showing within the chamber with 2 p.s.p. at least, that is the rate of the penetrating showers containing two particles at least. The lead volume available for the production of disintegrations that could be seen in the illuminated portion of the chamber was 6 900 cm^3. (Only the first eight plates downwards were considered.) Then one gets the rate of 0.05 disintegrations for day and lead gram. This figure is believed to be rather significant, because the number of disintegrations with 2 p.s.p. at least is just an experimental datum obtained without corrections.

More questionable is on the contrary the rate of occurrence of all the nuclear disintegrations in lead. In fact, to obtain this rate, we must correct the experimental figure in order to take into account those disintegrations with 0 or 1 p.s.p., whose heavily ionizing particles did not emerge from the lead plates. In Part A the total number of disintegrations was estimated as 1 760, which would give a rate of 1.3 disintegrations for day and lead gram. It must be emphasized, however, that this figure can only be regarded as indicative of an order of magnitude.

We have also observed a few disintegrations produced in collisions with nuclei of the gas filling the chamber (argon + ethil alcohol and water vapor, at total pressure of 65 cm_{Hg} and temperature about 18 °C). After rejecting the few cases in which some doubt could be left that the star seen in the gas was caused by radioactive contamination, we remain with 8 disintegrations (2 from ionizing and 6 from non-ionizing particles), recognized basing on the same criteria adopted in Part A for lead disintegrations ([13]). Now we have that, apart from the statistical significance, the 8 disintegrations referred to above would indicate a rate of occurrence notably higher than the lead rate. A similar observation had also been reported previously by Powell ([14]). In the present experiment the illuminated volume of gas within the chamber was about 25 dm^3, and if we suppose that the interactions observed took place in collisions against argon nuclei, we get a rate of 20 disintegrations per gram-atom and hour (11 disintegrations per day and gram of argon). Yet, in a recent research actually intended to the study of interactions in different gases at mountain height, Brown ([15]), including

([13]) Moreover we did find one event that could be reasonably ascribed to a V^0-decay (see Part A).

([14]) W. M. Powell: *Phys. Rev.*, **69**, 385 (1946).

([15]) W. W. Brown: *Phys. Rev.*, **93**, 528 (1954).

in the statistics all the stars releasing in the gas more than 8 MeV energy, finds for argon the value of 8.9 disintegrations per gram-atom and hour. We can indicate a possible reason for the discrepancy in the fact that the presence of many plates in our chamber presumably results in the production of a considerable local flux of neutrons.

4·2. *Association of events within the chamber.* – Given that the photographs we gathered were taken by the random expansion technique, we could propose to get an indication as to the rate at which the events caused by the nucleonic component may be accompanied, within the chamber volume, by other events, due to the same as well as to different components. To do that, we picked out the photographs showing nuclear disintegrations, and searched them for the presence of any accompanying event.

The association of nuclear disintegrations between themselves was first investigated. We found that in 29 photographs there was more than one nuclear disintegration. In 7 of these cases the coincidence of the events may be considered as being casual. The remaining 22 cases are most satisfactorily accounted for as examples of nuclear cascades inside the chamber: the « primary » events took place in the lead plates, and so did also all the « secondaries », but one which happened in the chamber gas. In Table II some data concerning the observed cascades are summarized.

TABLE II.

Link between primary and secondary disintegration	Number of observed cascades	Total number of p.s.p.; from	
		primary disintegrations	secondary disintegrations
Ionizing	10	13	9
Non ionizing	10	9	2
Undecided	2	0	0

The cascades reported in Table II do not represent, of course, the actual picture of the development of nuclear disintegrations through the lead plates, since many events certainly escaped the observation because of the thickness of the plates. Anyhow, given that the twofold events referred to above can be accounted for as nuclear cascades, we are not interested here in discussing them any further: their presence is conveniently explained by the knowledge now fairly well acquired ([16]) of the interaction lenghts of the particles emitted from nuclear disintegrations.

([16]) A. LOVATI, A. MURA, C. SUCCI and G. TAGLIAFERRI: *Nuovo Cimento*, **8**, 271 (1951); W. O. LOCK and G. YEKUTIELI: *Phil. Mag.*, **43**, 231 (1952).

The association of nuclear disintegrations with other types of events was examined in the following way. We took, out of the photographs showing nuclear disintegrations, 200 of them and searched on these photographs the presence of penetrating particles crossing two plates at least, electronic showers showing with 3 particles at least, and single heavily ionizing particles; moreover we counted also the particles that could be seen in the region between the chamber top and the first lead plate. The same research was performed on the 200 photographs that orderly followed, in the respective films, the ones showing the nuclear disintegrations. The results for the two samples of photographs are compared in Table III.

TABLE III.

	Number of p.p. crossing 2 plates at least	Number of electronic showers	Number of heavily ionizing particles	Number of particles from the chamber top
Photographs showing nuclear disintegrations (200) . . .	412	16	71	290
Photographs orderly following the ones showing nuclear disintegrations (200) .	385	19	80	310

As one can see, the nuclear disintegrations are not likely to be accompanied, within the chamber sensitive volume, by other events such as the ones investigated. We want to mention also that no sensible difference was noticed between the group of photographs showing more energetic nuclear disintegrations (with $\geqslant 2$ p.s.p.) and the group of photographs showing less energetic disintegrations (without p.s.p.).

The above results seem to indicate that at our observational height the particles of the nucleonic component with energies not higher than a few GeV are neither associated, within volumes of some tens dm^3, between themselves, nor with penetrating particles and electronic showers.

5. – Some Results on the Soft Component.

5·1. *Zenith angle dependence of the directional intensity.* – The showers that did come out frome the first lead plate with three electrons at least were selected and considered in the present analysis. These showers included both photon- and electron-initiaded cascades, and their minimum energy was of the order of 200 MeV. Care was taken to exclude the cases where the shower initiating

rays, on impinging on the first chamber plate, were closely accompanied by other particles. It may be believed that the showers observed in the chamber had not suffered any appreciable effect, as regards the nature, direction and energy of the shower initiating particle, while crossing the laboratory roof and chamber top, whose whole thickness was only 2 cm of light material (about 0.2 radiation lengths).

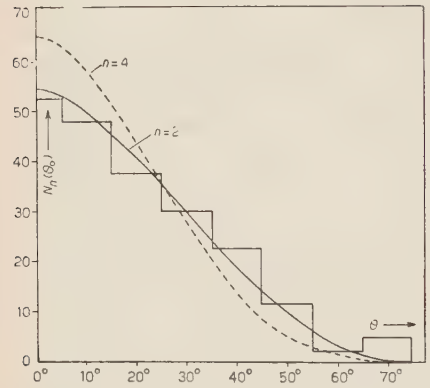

Fig. 3. – Distribution of the projected zenith angles ϑ_0 for 362 shower-producing electrons with energies greater than 200 MeV. The curves give the expected values according to law $I = I_v \cos^n \theta$, with $n = 2$ (solid line) and with $n = 4$ (broken line).

The zenith angle projected distribution was determined for the shower-producing electrons only, and not for the photons, due to the incertitude in individuating the direction of motion of the latters, especially when dealing with showers containing very few particles. The distribution resulting from 362 cases examined is shown in Fig. 3, and results in good agreement with a law $I = I_v \cos^2 \theta$. The same conclusion for the whole soft component was obtained by SANDS [17] with counter telescope technique.

5·2. *Rate of occurrence of the soft component.* – It is not easy to deduce the rate of occurrence of the soft component with the present technique. However, considering that the zenith angle distribution law is practically the same for the hard, as well as for the soft component, the comparison between the number of penetrating particles crossing the two first lead plates and the number of electron-photon showers coming out from the first plate can give a tentative indication of the intensity ratio of the hard and soft components. With our lower energy limits of about 90 and 300 MeV, respectively for μ-mesons and protons, and 200 MeV for electron-photon showers, this ratio turned out to be 8.2.

5·3. *Energy spectrum of electronic showers.* – The cascades, whose point of origin and direction of shower axis were such as to render very likely that they fully developped within the illuminated volume of the chamber, were classified according to the energy estimated from WILSON's [18] calculations up to 300 MeV and from ARLEY's [19] tables beyond 300 MeV (see Part A).

[17] M. SANDS: *Phys. Rev.*, **73**, 1338 (1948).
[18] R. R. WILSON: *Phys. Rev.*, **79**, 204 (1950).
[19] N. ARLEY: *Stochastic Processes and Cosmic Radiation* (New York, 1949).

In Fig. 4 the energy distribution for 563 showers is plotted in a bi-logarithmic scale: it is apparent that a straight line with a slope of — 2.5 can well approximate the experimental data for energies greater than 300 MeV. If we consider that value as the exponent of a simple power law representing the band here investigated of the differential energy spectrum, we can say that there is fair agreement between our results and HAZEN's ([20]) ones. No detectable difference appears between the energy spectra plotted separately for showers produced by electrons and by photons.

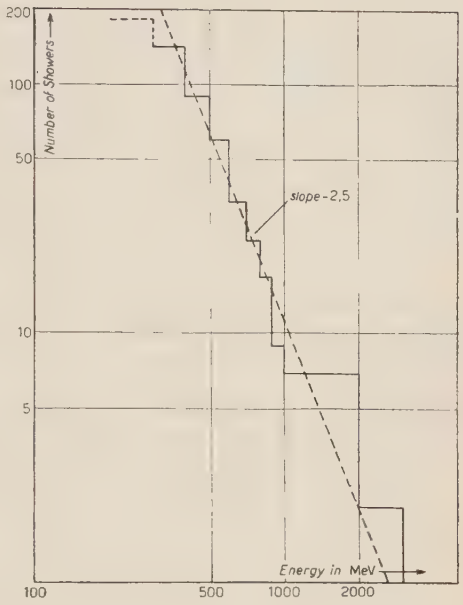

Fig. 4. – Differentilal energy spectrum of electron-photon showers at 3 500 m, obtained from a total of 563 events.

6. – Acknowledgments.

The authors wish to acknowledge the interest and encouragement of Professors G. POLVANI and P. CALDIROLA during the preparation of this paper. They are also deeply indebted to Dr. P. CASALE for his collaboration in the early part of the work, and to Drs. M. BOSSI and A. ROSSI for the assistance in carrying out the measurements.

The financial helps of the A.N.I.D.E.L. and of the « Gruppo Amici dell'Istituto » are gratefully acknowledged.

([20]) W. E. HAZEN: *Phys. Rev.*, **65**, 67 (1944).

RIASSUNTO

Il presente lavoro costituisce la seconda parte dell'analisi di alcuni aspetti della radiazione cosmica a quota di montagna, sulla base di 16 000 fotografie di espansioni a caso di una camera di Wilson. La camera di volume utile $60 \times 50 \times 15$ cm^3, conteneva 9 piastre di piombo dello spessore di 18 g cm^{-2} ciascuna. Della componente

penetrante è stata studiata la dipendenza dall'angolo zenitale della intensità direzionale, ritrovando una legge del tipo $I = I_v \cos^2 \theta$, e la frequenza di produzione di elettroni di knock-on. Si è ricavata la frequenza di produzione delle disintegrazioni nucleari in piombo e si è ricercata la correlazione fra le disintegrazioni nucleari ed altri eventi della radiazione cosmica. Della componente molle si è pure studiata la dipendenza dall'angolo zenitale della intensità direzionale, trovando di nuovo una legge del tipo $\cos^2 \theta$, e lo spettro differenziale di energia, che è risultato approssimabile con $N(E)\,\mathrm{d}E = k E^{-2.5}\,\mathrm{d}E$ per energie maggiori di 300 MeV.

On the Orbital Electron Capture in ^{195}Au.

A. Bisi and L. Zappa

Istituto di Fisica Sperimentale del Politecnico - Milano

(ricevuto il 26 Luglio 1954)

Summary. — The integrating features of the proportional counter spectrometer have been used to investigate the electron capture decay in ^{195}Au. The transition energies to the excited levels of ^{195}Pt were found to be $(E_0)_{d_{3/2}-f_{5/2}} = 143 \pm 17$ keV, $(E_0)_{d_{3/2}-p_{3/2}} = 172 \pm 17$ keV. The two transitions are classified as once-forbidden ($\Delta I = 0$, 1, yes).

1. – Introduction.

A long lived activity ($T_{\frac{1}{2}} = 185 \pm 3$ d) in gold isotopes from deuteron bombardments of platinum was assigned to ^{195}Au by Wilkinson [1]. The decay was attributed to K-capture, as no positrons were observed. A further determination of the half-life ($T_{\frac{1}{2}} = 180 \pm 15$ d) and an investigation of the decay scheme of this isotope were performed by Steffen, Huber and Humbel [2]. More recently the decay scheme of ^{195}Au was improved by de Shalit, Huber and Schneider [3] by means of coincidence measurements and of a careful investigation of the electron spectrum. The decay scheme is shown in Fig. 1 and in Table I are listed the conversion coefficients for the different γ-rays. Spin and magnetic moment of the ground state of ^{195}Pt have been measured [4]. The orbitals of the excited levels have been assigned through the measurement of conversion coefficients and on the basis of the nuclear

(1) G. Wilkinson: *Phys. Rev.*, **75**, 1019 (1949).
(2) R. M. Steffen, O. Huber and F. Humbel: *Helv. Phys. Acta*, **22**, 167 (1949).
(3) A. de Shalit, O. Huber and H. Schneider: *Helv. Phys. Acta*, **25**, 279 (1952).
(4) J. E. Mack: *Rev. Mod. Phys.*, **22**, 64 (1950).

TABLE I.

γ	$\bar{\alpha}$				α				K/L	L/M
	K	L	M	Tot.	K	L	M	Tot.		
29		$\geqslant 0.75$	$\geqslant 0.13$	$\geqslant 0.88$		$\geqslant 6.0$	$\geqslant 1.3$	$\geqslant 7.3$	—	4.6 ± 0.4
.97	0.74	0.13	0.03	0.90	7.4	1.3	0.3	9.0	5.8	—

shell model. The ground state of ^{195}Au has been classified $d_{\frac{3}{2}}$ by making analogy to the ground states of ^{193}Ir and ^{197}Au.

The aim of this work was the determination of the transition energy in the orbital electron capture of ^{195}Au and of the degree of forbidness of this transition.

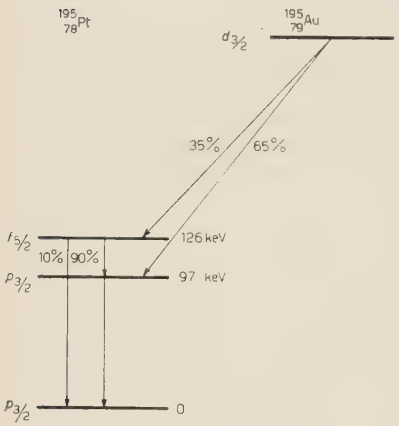

Fig. 1. – Decay scheme of ^{195}Au.

2. – Experimental Apparatus.

X- and γ-radiations from ^{195}Au were investigated by means of a proportional counter spectrometer described elsewhere (5). The counter filled with a 90% argon and 10% methane mixture (1.5 atm total pressure) was operated by a + 5 000 V regulated supply. This high voltage power supply shows a drift of not more than 0.01 percent for a period of some hours in continuous operation (6).

After amplification the pulse size was measured by means of a single channel (7) and a twenty channel (8) electronic pulse analyzer.

^{195}Au was produced by irradiation of Pt with deuterons in the cyclotron of Amsterdam. The active sample, a carrier free solution of $AuCl_3$ in diluted HCl, was studied long after the irradiation, when the short-lived activities had practically disappeared.

(5) G. BERTOLINI, A. BISI, E. LAZZARINI and L. ZAPPA: *Nuovo Cimento*, **11**, 539 (1954).

(6) W. A. HIGHINBOTHAM: *Rev. Sci. Instr.*, **22**, 429 (1951).

(7) J. E. FRANCIS jr., P. R. BELL and J. C. GUNDLACH: *Rev. Sci. Instr.*, **22**, 133 (1951).

(8) E. GATTI: *Nuovo Cimento*, **11**, 153 (1954).

3. – γ- and X-Radiations from ^{195}Au.

The following radiations were observed:

a) 29 keV γ-rays;

b) 97 keV γ-rays;

c) L X-rays characteristic of Pt from L- and K-capture and from internal conversion of the γ-rays;

d) K X-rays characteristic of Pt from K-capture and from K internal conversion of the γ-rays.

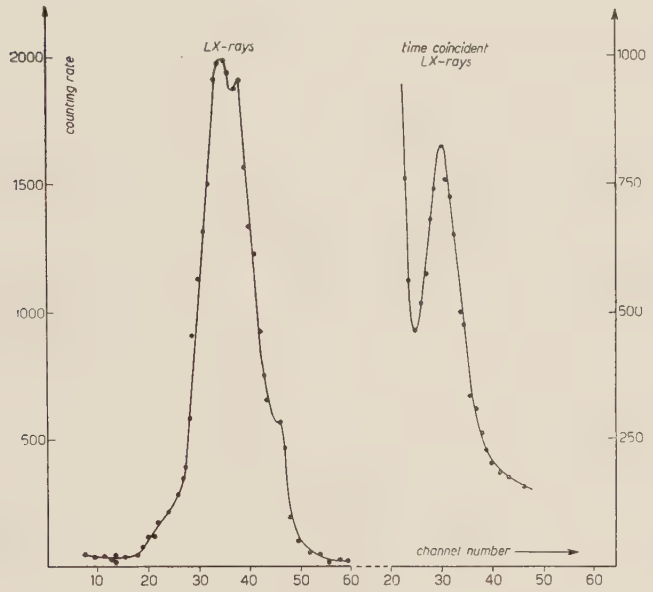

Fig. 2. – Pulse height distribution for L X-radiations from ^{195}Au.

Furthermore two peaks at energies 19 keV and 38.5 keV were observed. The appearance of these peaks can be easily understood when the integrating features of the proportional counter are taken into account. The 19 keV peak arises from two time coincident L X quanta, the 38.5 keV peak arises from the 29 keV and the L X time coincident quanta.

The height distributions of the obtained pulses are shown in Figs. 2, 3, 4. The 126 keV cross-over γ-ray was not observed owing to its low intensity and to the small efficiency of the counter in detecting high energy radiations.

The relative intensities of the different radiations were obtained from the areas under the peaks after subtracting the background and after correction for the detection efficiency of the counter (9). The results are summarized in Table II.

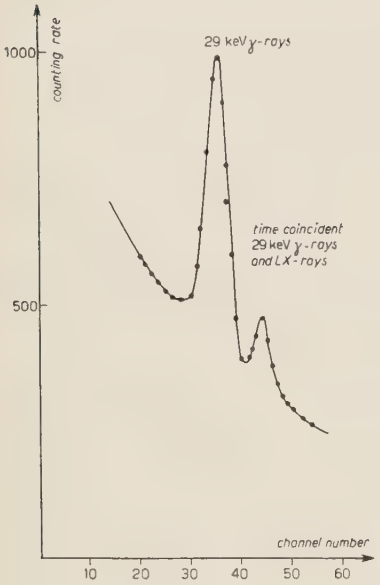

Fig. 3. – Pulse height distribution for 29 keV γ-radiations.

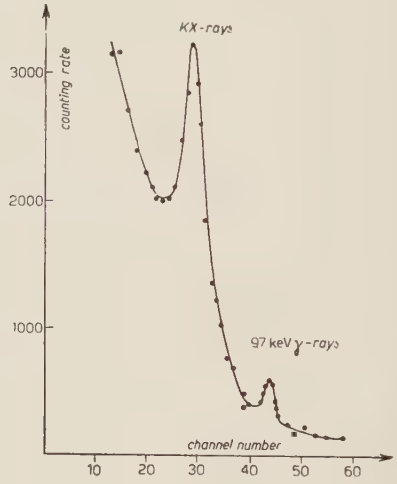

Fig. 4. – Pulse height distribution for K X- and 97 keV γ-radiations.

TABLE II.

ν	I_ν/I_K	I^*_{38}/I^*_ν
L	0.408 ± 0.016	—
29	0.0142 ± 0.0013	0.104 ± 0.002
97	0.141 ± 0.013	—

4. – Symbols.

In the following section we will adopt the following symbols:

I^*_ν = « measured » intensity of radiation of ν-type,

I_ν = « true » intensity of radiation of ν-type (measured intensity corrected for detection efficiency),

f_ν = detection efficiency of radiation of ν-type,

(9) A. BISI and L. ZAPPA: *Nuovo Cimento*, **12**, 211 (1954).

P^L_{a-b} and P^K_{a-b} = probabilities for the L-capture and for the K-capture in the a-b transition,

ε_{a-b} = branching of the ^{195}Au decay via a-b transition,

α^ν_K = K internal conversion coefficient of radiation of ν-type (α^ν_L, α^ν_M have analogous definition),

$\bar{\alpha}^\nu_K$ = K internal conversion ratio of radiation of ν-type ($\bar{\alpha}^\nu_L$, $\bar{\alpha}^\nu_M$ have analogous definition),

ω_K = K shell fluorescence yield of Pt,

ω_{LK} = fluorescence yield for transition to the L-level following the K-capture and the K internal conversion of γ-rays,

ω_{LL} = fluorescence yield for transition to the L-levels following the L-capture and the L internal conversion of γ-rays,

$(W_0)_{a-b}$ = nuclear energy change in the a-b transition,

W_K = $1 - \frac{1}{2}\alpha^2 Z^2_{\text{eff}}$ ($Z_{\text{eff}} = Z - 0.3$, $\alpha = \frac{1}{137}$) = K shell energy.

W_L = $1 - \frac{1}{8}\alpha^2 Z^2_{\text{eff}}$ ($Z_{\text{eff}} = Z - 4.15$) = L shell energy.

$(\psi_{L_I}/\psi_K)^2$ = ratio of L_I- and K-shell electron densities at the nuclear radius.

5. – L-Capture to K-Capture Ratio in $d_{3/2}$ - $f_{5/2}$ Transition.

The integrating features of the proportional counter provide a successful method for the determination of the ratio of L-capture to K-capture in the $d_{3/2}$ - $f_{5/2}$ transition of ^{195}Au. The existence in the γ-spectrum of a peak at 38.5 keV energy, due to the 29 keV and the L X time-coincident quanta was remarked in section 3. More exactly this peak arises from the following occurrences:

a) the L X-rays from L-capture or from the reorganization following K-capture, which are time coincident with the unconverted 29 keV γ-rays (no contribution from the conversion of the 97 keV γ-rays);

b) the L X-rays from L-conversion or from the reorganization following K-conversion of 97 keV γ-rays, which are time coincident with the unconverted 29 keV γ-rays (no contribution from the electron capture);

c) the L X-rays from electron capture which are time coincident with the unconverted 29 keV γ-rays and with the L X-rays from internal conversion of 97 keV γ-rays (one of the two L X-rays is not detected from the counter).

When the different occurrences *a*), *b*), *c*), are taken into account, one can easily deduce the following relation:

$$(1) \qquad \left\{P^L_{d_{3/2}\text{-}f_{5/2}}(\omega_{LL} - \omega_{LK}) + \omega_{LK}\right\}\left\{1 - f_L(\bar{\alpha}^{97}_L\omega_{LL} + \bar{\alpha}^{97}_K\omega_{LK})\right\} = \frac{2}{f_L}\frac{I^*_{38}}{I^*_{29}} - (\alpha^{97}_L\omega_{LL} + \bar{\alpha}^{97}_K\omega_{LK}) .$$

In equation (1) the efficiency f_L has been calculated as shown in a previous note ([9]). The $\bar{\varkappa}^{97}$ are listed in Table I. As regards the fluorescence yields ω_{LK}, ω_{LL} they have been deduced from the partial yields $\omega_{L_{\rm I}}$, $\omega_{L_{\rm II}}$, $\omega_{L_{\rm III}}$ and from the relative excitations (u_i and v_i) of the three L-levels. I.e.:

$$\omega_{LK} = u_1\omega_{L_{\rm I}} + u_2\omega_{L_{\rm II}} + u_3\omega_{L_{\rm III}}$$

$$\omega_{LL} = v_1\omega_{L_{\rm I}} + v_2\omega_{L_{\rm II}} + v_3\omega_{L_{\rm III}}$$

The partial yields are taken from KINSEY ([10]):

$$\omega_{L_{\rm I}} = 0.095\,, \qquad \omega_{L_{\rm II}} = 0.37\,, \qquad \omega_{L_{\rm III}} = 0.28\,.$$

The relative excitations v_i of the three L-subshells depend on the atomic number, on the quantum energy, and on the nature of the γ-transition. In our case (the 29 keV and 97 keV γ-radiations are classified $M\,1$) we have ([11]):

$$v_1 = 0.90\,, \qquad v_2 = 0.08\,, \qquad v_3 = 0.02\,. \tag{2}$$

The relative excitations of the three L-subshells from L-capture are not very different from (2). Within the accuracy of our measurements no serious error arises from assuming the values (2). Consequently we have:

$$\omega_{LL} = 0.12\,.$$

For the relative excitations u_i resulting from the reorganization following K-capture and K internal conversion we have approximately ([12]):

$$u_1 = 0\,, \qquad u_2 = 1/3\,, \qquad u_3 = 2/3\,.$$

This approximation is satisfactory for heavy elements where the K-shell is filled mostly by radiative transitions. Hence we have:

$$\omega_{LK} = 0.29\,.$$

From the indicated values of the fluorescence yields and using the data of Tables I and II, equation (1) gives:

$$\left(\frac{P^L}{P^K}\right)_{d_{3/2}\text{-}f_{5/2}} = 0.58 \pm 0.14\,.$$

([10]) B. B. KINSEY: *Canad. Journ. Res.*, **26***a*, 404 (1948).

([11]) M. RIOU: *Journ. de Phys. et Rad.*, **13**, 593 (1952).

([12]) E. H. S. BURHOP: *The Auger Effect and other Radiationless Transitions* (Cambridge, 1952), p. 45.

6. – Transition Energy.

A close correlation between the type of transition and the shell structure has been shown by MAYER, MOSZKOWSKI and NORDHEIM ([13]). They listed a group of odd A nuclei which shows a parity change and $\Delta I = 0$ or 1, and classified them as once-forbidden. These transitions have $\log ft$ ranging from 6 to 8 without a clear distinction between $\Delta I = 0$ and $\Delta I = 1$. A striking feature of these transitions is the allowed shape of their spectra.

On the basis of the decay scheme of Fig. 1 we confidently classify the two electron capture decays of ^{195}Au as once-forbidden. This assumption will be further justified from the results of the following sections.

Then MARSHAK's formulae ([14]) for allowed transitions can be used:

$$\frac{P^L}{P^K} = \left(\frac{\psi_{L_I}}{\psi_K}\right)^2 \left(\frac{W_0 + W_L}{W_0 + W_K}\right)^2 .$$

With $(P^L/P^K)_{d_{3/2}\text{-}f_{5/2}} = 0.58 \pm 0.14$ and the $(\psi_{L_I}/\psi_K)^2$ ratio calculated by ROSE and JACKSON ([15]) as a function of Z, we have for the transition energy:

$$(E_0)_{d_{3/2}\text{-}f_{5/2}} = 143 \pm 17 \text{ keV}$$

and consequently for the transition $d_{3/2}$ - $p_{3/2}$:

$$(E_0)_{d_{3/2}\text{-}p_{3/2}} = 172 \pm 17 \text{ keV} .$$

The correctness of these results can be proved by the following argument: by plotting the difference in the binding energy of the Au-Pt odd isobaric pairs ($A = 197$, 199) against the mass number we obtain for $(E_0)_{d_{3/2}\text{-}f_{5/2}}$ about 150 keV.

7. – L-Capture to K-Capture Ratio in $d_{3/2}$ - $p_{3/2}$ Transition.

From the results of the last section we can deduce the L-capture to K-capture ratio in $d_{3/2}$ - $p_{3/2}$ transition. We have:

$$\left(\frac{P^L}{P^K}\right)_{d_{3/2}\text{-}p_{3/2}} = 0.41 .$$

([13]) M. G. MAYER, S. A. MOSZKOWSKI and L. W. NORDHEIM: *Rev. Mod. Phys.*, **23**, 1315 (1951).

([14]) E. R. MARSHAK: *Phys. Rev.*, **61**, 431 (1942).

([15]) M. E. ROSE and J. L. JACKSON: *Phys. Rev.*, **76**, 1540 (1949).

Now we are able to calculate the relative intensity of the L X- and K X-radiations from ^{195}Au provided that the branching ratios $\varepsilon_{a\text{-}b}$ and the internal conversion coefficients of the different γ-rays are known. The following relation can be easily derived:

$$(3) \qquad \omega_{LK} - \frac{I_L}{I_K}\varepsilon_2\bar{\alpha}_K^{97}\omega_K + \varepsilon_2(\bar{\alpha}_L^{97}\omega_{LL} + \bar{\alpha}_K^{97}\omega_{LK}) + \\ + \varepsilon_1\left[(\bar{\alpha}_L^{29}\omega_{LL} + \bar{\alpha}_L^{97}\omega_{LL} + \bar{\alpha}_K^{97}\omega_{LK}) - \frac{I_L}{I_K}\bar{\alpha}_K^{97}\omega_K\right] = \\ = \frac{I_L}{I_K}\omega_K - (\varepsilon_1 P_1^L + \varepsilon_2 P_2^L)\left(\omega_{LL} - \omega_{LK} + \frac{I_L}{I_K}\omega_K\right).$$

$$\varepsilon_1 = \varepsilon_{d_{3/2}\text{-}f_{5/2}};\ P_1^L = P^L_{d_{3/2}\text{-}f_{5/2}}$$

$$\varepsilon_2 = \varepsilon_{d_{2/2}\text{-}p_{3/2}};\ P_2^L = P^L_{d_{3/2}\text{-}p_{3/2}}\ .$$

In eq. (3) the contribution of the 126 keV cross-over transition has been neglected; $\bar{\alpha}_K^{97}$, $\bar{\alpha}_L^{97}$, ε, ε_2 were taken from Tables I and II. The fluorescence yields have been previously discussed. $\bar{\alpha}_L^{29}$ have been calculated on the basis of our intensity measurements and the branching ratios of Fig. 1. We have obtained:

$$\alpha_{\text{tot}}^{29} = 32$$

and from Table I:

$$\alpha_L^{29} = 26\ .$$

This value agrees satisfactorily with the theoretical calculations of GELLMAN, GRIFFITH and STANLEY ([16]), for a $M1$ transition.

Finally eq. (3) gives:

$$\frac{I_L}{I_K} = 0.38\ ,$$

in satisfactory agreement with the measured value:

$$\frac{I_L}{I_K} = 0.408 \pm 0.016\ .$$

([16]) K. GELLMAN, B. A. GRIFFITH and J. P. STANLEY: *Phys. Rev.*, **80**, 866 (1 950).

8. – Conclusions.

The results of the previous sections lead to the following conclusions. ^{195}Au decays into excited states of ^{195}Pt through L- and K-capture; the two transitions, $d_{3/2} - f_{5/2}$ and $d_{3/2} - p_{3/2}$, can be classified, following MAYER MOSZKOWSKI and NORDHEIM ([14]), as parity forbidden with allowed shape. The two transition energies are respectively:

$$(E_0)_{d_{3/2}-f_{5/2}} = 143 \pm 17 \text{ keV}$$

$$(E_0)_{d_{3/2}-p_{3/2}} = 172 \pm 17 \text{ keV}$$

and the log ft values ($T_{\frac{1}{2}} = 185$), from Feenberg and Trigg's formula ([17]) (corrected for L-capture) are:

$$(\log ft)_{d_{3/2}-f_{5/2}} = 6.5 , \qquad (\log ft)_{d_{3/2}-p_{3/2}} = 6.6 .$$

No difference can be noted between the $\Delta I = 1$ and $\Delta I = 0$ transitions. From this it can be argued that the matrix elements of the two transitions are nearly equal. A more striking proof comes from following argument: assuming the matrix element for the two transitions is the same we can deduce the branching ratio ε from the transition probabilities:

$$\varepsilon_{d_{3/2}-f_{5/2}} = 0.43; \qquad \varepsilon_{d_{3/2}-p_{3/2}} = 0.57 ,$$

in a rather surprising agreement with the measured value (3).

We wish to thank Professor G. BOLLA, director of the Institute, for his kind interest in this work, and Professor B. FERRETTI for a helpful discussion.

([17]) E. FEENBERG and G. TRIGG: *Rev. Mod. Phys.*, 22, 399 (1950).

RIASSUNTO

Viene studiato il decadimento per cattura elettronica dell'^{195}Au sfruttando le proprietà integratrici dello spettrometro a contatore proporzionale. Le energie di transizione ai livelli del ^{195}Pt risultano: $(E_0)_{d_{3/2}-f_{5/2}} = 143 \pm 17$ keV, $(E_0)_{d_{3/2}-p_{3/2}} = 172 \pm$ ± 17 keV. Le due transizioni sono classificate 1° - proibite ($\Delta I = 0$, 1, con cambio di parità).

Correlazioni tra disintegrazioni nucleari provocate da raggi cosmici.

M. di Corato, R. Levi Setti, M. Panetti e P. Pinto

Istituto di Scienze Fisiche dell'Università - Milano
Istituto Nazionale di Fisica Nucleare - Sezione di Milano

A. Milone

Istituto di Fisica dell'Università - Genova

(ricevuto il 3 Agosto 1954)

Riassunto. — L'analisi statistica della distribuzione di circa 3000 stelle prodotte da raggi cosmici in lastre fotografiche nucleari ha rivelato la presenza di correlazioni tra le stelle stesse, che non risultano distribuite a caso. L'entità dell'effetto di associazione osservato e il suo andamento in funzione delle distanze reciproche tra le stelle fanno ritenere che esso sia dovuto alle interazioni secondarie dei neutroni veloci emessi dalle stelle nell'emulsione.

Introduzione.

Le interazioni secondarie di particelle cariche emesse da disintegrazioni nucleari in lastre fotografiche sono osservabili come «stelle doppie» (stelle legate da un ramo ionizzante). La presenza invece di interazioni secondarie prodotte da particelle neutre emesse da stelle nell'emulsione può essere rivelata e studiata soltanto con metodi statistici. Mentre la distribuzione spaziale delle stelle primarie obbedisce generalmente alla legge del caso, la distribuzione complessiva delle primarie e delle secondarie ne differisce per un eccesso di coppie di stelle a piccole distanze reciproche.

Alcuni autori ([1-7]) hanno studiato tale problema con emulsioni nucleari esposte alla radiazione cosmica. Alcuni di essi non hanno trovato deviazione significativa tra i risultati sperimentali e quelli previsti dalla legge del caso, altri hanno segnalato la presenza di un effetto di associazione più o meno rilevante, tale, in alcune circostanze, da non essere interpretabile sulla base di processi di cascata nucleonica noti.

Nel presente lavoro si effettua una analisi statistica della distribuzione delle stelle in lastre nucleari e, ammettendo che le particelle responsabili dell'effetto di correlazione siano neutroni veloci emessi dalle stelle primarie presenti nell'emulsione, si determina il valore del prodotto, $q\sigma$, del numero di neutroni emessi in media in ogni disintegrazione per la sezione di produzione di stelle da parte di neutroni.

1 - Distribuzione statistica delle stelle.

1·1. *Metodo sperimentale.* – Su una superficie di 487 cm² di lastre Ilford G5 di 400 μ di spessore, esposte per due ore a circa 20 000 m di quota, sono state osservate 2118 stelle con 4 o più rami ionizzanti, 603 stelle a tre rami e 269 stelle a 2 rami; inoltre 13 stelle doppie, non comprese quelle originate da mesoni σ. Per la discriminazione delle stelle a due rami, sono stati adottati i criteri suggeriti da MERLIN e PIERUCCI ([8]).

Le coordinate delle stelle, proiettate sul piano della lastra, sono state riportate in scala su piantine per zone di emulsione di (3×5) cm². Prima di esaminare la distribuzione alle piccole distanze, dove si può prevedere di osservare l'effetto di correlazione, è sembrato conveniente verificare l'uniformità di esplorazione delle lastre impiegate, su aree ancora abbastanza grandi da non risentire dell'effetto stesso. Una eventuale esplorazione selettiva, tendente a segnalare di preferenza le stelle vicine, può portare infatti ad effetti spuri di associazione. Il controllo è stato effettuato nel modo seguente: la zona esplorata è stata divisa in quadratini di (0.5×0.5) cm², e la distribuzione del numero di quadratini in funzione del numero delle stelle con 2 o più rami contenute in ciascuno di essi, è stata messa a confronto con la distribuzione di Poisson.

([1]) L. LEPRINCE-RINGUET e J. HEIDEMANN: *Nature*, **161**, 844 (1948).
([2]) T. T. LI e D. H. PERKINS: *Nature*, **161**, 844 (1948).
([3]) T. T. LI: *Phil. Mag.*, **41**, 1152 (1950).
([4]) G. DAVIS: *Phil. Mag.*, **43**, 472 (1952).
([5]) L. BARBANTI SILVA, C. BONACINI C. DE PIETRI, G. LOVERA e R. PERILLI FEDELI: *Nuovo Cimento*, **9**, 630 (1952).
([6]) K. E. DAVIS, J. B. MARION, J. F. DELORD e K. M. KING: *Phys, Rev.*, **88** 368 (1952).
([7]) F. B. BROWN e A. V. MASKET: *Phys. Rev.*, **88**, 1204 (1952).
([8]) M. MERLIN e O. PIERUCCI: *Nuovo Cimento*, **8**, 518 (1951).

Con le dimensioni scelte per la cella elementare, il massimo della distribuzione di frequenza si ha per celle contenenti una sola stella. In tal modo si ottiene la massima informazione sulla efficienza di osservazione di stelle isolate.

La fig. 1 mostra il confronto tra la distribuzione di Poisson e quella trovata sperimentalmente. L'accordo è molto buono e il metodo del χ^2 fornisce una probabilità del 97 % che le deviazioni esistenti tra le due distribuzioni siano casuali. Si può quindi escludere che vi sia stata esplorazione preferenziale di stelle vicine a danno di quelle isolate.

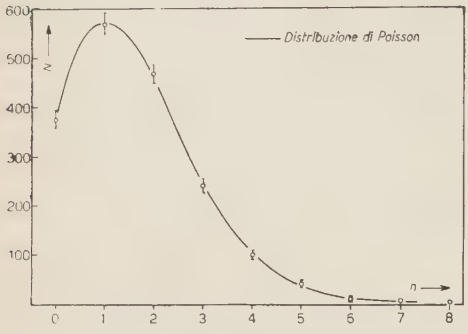

Fig. 1.

Ciò posto, si è determinata la distribuzione del numero di coppie di stelle in funzione della loro distanza reciproca in proiezione, per intervalli Δr di 0,5 mm, separatamente per stelle con numero di rami $\nu \geqslant 2$, $\geqslant 3$, $\geqslant 4$. Nella statistica non sono state incluse le stelle doppie. Le distanze comprese tra 0 e 0,5 mm sono state misurate direttamente al microscopio, le distanze maggiori tramite le coordinate delle stelle. Dal confronto tra le distanze misurate al microscopio e quelle calcolate dalle coordinate, si ricava l'errore quadratico medio su queste ultime, che risulta di circa 50 μ.

Si è quindi valutato l'errore sul numero sperimentale N_i di distanze che cadono nell'intervallo i-esimo, (r_i, r_{i-1}), derivante dall'errore di misura sulle distanze stesse: esso risulta indipendente da r_i ed uguale a $\sqrt{0.16 N_i}$. Pertanto, considerando indipendenti gli errori di misura e quelli statistici, si trova che l'errore su N_i è $\sqrt{1{,}16 N_i}$ (*).

1·2. *Previsioni statistiche* – Data una zona rettangolare di lati a, b $(b \leqslant a)$, sulla quale siano distribuite a caso N stelle, il numero medio di coppie di stelle aventi distanze reciproche comprese tra r ed $r+\mathrm{d}r$ è dato da

$$N_c(r)\,\mathrm{d}r = [N(N-1)/2]\cdot f(r)\,\mathrm{d}r\,, \tag{1}$$

dove [3]
$$f(r) = 2r/ab[\pi - 2(a+b)r/ab + r^2/ab]\,, \qquad \text{per } r \leqslant b.$$

(*) Nella valutazione dell'errore statistico sui valori N_i si dovrebbe tener conto del fatto che solo una parte, e precisamente $2N-3$, delle $N(N-1)/2$ distanze possibili, sono tra loro indipendenti, ove N è il numero di stelle contenute in una zona. Nel caso presente, tuttavia, la densità superficiale di stelle e le distanze considerate sono tali che il numero di coppie non indipendenti incluse nella statistica risulta trascurabile.

Integrando la (1) tra r_i e r_{i+1} e sommando i risultati relativi a tutte le zone, si ottengono i numeri $(N_c)_i$ di coppie di stelle da attendersi in media nel caso di distribuzione casuale.

Introduciamo ora l'ipotesi che abbia luogo un processo di produzione di stelle secondarie dovuto a particelle neutre, che per la presente trattazione supponiamo neutroni, e determiniamo la funzione di frequenza $N_{q\sigma}(r)$ delle coppie di stelle casuali e non casuali, eccettuando le stelle secondarie che sono legate alla loro primaria da un legame ionizzante. La probabilità $\Phi(r)\,\mathrm{d}r$ che un neutrone emesso da una stella nell'emulsione generi una stella secondaria nella stessa zona, ad una distanza compresa tra r e $r+\mathrm{d}r$, è espressa da:

$$\Phi(r)\,\mathrm{d}r = \sigma F(r)\,\mathrm{d}r\,, \tag{2}$$

con [9]:

$$F(r)\,\mathrm{d}r = L \exp\left[-L'\sigma' r\right]\left[\operatorname{arctg} h/r - (r/2h)\log\left(1 + h^2/r^2\right)\right](ab/2\pi r) f(r)\,\mathrm{d}r\,,$$

essendo:

L = numero di nuclei per unità di volume dell'emulsione, escluso l'idrogeno;

L' = numero di nuclei per unità di volume dell'emulsione, idrogeno incluso;

σ = sezione media di produzione di stelle da neutroni, dei nuclei dell'emulsione, idrogeno escluso;

σ' = sezione geometrica media dei nuclei dell'emulsione;

h = spessore dell'emulsione.

Si ricava $N_{q\sigma}(r)$ valutando i numeri di coppie formate da associazioni « primaria-primaria », « secondaria-secondaria », « primaria-secondaria di un'altra stella », e « primaria-secondaria propria »:

$$N_{q\sigma}(r)\,\mathrm{d}r = \left[M(M-1)/2 + (N-M)(N-M-1)/2 + (N-M)(M-1)\right]\cdot f(r)\,\mathrm{d}r + Mq\,\Phi(r)\,\mathrm{d}r\,, \tag{3}$$

dove N è il numero di stelle nella zona considerata ed M è il numero di primarie. Tenendo conto che il numero $N-M$ di stelle secondarie soddisfa alla relazione:

$$N - M = Mq\sigma \int_0^{\sqrt{a^2+b^2}} F(r)\,\mathrm{d}r\,, \tag{4}$$

(9) M. Di Corato: *Tesi* Università di Milano (1953).

e ponendo:

$$\int_0^{\sqrt{a^2+b^2}} F(r)\,dr = K\,; \qquad \int_{r_i}^{r_{i+1}} [F(r) - Kf(r)]\,dr = K_i\,,$$

dalla (3), integrando tra i limiti r_i ed r_{i+1} e sommando i risultati relativi a tutte le zone, si ottengono le frequenze:

$$(N_{q\sigma})_i = (N_c)_i + Nq\sigma K_i/(1 + q\sigma K)\,. \tag{5}$$

2. - Stima del parametro $q\sigma$.

Dalla (5) e dai valori sperimentali N_i, imponendo che sia $(N_{q\sigma})_i = N_i$, si può determinare il valore più probabile di

$$\alpha = Nq\sigma/(1 + q\sigma K)\,, \tag{6}$$

con un calcolo di media ponderata sui valori di $\alpha_i = [N_i - (N_c)_i]/K_i$.

$$\bar{\alpha} = \frac{\sum_i \{(N_i - (N_c)_i)/K_i\} K_i^2/1{,}16\, N_i}{\sum K_i^2/1{,}16\, N_i} \tag{7}$$

L'errore su $\bar{\alpha}$ è dato da

$$(\textstyle\sum_i K_i^2/1{,}16 N_i)^{-\frac{1}{2}}\,. \tag{8}$$

Dalle relazioni (6), (7), (8) si ricava il valore più probabile di $q\sigma$ e il relativo errore.

I risultati relativi alle analisi della distribuzione di 2 983 stelle con numero di rami $\nu \geqslant 2$ sono contenuti nella tabella I: nella penultima riga sono indicati i valori di $(N_{q\sigma})_i$ dedotti dalla (5) introducendovi il valore più probabile di $q\sigma$:

$$q\sigma = (4{,}4 \pm 2)\cdot 10^{-24}\ \text{cm}^2\ (*).$$

(*) Allo stesso risultato si giunge applicando il metodo della massima verosimiglianza.

TABELLA I.

Δr (mm)	0–0.5	0.5–1	1–1.5	1.5–2	2–2.5	2.5–3	3–3.5	3.5–4
N_i	106 ± 11	227 ± 16	369 ± 21	492 ± 24	660 ± 28	756 ± 30	875 ± 32	$1\,004 \pm 34$
$(N_c)_i$	78.5	231.1	378.1	519.6	655.4	785.9	910.8	1 030.3
$10^3\,[N_i - (N_c)_i]/N$	9.2	— 1.4	— 3.3	— 9.3	1.5	— 10	— 12	— 8.8
χ_i^2	9.6337	0.0727	0.2190	1.4661	0.0323	1.1376	1.4071	0.6713
$(N_{\overline{qq}})_i$	101.8	239.3	382.9	522.9	657.9	787.8	912.2	1 031.4
$(\chi_{aa}^2)_i$	0.2578	0.6025	0.4975	1.8260	0.0067	1.2915	1.5330	0.7384

$\nu \geqq 2$, 2983 stelle.

TABELLA II.

Δr (mm)	0–0.5	0.5–1	1–1.5	1.5–2	2–2.5	2.5–3	3–3.5	3.5–4
N_i	81 ± 10	184 ± 15	293 ± 18	418 ± 22	545 ± 25	627 ± 27	750 ± 29	838 ± 31
$(N_c)_i$	65.2	192.1	314.2	431.7	544.6	652.9	756.8	856.1
$10^3\,[N_i - (N_c)_i]/N$	5.8	— 3.4	— 7.8	— 5	0.15	— 9.5	— 4	— 6.7
χ_i^2	3.8288	0.3415	1.4304	0.4348	0.0003	1.0274	0.0611	0.3827
$(N_{\overline{qq}})_i$	77.7	196.5	316.7	433.5	545.8	653.9	757.6	856.6
$(\chi_{aa}^2)_i$	0.2297	0.7586	1.7592	0.5542	0.0012	1.1147	0.0782	0.4125

$\nu \geqq 3$, 2721 stelle.

TABELLA III.

Δr (mm)	0–0.5	0.5–1	1–1.5	1.5–2	2–2.5	2.5–3	3–3.5	3.5–4
N_i	49 ± 8	108 ± 11	169 ± 14	238 ± 17	317 ± 19	372 ± 21	451 ± 23	503 ± 24
$(N_c)_i$	39.2	115.5	189.1	259.7	328.9	392.7	455.1	514.9
$10^3\,[N_i - (N_c)_i]/N$	4.6	— 3.5	— 9.5	— 10.2	— 5.6	— 9.8	— 1.9	— 5.6
χ_i^2	2.4500	0.4870	2.1365	1.8132	0.4306	1.0911	0.0369	0.2750
$(N_{qq})_i$	45.5	117.6	190.3	260.5	329.5	393.2	455.4	515.1
$(\chi_{aa}^2)_i$	0.3556	0.7681	2.3841	1.9434	0.4742	1.1430	0.0455	0.2889

$\nu \geqq 4$, 2118 stelle.

La fig. 2*a* mostra la distribuzione di N_i e di $(N_c)_i$ in funzione di r; la fig. 2*b* mostra le deviazioni osservate tra N_i ed $(N_c)_i$ in funzione di r e la curva che rappresenta l'andamento delle deviazioni di $(N_{q\bar{\sigma}})_i$ da $(N_c)_i$. Il metodo del χ^2 indica una probabilità del 5% che l'insieme delle deviazioni osservate tra N_c ed $(N_c)_i$ sia casuale; la probabilità è circa il 50% per le deviazioni tra N_i ed $(N_{q\sigma})_i$.

I risultati analoghi per 2721 stelle con $\nu \geqslant 3$ e per 2118 stelle con $\nu \geqslant 4$,

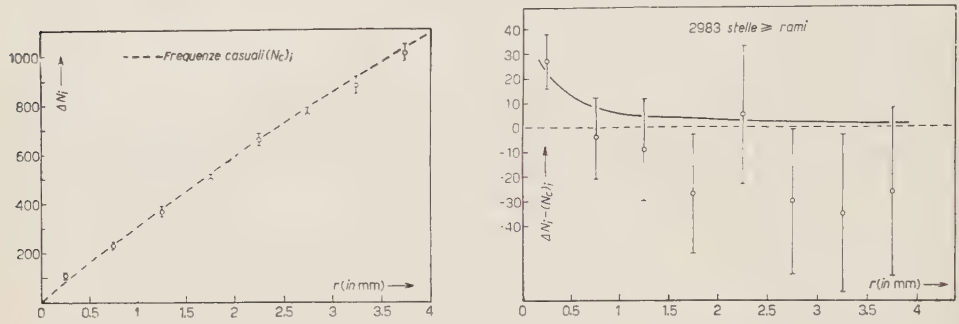

Fig. 2 *a-b*.

sono contenuti rispettivamente nelle tabelle II e III. Il valore più probabile di $q\sigma$ per le stelle con 3 o più rami risulta $2{,}4 \pm 1{,}9$; per le stelle con 4 o più rami risulta $1{,}5^{+1{,}9}_{-1{,}5}$.

Il criterio del χ^2 fornisce probabilità 40% e 28% nei due casi rispettivamente, per le deviazioni tra N_i e $(N_c)_i$; queste probabilità sono circa il 70% ed il 40% nel confronto tra i valori di N_i e di $(N_{\bar{q}\bar{\sigma}})_i$.

3 - Discussione.

L'analisi statistica descritta ha rivelato deviazioni significative tra N_i e $(N_c)_i$ per $\nu \geqslant 2$: la distribuzione degli N_i risulta invece in buon accordo con quella di $(N_{q\sigma})_i$, come s'è visto al paragrafo precedente dal confronto effettuato col metodo del χ^2. Per le statistiche comprendenti stelle con $\nu \geqslant 3$, $\nu \geqslant 4$, la probabilità che le deviazioni tra N_i e $(N_c)_i$ siano casuali è considerevole; tuttavia un accordo anche migliore si ottiene tra N_i ed $(N_{q\sigma})_i$, in senso concorde con quanto osservato per $\nu \geqslant 2$. L'insieme dei risultati permette dunque di stabilire l'esistenza di un effetto di associazione, sensibile se si includono nella statistica le stelle a due rami, ed inoltre induce a ritenere plausibile l'ipotesi che le deviazioni siano dovute alle interazioni secondarie di particelle neutre emesse dalle stelle.

È importante notare che, per poter rivelare un effetto significativo di correlazione tra le stelle dovuto a particelle neutre emesse dalle stesse, è necessario eseguire l'analisi statistica descritta su materiale sperimentale che soddisfaccia a particolari condizioni. Si può facilmente dimostrare che il rapporto segnale/disturbo $[(N_{q\sigma})_i - (N_c)_i]/(N_c)_i$, per un certo intervallo è inversamente proporzionale alla densità superficiale δ di stelle nelle lastre impiegate ed è funzione crescente del loro spessore tramite K_i:

$$[(N_{q\sigma})_i - (N_c)_i]/(N_c)_i \propto q\sigma K_i/\delta \,.$$

Altrettanto immediato è considerare il rapporto segnale/errore statistico: esso dipende dalla superficie totale esplorata S e ancora dallo spessore della lastra tramite K_i: Si può scrivere:

$$[(N_{q\sigma})_i - (N_c)_i]/\sqrt{(N_c)_i} \propto q\sigma K_i \sqrt{S} \,.$$

Entrambi i rapporti decrescono poi rapidamente al crescere di r, a causa dell'andamento di K_i, tanto che per distanze di alcuni millimetri diventa praticamente impossibile la rivelazione di effetto di associazione.

Nella presente esperienza, con una densità di 6,1 stelle/cm², $q\sigma = 4{,}4$, il rapporto segnale/disturbo è circa 0,35 per l'intervallo $0 \div 0{,}5$ mm; con una superficie esplorata di 487 cm² per lo stesso intervallo il rapporto segnale/errore risulta circa 2,8. La dipendenza di questi rapporti dallo spessore delle lastre è indicata dai seguenti dati: se la nostra esperienza fosse stata effettuata su lastre di 200 μ o di 50 μ anzichè di 400 μ (a parità di δ, $q\sigma$, S e Δr), il rapporto segnale/disturbo sarebbe stato circa 0,25 e 0,085 rispettivamente, e il rapporto segnale/errore rispettivamente 2 e 0,7.

Dalle considerazioni svolte si deduce che i requisiti cui devono soddisfare le lastre da impiegarsi in una analisi statistica di correlazioni tra stelle sono essenzialmente: grande spessore per aumentare l'angolo solido entro cui possono aver luogo interazioni secondarie visibili e breve esposizione per ridurre il disturbo dovuto alle coppie casuali; la statistica raccolta nella presente esperienza, pur non essendo oltremodo estesa, risulta adeguata alla rivelazione di una deviazione significativa tra N_i ed $(N_c)_i$ proprio per le condizioni di densità di stelle e di spessore delle lastre impiegate.

Si è finora assunto che le particelle neutre responsabili del fenomeno di associazione fossero neutroni; tuttavia il procedimento seguito per la stima di $q\sigma$ risulta del tutto generale e non implica nessuna supposizione sulla natura delle particelle stesse, eccettuata quella che esse abbiano un cammino di assorbimento non molto inferiore a quello geometrico (questo compare nel fattore correttivo in (2), § 1·2, che tiene conto della perdita di particelle per assor-

bimento: la correzione è comunque molto piccola rispetto al fattore di perdita geometrica).

Al fine di dedurre se i valori di q determinati sperimentalmente sono compatibili con l'interpretazione del fenomeno in studio secondo un processo generativo da soli neutroni, è conveniente valutare l'ordine di grandezza del numero di neutroni veloci emessi in media per disintegrazione sulla base dei dati esistenti sulla frequenza e sullo spettro di energia di emissione di protoni veloci da stelle in lastre esposte ad una quota paragonabile a quella della presente esperienza ([10]). Ponendo un limite inferiore di circa 40 MeV per l'energia necessaria a un neutrone per produrre una stella a due rami visibili, e supponendo inoltre che nella regione di energia considerata gli spettri energetici dei protoni e dei neutroni emessi siano confrontabili e che il rapporto n/p per questi sia uguale in media al rapporto di abbondanza medio per i nuclei dell'emulsione (1,25), si ricava un valore di $2 \div 2{,}5$ neutroni con $E \geq 40$ MeV emessi in ogni disintegrazione.

Per ricavare il valore di q dai nostri risultati sarebbe necessario conoscere σ, sezione d'urto media per produzione di stelle a due o piú rami da parte di neutroni, relativa alla parte dello spettro di energia di produzione dei neutroni al di sopra di circa 40 MeV. In considerazione degli errori sperimentali sui valori di $q\sigma$ ottenuti, non sembra giustificata però una valutazione di σ se non approssimativa. Sembra sufficiente, per i presenti scopi, ritenere che σ non sia molto differente dalla sezione geometrica, mediata per i nuclei dell'emulsione diversi da idrogeno, uguale a $0{,}84 \cdot 10^{-24}$ cm^2. Con questa ipotesi si ottengono per q valori di circa 5, 3 e 2, rispettivamente per produzione di stelle aventi $r \geq 2$, ≥ 3 e ≥ 4: tenendo conto degli errori sperimentali su $q\sigma$, dal confronto tra questi valori e quello previsto di $2 \div 2{,}5$ neutroni per stella, si deduce che i risultati ottenuti sono compatibili con l'ipotesi che al fenomeno di correlazione partecipino i neutroni soltanto. Anche il valore di q relativo a $r \geq 2$, sebbene alquanto elevato, non si può ritenere in disaccordo in considerazione oltre che dell'errore sperimentale anche dell'indeterminazione su σ, e infine perchè non è escluso che nella statistica fossero presenti stelle prodotte da neutroni di energia inferiore a 40 MeV.

Concludendo, si può affermare che l'entità dell'effetto di correlazione osservato e la sua variazione in funzione delle distanze reciproche tra le stelle sono compatibili con l'ipotesi che esso sia dovuto alle interazioni secondarie dei neutroni emessi dalle stelle. Non si può escludere la possibilità che altri fenomeni abbiano contribuito all'effetto, tuttavia la presente esperienza non sembra fornire alcun elemento a favore di altre interpretazioni.

([10]) U. Camerini, P. H. Fowler, W. O. Lock e H. Muirhead: *Phil. Mag.*, **41**, 413 (1950).

Esprimiamo la nostra gratitudine ai Professori PANCINI e POLVANI, per il loro costante interessamento e per le utili discussioni e consigli.

SUMMARY

The statistical analysis of the distribution of about 3000 cosmic ray stars in nuclear emulsions has demonstrated the presence of a correlation between them, giving a non-random distribution of the stars. The magnitude of the effect and its variation with the inverse distance between the stars suggests that it is due to secondary interactions produced by fast neutrons emitted from the stars in the emulsion.

On the Field Measurements and the State Definition in Quantum Electrodynamics.

B. FERRETTI

Istituto di Fisica e Scuola di Perfezionamento in Fisica Nucleare dell'Università - Roma
Istituto Nazionale di Fisica Nucleare - Sezione di Roma

(ricevuto il 9 Agosto 1954)

The very illuminating discussion by BOHR and ROSENFELD [1] on the problem of field quantities measurability in Quantum-Electrodynamics, gives results which may be considered hardly open to any doubt [2] on all the aspects of the question considered by the Authors.

There is however one point which may have some interest in the discussion of the quantum electrodynamics formalism from a physical point of view, and which has not been considered by BOHR and ROSENFELD.

The point is the following: how is it

[1] N. BOHR and L. ROSENFELD: *Kgl. Danske Vid. Selsk. Math. Fys.*, **12**, n. 8 (1933); *Phys. Rev.*, **78**, 794 (1950).

[2] In a well known paper HALPERN and JOHNSON (O. HALPERN and M. H. JOHNSON: *Phys. Rev.*, **59**, 896 (1941)) have stated that « admitting the existence of arbitrarily constituted test bodies, the accuracy of the measurement (of field strengths) still cannot exceed certain limits which are mainly defined by the wave-length of the field and the spatial and temporal domain of measurement ».

The argument is that the electric charge density of the test bodies cannot be thought arbitrarily high because of the « vacuum disruptive currents » which take place for the creation of (real) electron positron pairs.

Recently Prof. HALPERN has further emphasized that due to the mentioned circumstance, when the charge density of the test body should be too high, it is even impossible to prepare the device for Bohr-Rosenfeld's ideal field measurements (private communication).

Now it seems that this kind of argument cannot possibly be completely correct, merely for relativistic reasons. Such notions as the wave length of the field and so on, are not indeed relativistic invariant, and if therefore we change frame of reference we can pass from a wave length as short as we like to a wave lengths as long as we like in the same physical circumstances (at least in the case of progressive waves). The same may be stated for charge density. We can realize a charge density as high as we like taking a body charged at rest with a moderate charge density and moving it sufficiently fast. It should however be remarked that we have then, toghether with the charge density, an electric current different from zero.

This last point gives us the key for the solution of the supposed paradoxe concerning Bohr-Rosenfeld's measurement devices.

One may think in effect of compensating the vacuum disruptive currents, by some suitable low-resistence source of e.m. force between the charged test-bodies of Bohr-Rosenfeld's devices and the neutralising bodies.

The essential point here is that, as long as the dimension and the density of the charge of the test body are finite, the intensity of the

possible to define *states* of the e.m. field by measurements, or, which is the same, how is it possible to perform *complete sets* of measurements of the field quantities?

Even in the classical theory this point is not trivial. Considering in effect the field like a mechanical system with an infinite number of degrees of freedom, it would appear to be necessary in general a set of an infinite number of measurements for defining exactly and completely the state of the system in the classical sense, and this of course would be an impossibility.

In Quantum Theory however this difficulty luckily does'nt arise, but, with all that, a thorough discussion of the question taking into account the interaction with the positron-electron field, would not be too easy.

In this letter I only like to consider the case of the electromagnetic field without the interaction with the electron-positron field.

First it should be noted that, in order to have the possibility of defining the state of the system by a convenient set of measurements, we cannot take in consideration the case of the field in the infinite space, but we have to think of a bounded region of the space only, like for instance that inclosed in a box with perfectly reflecting walls (3).

It is quite easy then to see that «closed sets» of measurements exist which allow to define completely (in quantum mechanical sense) the state of the system. The «vacuum state» for instance may be defined by a weighing operation of the field containing box. It may be remarked however that this kind of operation is not a measurements of the field strenghts but merely of the total energy of the field.

It is fitting to point out immediately that it is impossible to put up a complete set of measurements by measuring field strengths only. This circumstance however does not forbid the possibility of performing a complete set of measurements by measuring field strenghts and some other quantity toghether.

One convenient manner of carrying on the analysis of the present problem is to consider for instance the normal modes of vibration of the field containing box.

If $\boldsymbol{k}$ are the propagation vectors and $\boldsymbol{u}_{ik}$, $\boldsymbol{v}_{ik}$ are the polarization versors defining this normal modes, ($\boldsymbol{u}_{ik}$ parallel to the electric field and $\boldsymbol{v}_{ik}$ parallel to the magnetic field) and if $\boldsymbol{E}$ and $\boldsymbol{H}$ are the electric and magnetic fields, putting

$$(1) \qquad \begin{cases} H'_{ak} = \int\limits_{\dot{\Omega}} \boldsymbol{a} \times \boldsymbol{H} \cos \boldsymbol{k} \times \boldsymbol{r} \, \mathrm{d}\boldsymbol{r}, \\ H''_{ak} = \int\limits_{\dot{\Omega}} \boldsymbol{a} \times \boldsymbol{H} \sin \boldsymbol{k} \times \boldsymbol{r} \, \mathrm{d}\boldsymbol{r}, \\ \cdots\cdots\cdots\cdots \end{cases}$$

and so on (where the integration is extended to the volume of the field containing box and $\boldsymbol{a}$ and $\boldsymbol{b}$ are given versors) we have, as well known, the

vacuum disruptive currents is not infinite; this circumstance may reasonably be suspected from the previous relativistic argument and may be confirmed by a more direct argument. A compensation of the vacuum disruptive currents is therefore possible and no real difficulty arises in preparing Bohr-Rosenfeld's measurements.

(3) This is a trivial example of the limitation that from physical requirements may be put on the mathematical formalism in quantum electrodynamics. It is a known thing that from a mathematical point of view it is essentially different to consider the Hohlraum infinite from the beginning, or finite, and then, if it is the case, to make its volume going to infinite. (See for instance S. T. Ma: *Phys. Rev.*, **87**, 652 (1952); B. Ferretti: *Nuovo Cimento*, **10**, 1079 (1953), App. I). It seems here clearly indicated that when a difference arises in the two treatments the second one should be preferred for physical reasons.

following commutation rules:

$$(2)\quad \begin{cases} [H'_{ak}, H''_{bk'}]_- = [E'_{ak}, E''_{bk'}]_- = 0 \\ [E'_{ak}, H'_{bk'}]_- = [E''_{ak}, H''_{bk'}]_- = 0 \\ [E'_{ak}, H''_{bk'}]_- = [E''_{ak}, H'_{bk'}]_- = \\ = -ih\Omega k\, \delta_k\, c_{k'} \sum_i (\boldsymbol{u}_{ik} \times \boldsymbol{a})(\boldsymbol{v}_{ik} \times \boldsymbol{b}). \end{cases}$$

Further the field strengths and the photon occupation numbers concerning different propagation vectors are commuting.

In order to verify the general physical consistency of the relations (2) it is necessary to verify that it is possible to measure *together any number* (and not only one or two) of field strengths components (1), concerning different vectors k with any wanted accuracy. This is the case provided the number of field strengths components to be measured keeps finite.

In order to measure in effect one field strength component (1) one may set up a test body with a suitable distribution of charges or currents filling almost completely the box Ω, and then proceed in a manner similar to that suggested by Bohr and Rosenfeld for the measure of the average field strength in a given space-time volume. (In our case the time of the measurement should be very short compared with the period of the field strength component (1) to be measured).

It is possible then to show that the disturbance created by the measure of one field strength component on the measure of others belonging to different k is proportional to $\varrho_0 \Delta x^2$ where ϱ_0 is the maximum density of charge (or current) of the test body and Δx is the indetermination of the test body location.

For a given accuracy, $\varrho_0 \Delta x$ keeps finite, and Δx may be as small as we want. There is not therefore any need of further compensation for getting the stated result.

It is a nice, although a not quite essential feature, of this method that the accuracy of measurement of such field components as E'_{ak} and E''_{bk} belonging to the same k, is again without need of any further compensation, the one to be expected from the commutation relation (2). In this respect this treatment is much simpler than Bohr-Rosenfeld's.

If however the number of field components to be measured increases beyond any limit, in order to have a finite accuracy Δx should be equal to zero (in all but a finite number of measurements) which is to be considered by itself an impossibility ([4]).

It is possible to show further that no compensation of the error proportional to Δx^2 is possible without contraddicting the indetermination principle.

For this reason (quite apart from the impossibility of an infinite number of different measurements) it is impossible to define completely the state of the field measuring field strength components only.

A complete set of measurements may however be carried on for instance like following: measuring all the necessary (commutable) field components until to a certain frequency ν_1, and then the photon occupation numbers for frequency greater than ν_1. If all these numbers are zero for frequencies greater than $\nu_2 \geqslant \nu_1$, it is possible to perform the complete set of measurements again by a weighing operation like in the vacuum case, but using this time screens of very high mass perfectly transparent for radiation of frequency lower than ν_2 and perfectly reflecting for frequency greater than ν_2.

It should be noted that under this respect the situation is essentially more complicated when the interaction with the electron-positron field is considered, and it is still matter of further investigation to find out the implication on quantum electrodynamics of the requirement that complete sets of measurements on the electromagnetic field should be possible.

([4]) This point should be related to the fundamental result of Bohr and Rosenfeld that it is impossible to measure a field strength in a geometrical point and such a notion has no physical meaning.

Non-Perturbative Equations for Propagation Kernels.

E. R. Caianiello

Istituto di Fisica e Scuola di Perfezionamento in Fisica Nucleare dell'Università - Roma
Istituto Nazionale di Fisica Nucleare - Sezione di Roma

(ricevuto il 20 Agosto 1954)

In a previous work [1], complete sets of equations defining the propagation kernels in theories with linear coupling among fermion and boson fields have been given. These equations, which are independent of perturbation expansions, fall into two classes, the second of which contains the derivatives of the kernels with respect to the interaction strength λ; both are infinite sets—a well-known feature.

It is the purpose of the present letter to point out that, by suitably working on the eq.'s of ref. [1], it is possible to deduce from them, for any given kernel, single equations which give more information than relations of the type exemplified in ref. [1], sect. 4·5. We present here only the simplest case, with an oversimplified notation, and refer the reader for the proof and a fuller study of the question (in particular, of the degree of uniqueness of the solution) to a work which will appear as a continuation to that of ref. [1]. The analogous equation for the general case differs but little from the one we report here, which refers to the kernel $K\begin{pmatrix} xz \\ yz \end{pmatrix} x\Big)$. It is:

$$\frac{\mathrm{d}}{\mathrm{d}\lambda}\left\{\lambda\left[\lambda\frac{\mathrm{d}}{\mathrm{d}\lambda}+3-\Omega\,\delta(0)\right]K\begin{pmatrix} xz \\ yz \end{pmatrix} x\Big)-\frac{1}{\lambda}\int \mathrm{d}\xi_1\int \mathrm{d}\xi_2\,\delta(\xi_1-\xi_2)\Lambda_{\xi_1}D_z\Lambda_x K\begin{pmatrix} x\xi_1 \\ y\xi_2 \end{pmatrix} z\Big)\right\} =$$

$$=\left[\lambda\frac{\mathrm{d}}{\mathrm{d}\lambda}+3-\Omega\,\delta(0)\right]\cdot\left\{\delta(x-y)\int \mathrm{d}\xi\,K\begin{pmatrix} z\xi \\ z\xi \end{pmatrix}\xi\Big)-\delta(x-z)\int \mathrm{d}\xi\,K\begin{pmatrix} x\xi \\ y\xi \end{pmatrix}\xi\Big)\right\}.$$

Here, we have omitted writing the γ-matrices, whose appearence is quite automatic in the formalism and can be easily inferred; Ω is the 4-dimensional volume of integration: Λ_x and D_x are the differential operators such that $\Lambda_x(xy)=\delta(x-y)$, $D_x[xy]=\delta(x-y)$ (they may contain counter terms, external fields, and be reduced to multiplicative factors with simple manipulations and passage to momentum space). The divergence implied by the appearence of the infinite quantity $\Omega\,\delta(0)$

[1] E. R. Caianiello: *Nuovo Cimento*, **11**, 492 (1954).

is quite trivial, and could be easily removed; we think it more significant, at this stage, to leave it there. The equation is singular for $\lambda = 0$.

A simple way to check the correctness of this equation is to use the formal power-series expansions of $K\left(\begin{matrix}x_1 x_2\\ y_1 y_2\end{matrix}\middle| t\right)$; formula (30) of ref. [1]. Clearly, once one knows the solutions of equations of this type the problem of determining the kernels becomes trivial. This can be seen in many ways, for instance, in our case, most simply by integrating the equation written above with respect to the variable z, after the known value of K is substituted in all terms but the last: one gets then immediately $\int \mathrm{d}\xi\, K\left(\begin{matrix}x\xi\\ y\xi\end{matrix}\middle| \xi\right)$, that is $\dfrac{\mathrm{d}}{\mathrm{d}\lambda} K\left(\begin{matrix}x\\ y\end{matrix}\right)$.

Thanks are due to Prof. B. Ferretti for stimulating discussions.

The Green's Functions of Quantised Fields.

P. T. Matthews

Department of Mathematical Physics, The University, Birmingham, England

A. Salam

St. John's College, Cambridge, England

(ricevuto il 25 Agosto 1954)

The generalised form of Feynman's dynamical principle [1] for quantised, interacting, Fermi and neutral Bose fields, $\boldsymbol{\psi}(x)$ and $\boldsymbol{\varphi}(x)$, expresses the matrix element of the chronological product of field operators, $\boldsymbol{A}(1)$, $\boldsymbol{B}(2)$, ..., $\boldsymbol{C}(n)$, as

$$(1) \qquad \delta(\xi'\,\sigma_1|(\boldsymbol{A}(1),\boldsymbol{B}(2),\ldots,\boldsymbol{C}(n))_+|\xi'',\sigma_2) = \frac{1}{N}\int \delta\psi\;\delta\bar{\psi}\;\delta\varphi\left\{A(1)B(2)\ldots C(n)\exp\left[i\int_{\sigma_2,\xi''}^{\sigma_1,\xi'}\mathcal{L}(x)\,\mathrm{d}^4x\right]\right\},$$

where $\mathcal{L}(x)$ is the Lagrangian density, and all expressions in the integrand are treated as classical functions, except that Fermi fields anti-commute. N is a normalising factor defined so that the vacuum to vacuum transition amplitude is unity for infinite time interval, and zero external fields.

By including external sources in the Lagrangian, and making a Maclaurin expansion of $(0,+\infty|0,-\infty)$ with respect to them [2], the n nucleon, m meson Green's function can be derived, which directly determines the corresponding scattering amplitude. Using (1), this can be expressed in a compact form, and actually evaluated if a technique of functional integration can be developed.

For example, the one particle Green's function for the quantised Fermi field, $\boldsymbol{\psi}$, in scalar interaction with a given classical, external, neutral, scalar field, φ^{ex}, is

$$(2) \qquad K(1,2;\varphi^{\mathrm{ex}}) = (0,+\infty|(\boldsymbol{\psi}(1),\boldsymbol{\psi}(2))_+|0,-\infty) = \frac{1}{N(\varphi^{\mathrm{ex}})}\int \delta\psi\;\delta\bar{\psi}\;\psi(1)\bar{\psi}(2)\exp\left[i\int\bar{\psi}(x)\mathcal{D}_{xy}(\varphi^{\mathrm{ex}})\psi(y)\,\mathrm{d}x\,\mathrm{d}y\right],$$

[1] R. P. Feynman: *Rev. Mod. Phys.*, **20**, 367 (1948).
[2] D. J. Candlin: *Nuovo Cimento*, **12**, 380 (1954).

where

$$\mathcal{D}_{xy}(\varphi^{\mathrm{ex}}) = \delta(x-y)\left(\gamma\frac{\mathrm{d}}{\mathrm{d}x} + k + g\varphi^{\mathrm{ex}}(x)\right), \tag{3}$$

and

$$N(\varphi^{\mathrm{ex}}) = \int \delta\psi\,\delta\bar{\psi}\,\exp\left[i\int \bar{\psi}(x)\mathcal{D}_{xy}(\varphi^{\mathrm{ex}})\psi(y)\,\mathrm{d}x\,\mathrm{d}y\right]. \tag{4}$$

Thus

$$K(1,2;\varphi^{\mathrm{ex}}) = \frac{\delta}{\delta\mathcal{D}_{12}} N(\varphi^{\mathrm{ex}})/N(\varphi^{\mathrm{ex}}). \tag{5}$$

This integral has been evaluated by FEYNMAN [3] and yields the familiar result

$$K(1,2;\varphi^{\mathrm{ex}}) = [\mathcal{D}_{12}(\varphi^{\mathrm{ex}})]^{-1}. \tag{6}$$

$N(\varphi^{\mathrm{ex}})/N(0)$ is the vacuum to vacuum transition amplitude, a most important quantity in the later theory.

Extension of this argument to the n-particle propagator, $K^{(n)}(\varphi^{\mathrm{ex}})$, expresses it as a determinant of one particle propagators in accordance with the Pauli exclusion principle.

The one nucleon propagator for coupled quantised fields is

$$K(1,2) = \frac{1}{N}\int \delta\psi\,\delta\bar{\psi}\,\delta\varphi\left\{\psi(1)\bar{\psi}(2)\cdot\exp\left[i\int \bar{\psi}(x)\mathcal{D}_{xy}(\varphi)\psi(y) + q(x)\mathcal{K}_{xy}q(y)\,\mathrm{d}x\,\mathrm{d}y\right]\right\}, \tag{7}$$

where

$$\mathcal{K}_{xy} = \delta(x-y)(\Box_x - \mu^2), \tag{8}$$

and

$$N = \int \delta\psi\,\delta\bar{\psi}\,\delta\varphi\,\exp\left[i\{\bar{\psi}\mathcal{D}(\varphi)\psi + \varphi\mathcal{K}\varphi\}\right]. \tag{9}$$

In the final expression an obvious contracted notation has been introduced. Equation (7) can be written

$$K(1,2) = \frac{\int \delta\psi\,\delta\bar{\psi}\,\delta\varphi\,\delta/\delta\mathcal{D}_{12}(\varphi)\,\exp\left[i\{\bar{\psi}\mathcal{D}(\varphi)\psi + \varphi\mathcal{K}\varphi\}\right]}{\int \delta\psi\,\delta\bar{\psi}\,\delta\varphi\,\exp\left[i\{\bar{\psi}\mathcal{D}(\varphi)\psi + \varphi\mathcal{K}\varphi\}\right]}. \tag{10}$$

Performing the integrations over ψ and $\bar{\psi}$ (which are the same as in (5)), and using (5),

$$K(1,2) = \frac{\int \delta\varphi\,K(1,2;\varphi)N(\varphi)\,\exp\left[i\varphi\mathcal{K}\varphi\right]}{\int \delta\varphi\,N(\varphi)\,\exp\left[i\varphi\mathcal{K}\varphi\right]}. \tag{11}$$

[3] R. P. FEYNMAN: *Phys. Rev.*, **84**, 108 (1951); Appendix C.

This result generalises immediately to the n-particle, m-meson propagator,

$$K^{(n,m)} = \frac{\int \delta\varphi(\varphi)^m \, K^{(n)}(\varphi) N(\varphi) \exp[i\varphi\mathcal{K}\varphi]}{\int \delta\varphi \, N(\varphi) \exp[i\varphi\mathcal{K}\varphi]} . \tag{12}$$

where, by definition,

$$K^{(0)}(\varphi) = 1 . \tag{13}$$

Dividing the numerator and denominator of (12) by $N(0)$, all propagators are expressed as functional integrals over φ of the one particle propagator, and the vacuum to vacuum transition amplitude in a given external field. The former is the solution of a Fredholm integral equation (4), and the latter the corresponding Fredholm determinant, $\mathrm{d}(\varphi)$,

$$\mathrm{d}(\varphi) = N(\varphi)/N(0) . \tag{16}$$

The Fredholm determinant can be expressed as an exponential

$$\mathrm{d}(\varphi) = \exp[-L(\varphi)] . \tag{15}$$

Thus, for example,

$$K(1, 2) = \frac{\int \delta\varphi \, K(1, 2; \varphi) \exp[i\varphi\mathcal{K}\varphi - L(\varphi)]}{\int \delta\varphi \exp[i\varphi\mathcal{K}\varphi - L(\varphi)]} . \tag{16}$$

An approximate form of (16) has been obtained previously by PEIERLS and EDWARDS (5), starting from Schwinger's dynamical principle (6), which is the variational equivalent of Feynman's. The approximation which they made in the field equations amounts, in this formulation, to using the zero order approximation to (15), that is, to replacing $\mathrm{d}(\varphi)$ by unity. The final functional integral over φ has been carried out by these authors for two special cases.

This work is the direct result of numerous stimulating conversations with Prof. R. E. PEIERLS and most particularly Dr. S. F. EDWARDS, to whom we express our thanks. A more detailed account will be published elsewhere.

(4) M. NEUMAN: *Phys. Rev.*, **83**, 1258 (1951); **85**, 129 (1952); A. SALAM and P. T. MATTHEWS: *Phys. Rev.*, **90**, 690 (1953); J. SCHWINGER: *Phys. Rev.*, **93**, 616 (1954).

(5) R. E. PEIERLS and S. F. EDWARDS: *Proc. Roy. Soc.*, A **224**, 24 (1954).

(6) J. SCHWINGER: *Proc. Nat. Acad. Sci.*, **37**, 452 (1951).

IL NUOVO CIMENTO Vol. XII, N. 4 1° Ottobre 1954

Commutation Relations between Different Fields.

H. Umezawa

Physical Laboratories, University of Manchester

S. Oneda

Kanazawa University, Japan

(ricevuto il 10 Settembre 1954)

1. – We shall show in what manner the commutation relations between different fields are restricted by the form of the interaction Hamiltonian, and so by the possible transmutations. Further restrictions follow from the requirement that fermions form « families ».

2. – From the canonical invariance of quantum field theory, the following theorems can be proved (Oneda and Umezawa (1953) [1], Takahashi and Umezawa (1953) [2]):

(i) Each interaction Hamiltonian must contain an even number $A_1, \ldots, A_{2n}$ of field operators which anticommute (*) with a field X. Thus, each transmutation process must involve an even number of particles A_k.

(ii) If a field operator A commutes (anticommutes) with a field X, then the hermitian conjugate A^* also commutes (anticommutes) with X.

3. – The above theorems do not restrict the commutation relations if the interaction Hamiltonian is made up of pairs of anticommuting fields only. That is the case, e.g., for the electrostatic interaction and low energy nuclear interactions. Indeed, Klein (1938) [3] has shown that the electrostatic interaction is compatible with any type of commutation relations.

For more general interactions, theorems (i) and (ii) do impose restrictions on the commutation relations, but they do not always determine them completely. For the baryon-π system, e.g., the wave functions of Λ, P, N, $\pi^{\pm}$ cannot all commute with each other, and π^0 must commute with all fields. In this case, theorems (i) and (ii) admit of two types of commutation relations.

(*) In this paper, « commuting » and « anticommuting » refer to field operators in different space points at the same time.

(1) S. Oneda and H. Umezawa: *Prog. Theor. Phys.*, **9**, 685 (1953).

(2) Y. Takahashi and H. Umezawa: *Prog. Theor. Phys.*, **9**, 14 (1953).

(3) O. Klein: *Journ. de Phys.*, **9**, 1 (1938).

4. – This result can be made unique by an additional assumption. We require that all fermions form « families » with the following properties:

Any two members of a family anticommute, and each of them commutes with any field outside the family. Thus, we assume that

$$[\varphi^1, \varphi^2]_+ = 0 \quad \text{and} \quad [\varphi^1, \varphi^3]_+ = 0 \quad \text{imply} \quad [\varphi^2, \varphi^3]_+ = 0 ,$$

and that

$$[\varphi^1, \varphi^2]_+ = 0 \quad \text{and} \quad [\varphi^1, \chi]_- = 0 \quad \text{imply} \quad [\varphi^2, \chi]_- = 0 .$$

This construction is internally consistent: the family requirement is compatible with theorems (i) and (ii).

5. – For the baryon-π system the family hypothesis leads to the commutation relations

$$[\Lambda, \mathrm{P}]_+ = [\Lambda, \mathrm{N}]_+ = [\mathrm{P}, \mathrm{N}]_+ = 0 ,$$

$$[\pi, \Lambda]_- = [\pi, \mathrm{P}]_- = [\pi, \mathrm{N}]_- = 0 .$$

From $\mathrm{N} \to \mathrm{P} + e + \nu$ it follows then that the leptons form an anticommuting set. However, we cannot decide whether they constitute a separate family or whether they belong to the baryon family, because even numbers of both nucleons and leptons are involved and so Klein's result holds.

In a forthcoming paper in which details of the theory will be given the method will be applied to the set Λ, P, N, π, θ, τ, $\varkappa$, μ, e, ν.

6. – We have defined families, essentially, as sets of fields with the same commutation relations. We believe, however, that the commutation properties cannot be considered to be the ultimate basis of the family concept which probably, needs a group theoretical foundation. Thus it may be fortuitous that, for fermions, the commutation relations enable us to build up families from the known transmutations.

We wish to thank Professor L. Rosenfeld, Dr. A. Visconti and Dr. J. Podolanski fot many inspiring discussions.

Matrix Elements for Double Pion Photoproduction.

R. Gatto

Istituto di Fisica dell'Università - Roma
Istituto Nazionale di Fisica Nucleare - Sezione di Roma

(ricevuto l'11 Settembre 1954)

The treshold photon energy for two meson production in photon-nucleon collisions lies at about 322 MeV. The ratio of the pair cross-section to the single meson cross-section may roughly be estimated, from pseudoscalar meson theory, to be about one forth for γ-rays of 600 MeV and about unity for γ-rays of 1 000 MeV in the laboratory system [1]. Experiments to detect this process are now being carried out at the California Institute of Techhology [2]. It seems of interest, at this stage, to investigate the consequences of the hypothesis of charge independence for double pion photoproduction. A discussion of the implications of charge independence on single photo-nucleon production of pions has been given by Watson [3]. In this note we shall briefly deal with the extension of Watson's analysis to the case of double photoproduction. Some general consequences of charge independence for multiple photoproduction will also be stated.

It appears a reasonable hypothesis to assume that the matrix element responsible for the process can be expanded in powers of the electric charge, and that only the first term in such expansion needs to be considered [3]. In this case one may expect the interaction to contain terms which rotate in charge space as scalars and terms which rotate as zero-components of spherical tensors of first rank. We call $[p+--]$ the matrix element for the process $\gamma+\mathrm{p}\to\mathrm{p}+\pi^+ +\pi^-$ and use similar notations for the other processes differing from this only in the charge of the particles. It must be stressed that such matrix elements always refer to well defined space and ordinary spin states for the incoming and the outgoing particles. As a consequence $[p+--]$ is in general distinct from $[p--+]$ [4]. Such a distinction may prove useful also in evaluating total cross-sections since it immediately shows which matrix elements do not contribute. The isotopic spins of the final particles may be added to form isotopic spin states of total isotopic spin 1/2, 3/2, 5/2. However only matrix elements which lead to final states of total isotopic spin 1/2 and 3/2 need to be considered because of the assumed properties of the interaction respect to rotation in charge space. Two indipendent states of total isotopic spin 1/2 may be constructed,

(1) K. A. Brueckner and K. M. Watson: *Phys. Rev.*, **87**, 621 (1952).
(2) Kindly communicated by Prof. G. Bernardini.
(3) K. M. Watson: *Phys. Rev.*, **85**, 852 (1952).
(4) L. Van Hove, R. Marshak and A. Pais: *Phys. Rev.*, **88**, 1211 (1952).

one spatially symmetric in the two pions, the other spatially antisymmetric; and similarly two independent states of total isotopic spin 3/2 may be constructed, the first spatially symmetric in the two pions, the other spatially antisymmetric. Taking the interaction in the form $T_0+T_1^0$ [3] (T_0 rotates in charge space as a scalar, T_1^0 as a zero spherical component of a vector) one gets a total of six independent matrix elements, which we call:

$$\mathcal{A}_+ = \sqrt{\tfrac{1}{3\,0}}\,\langle +;\tfrac{3}{2},m\,|\,T_1^0\,|\,\tfrac{1}{2},m\rangle = \sqrt{\tfrac{1}{1\,5}}\,\langle +;\tfrac{3}{2}\|T_1\|\tfrac{1}{2}\rangle$$

$$\mathcal{A}_- = \sqrt{\tfrac{1}{6}}\,\langle -;\tfrac{3}{2},m\,|\,T_1^0\,|\,\tfrac{1}{2},m\rangle = \sqrt{\tfrac{1}{3}}\,\langle -;\tfrac{3}{2}\|T_1\|\tfrac{1}{2}\rangle$$

$$\mathcal{B}_- = \sqrt{\tfrac{1}{6}}\,[\langle -;\tfrac{1}{2},m\,|\,T_1^0\,|\,\tfrac{1}{2},m\rangle(-)^{\frac{1}{2}-m} + \langle -;\tfrac{1}{2},m\,|\,T_0\,|\,\tfrac{1}{2},m\rangle] =$$
$$= \sqrt{\tfrac{1}{6}}\,[\,|\,m\,|\langle -;\tfrac{1}{2}\|T_1\|\tfrac{1}{2}\rangle + \langle -;\tfrac{1}{2}\|T_0\|\tfrac{1}{2}\rangle]$$

$$\mathcal{B}'_- = \sqrt{\tfrac{1}{6}}\,[\langle -;\tfrac{1}{2},m\,|\,T_1^0\,|\,\tfrac{1}{2},m\rangle(-)^{\frac{1}{2}-m} - \langle -;\tfrac{1}{2},m\,|\,T_0\,|\,\tfrac{1}{2},m\rangle] =$$
$$= \sqrt{\tfrac{1}{6}}\,[\,|\,m\,|\langle -;\tfrac{1}{2}\|T_1\|\tfrac{1}{2}\rangle - \langle -;\tfrac{1}{2}\|T_0\|\tfrac{1}{2}\rangle]$$

$$\mathcal{B}_+ = \sqrt{\tfrac{1}{3}}\,[\langle +;\tfrac{1}{2},m\,|\,T_1^0\,|\,\tfrac{1}{2},m\rangle(-)^{\frac{1}{2}-m} + \langle +;\tfrac{1}{2},m\,|\,T_0\,|\,\tfrac{1}{2},m\rangle] =$$
$$= \sqrt{\tfrac{1}{3}}\,[\,|\,m\,|\langle +;\tfrac{1}{2}\|T_1\|\tfrac{1}{2}\rangle + \langle +;\tfrac{1}{2}\|T_0\|\tfrac{1}{2}\rangle]$$

$$\mathcal{B}'_+ = \sqrt{\tfrac{1}{3}}\,[\langle +;\tfrac{1}{2},m\,|\,T_1^0\,|\,\tfrac{1}{2},m\rangle(-)^{\frac{1}{2}-m} - \langle +;\tfrac{1}{2},m\,|\,T_0\,|\,\tfrac{1}{2},m\rangle] =$$
$$= \sqrt{\tfrac{1}{3}}\,[\,|\,m\,|\langle +;\tfrac{1}{2}\|T_1\|\tfrac{1}{2}\rangle - \langle +;\tfrac{1}{2}\|T_0\|\tfrac{1}{2}\rangle]$$

where + or − denotes spatial symmetry or spatial antisymmetry respectively in the two final pions, and the dependence of the matrix elements on m follows from elementary use of the Wigner-Eckart theorem. The matrix elements for the different reactions may the be written:

$$[p+-] = \sqrt{2}\,\mathcal{A}_+ - \sqrt{2}\mathcal{A}_- - \mathcal{B}_- + \mathcal{B}_+$$
$$[p\;0\;0\,] = \sqrt{8}\,\mathcal{A}_+ - \mathcal{B}_+$$
$$[p-+] = \sqrt{2}\,\mathcal{A}_+ + \sqrt{2}\,\mathcal{A}_- + \mathcal{B}_- + \mathcal{B}_+$$
$$[n+0\,] = -3\mathcal{A}_+ - \mathcal{A}_- + \sqrt{2}\,\mathcal{B}_-$$
$$[n\;0+] = -3\mathcal{A}_+ + \mathcal{A}_- - \sqrt{2}\,\mathcal{B}_-$$
$$[p\;0-] = \;\;3\mathcal{A}_+ - \mathcal{A}_- + \sqrt{2}\,\mathcal{B}'_-$$
$$[p-0\,] = \;\;3\mathcal{A}_+ + \mathcal{A}_- - \sqrt{2}\,\mathcal{B}'_-$$
$$[n+-] = -\sqrt{2}\,\mathcal{A}_+ - \sqrt{2}\,\mathcal{A}_- - \mathcal{B}'_- - \mathcal{B}'_+$$
$$[n\;0\;0\,] = -\sqrt{8}\,\mathcal{A}_+ + \mathcal{B}'_+$$
$$[n-+] = -\sqrt{2}\,\mathcal{A}_+ + \sqrt{2}\,\mathcal{A}_- + \mathcal{B}'_- - \mathcal{B}'_+\,.$$

To get the total cross-sections from the above formulae it is convenient first to sum the two cross-sections for interchanged final states of the two pions when they have different charge (for instance, $|[p+-]|^2+|[p-+]|^2$). In this manner one has two advantages: firstly, some interference terms are immediately removed, secondly, the indistinguishability of the final pions when they have the same charge

is automatically taken into account. Total cross-sections are then obtained after averaging and summing over polarizations and after summing over all possible directions for the final particles (for the two pions each pair of directions and polarizations has to be counted only once).

The above equations have been essentially derived on the hypothesis of a charge independent pion-nucleon interaction. Additional hypotheses, if they should prove to be valid, could greatly reduce the number of distinct matrix elements. Suppose, for instance, that the interaction in the states of total isotopic spin 3/2 predominates, so that the influence of the other states may be neglected. In this case only $\mathcal{A}_+$ and $\mathcal{A}_-$ would remain in the above formulae. One obtains of course the same result, if one assumes that an excited state of the nucleon ([5]) with isotopic spin 3/2 is first formed, which successively decays into the final particles; the life time of this excited state being just long enough so that its production and its decay may be regarded as independent processes ([6]). Of course, from the assumed properties of the interaction, only excited states of the nucleon having isotopic spin 1/2 and 3/2 may be produced. Recently some evidence has been found in high energy pion-nucleon scattering for an excited state perhaps having isotopic spin 1/2 ([7]). If, at some energy, photoproduction through this excited state should predominate, it may be of interest to observe that, for that case, a relation similar to that found by WATSON ([3]) for the case of pion production in nucleon-nucleon collisions can be derived. Denoting by N^+, N^0 and N^- respectively the average numbers of positively charged, neutral charged and negatively charged pions produced, it can be shown that the relation $N^+ + N^- = 2N^0$ holds whatever the number of pions produced and independently of the charge of the bombarded nucleon. Similarly, for the case of photoproduction through an excited state having isotopic spin 3/2, it can be shown that the relation $N_p^+ - 2N_p^0 + N_p^- = N_n^+ - 2N_n^0 + N_n^-$ holds whatever the number of pions produced. Here we denote by N_p^+ the average number of positively charged pions produced when the target nucleon is a proton, by N_n^+ the average number of positively charged pions produced when the target nucleon is a neutron, and so on. The proofs of the above relations follow from simple extensions of Watson's group-theoretical argument. (Note that in our case charge independence does not hold for the whole process; it only holds for the decay of the excited nucleon.)

Concluding, I would like to stress the viewpoint that experiments on double pion production should deserve special interest in view of the possibility of obtaining information on the scarcely known pion-pion interaction. In this connection such experiments should be specially instructive at energies near the tresholds ([1]).

I wish to express my gratitude to Prof. G. BERNARDINI, who has read the manuscript and has made helpful comments and suggestions. I am also indebted to Prof. L. RADICATI for discussions on these topics.

([5]) We use the therm « excited nucleon » exactly as defined by FERRETTI (see: J. G. WILSON: *Progress in Cosmic Ray Physics*, II (Amsterdam, 1954), p. 104).

([6]) F. J. BELINFANTE: *Phys. Rev.*, **92**, 145 (1953).

([7]) See *Proceedings of the 4-th Rochester Conference.*

Remark on an Unusual Cosmic Ray Event.

E. Corinaldesi

Dublin Institute for Advanced Studies

(ricevuto il 18 Settembre 1954)

An unusual event, recently found by Schein and co-workers (1), has been tentatively explained as being due to the annihilation of an antiparticle. This may be believed to be an antiproton, the annihilation occurring in flight. In the system of the centre of gravity of the antiproton and the proton, the annihilation would take place with emission of some high energy neutral particles, responsible for the conservation of energy and momentum, accompanied by a number of low energy photons. The latter would assume rather high energies when transformed to the laboratory system. On this hypothesis, and by using the Bloch-Nordsieck method, it is easy to evaluate the average number of soft photons emitted in a certain energy range. The calculation is similar to that for the Compton scattering (2), and leads to the formula ($\hbar = c = 1$)

$$\bar{n} = \frac{e^2}{(2\pi)^3} \int_{\Delta} \delta(k^2) \left[\frac{(p\boldsymbol{e})}{(pk)} - \frac{(p'\boldsymbol{e})}{(p'k)} \right]^2 \mathrm{d}^4k \ .$$

Here p and p' denote the 4-momenta of the antiproton before and after annihilation, the process being described as the transition from a state with a given momentum and positive energy to one with the same momentum and negative energy (3). The 4-momentum of the soft photon is denoted by k, Δ is the energy interval in question and $\boldsymbol{e}$ the polarization vector. The probability for the emission of n photons in the energy range Δ follows a Poisson distribution: $\bar{n}^n \exp[-\bar{n}]/n!$

In the c.g.s. the momenta of the proton and of the antiproton are denoted by $\pm P$. After averaging over the polarization one obtains

$$\bar{n} = \frac{e^2}{4\pi^2} \left[\frac{2P^2 + M^2}{2P\sqrt{P^2 + M^2}} \ln \left(\frac{\sqrt{P^2 + M^2} + P}{\sqrt{P^2 + M^2} - P} \right) - 1 \right] \ln \frac{K_{\max}}{K_{\min}} \ .$$

---

(1) M. Schein, D. M. Haskin and R. G. Glasser: *Narrow Shower of Pure Photons at* 100 000 *Feet* (pre-publication).

(2) R. Jost: *Phys. Rev.*, **72**, 815 (1947); W. Thirring and B. Touschek: *Phil. Mag.*, **42**, 244 (1951).

(3) W. Heitler: *The Quantum Theory of Radiation* (Oxford, 1954), p. 268.

Here M is the proton mass, and it will be assumed that $P \gg M$. The limits $K_{\max}$ and $K_{\min}$ are not very well defined. If, however, $K_{\max}$ is put equal to P, and $K_{\min}$ is chosen as the energy assumed in the c.g.s. by a photon belonging to the visible spectrum in the laboratory system, one finds

$$\bar{n} \lesssim \frac{e^2}{\pi^2}(z^2 + 10z + 2);$$

with $z \equiv \ln (P/M)$.

Thus the average number of soft photons accompanying the annihilation increases slowly with P. Conversely, it is easy to show that for $\bar{n}$ to be of the order of 20, P should be exceedingly large, in fact, of the order of 10^{52} eV. At a lower energy, such as that of 10^{13} eV suggested by SCHEIN and co-workers, so large a number of photons could of course still be emitted. The probability of this happening would however be very small, as can be seen from the Poisson formula, possibly as small as the probability of the event being a fluctuation in a normal electron-photon cascade.

The writer is indebted to the Rev. Prof. J. MCCONNELL and to Profs. C. B. A. MCCUSKER and E. CLEMENTEL for their interest in this remark.

Direttore responsabile: G. POLVANI Tipografia Compositori - Bologna

Questo fascicolo è stato licenziato dai torchi il 23-IX-1954